POLITECNICO
MILANO 1863

Cal Agua
Unidad Mixta UV-UPV

Calibration and Validation of a Microalgae Model applied to a Lab-scale Photobioreactor for Municipal Wastewater Treatment

Master of science in
ENVIRONMENTAL AND LAND PLANNING ENGINEERING
SCHOOL OF CIVIL, ENVIRONMENTAL AND LAND MANAGEMENT ENGINEERING

Enrico Giuliani - 968190

Advisor: Prof.ssa Elena Ficara
Co-advisors: Prof. Ángel Robles Martínez, Prof. José Ferrer Polo
Academic Year 2022-2023

Abstract

In the framework of strategies toward a sustainable development, an important factor is the technological progress in the water sector. The present thesis was developed within the CALAGUA research group formed by personnel from the Research Institute of Water and Environmental Engineering of the Polytechnic University of Valencia and the Department of Chemical Engineering of the University of Valencia.
The development of new technologies based on microalgae applications is a significant player in achieving sustainable goals and moving towards the concept of circular economy [74]. One of the principles of the circular economy is the recovery of useful and valuable substances that are considered waste in the traditional consumer economy. The potential applications of microalgae range across a multitude of sectors such as wastewater remediation, biorefineries, pharmaceuticals and chemical building blocks synthesis. The present work is structured on experimental assays at a laboratory scale, aiming to calibrate and validate the parameters of a microalgal kinetic model associated with microalgal growth rate and pH. All the development of the thesis was performed at a laboratory scale. The scope of the investigation is to obtain further knowledge of the microalgae pure culture. Indeed, the reference algal model is the one developed by Viruela et al. [117] that is then coupled with a bacterial model to obtain a microalgae-bacteria consortium model. However, the microalgae model was less accurate than the bacterial one, making it necessary to recalibrate some parameters. Several tests have been performed by varying the values of the factors affecting the algal growth rate such as pH, light intensity and biomass concentration. The choice of the values of the mentioned factors has been driven by the scientific literature so that the research covers the average growth conditions applied in the commonest experimental activities. After the data collection and the data cleaning, calibration and validation of the interested parameters are performed.

Keywords: microalgae; modeling; bioreactor; pH

Sintesi

Fra le varie strategie verso uno sviluppo sostenibile un ruolo rilevante è costituito dal progresso tecnologico del settore dell'acqua. La tesi qui proposta è stata sviluppata all'interno del centro di ricerca CALAGUA, gruppo congiunto fra il Research Institute of Water and Environmental Engineering della Università Politecnica di Valencia e il dipartimento di ingegneria chimica della Univeristà di Valencia.
Lo sviluppo di nuove tecnologie basate sull'applicazione delle microalghe può rappresentare un fattore aggiunto per il raggiungimento degli obiettivi di sviluppo sostenibile dell'agenda ONU 2030 e verso un'economia circolare [74]. Uno dei principi dell'economia circolare è il recupero di sostanze utili e con valore aggiunto, sostanze le quali tradizionalmente erano considerate rifiuti da gestire. Le potenziali applicazioni delle microalghe spaziano in molteplici settori come per esempio il trattamento delle acque di rifiuto, la bioraffineria, nel campo farmaceutico e nella chimica di sintesi. L'obiettivo finale di questo lavoro di tesi è la calibrazione e validazione di parametri cinetici di un modello cinetico microlagale legati al tasso di crescita microalgale e al pH. Lo studio proposto è stato svolto interamente in scala laboratoriale. Lo scopo della ricerca è l'investigazione delle dinamiche biologiche di una coltura microalgale pura per sviluppare il modello algale proposto da Viruela et al. [117] da accoppiare successivamente con un modello batterico. Il modello batterico già presenta una buona accuratezza, al contrario quello delle sole microalghe non mostra una affidabilità elevata e si è perciò reso necessario uno studio più approfondito del tema. Numerosi esperimenti sono stati svolti in differenti condizioni, variando i fattori che influenzano il tasso di crescita algale. Fra questi sono stati testati vari valori di pH, intensità luminosa e concentrazione della biomassa. I livelli definiti di questi fattori sono stati scelti a valle di una ricerca bibliografica. In questo modo la ricerca copre un campo applicativo che presenta i valori più comunemente adottati nei lavori sperimentali. La calibrazione e validazione dei parametri di interesse è svolta successivamente alle operazioni di raccolta, esplorazione e pulizia dei dati.

Parole chiave: microalghe; modellizzazione; bioreattore; pH

Contents

1 | Introduction

Starting from the Industrial Revolution in the XVIII century, humankind has experienced the fastest technological development in its history. Even though it regarded only a small part of the world, the western one, it resulted in an incomparable step toward a higher quality of life.
Then, in the last century, this progress involved finally almost all of the world, mainly due to globalization. However, this unprecedented progress has produced drawbacks affecting the Earth system's functionality and integrity.
The world population has grown to 8 billion and the trend suggests that the global population could grow to around 8.5 billion in 2030, 9.7 billion in 2050 and 10.4 billion in 2100 [111].
Moreover, with the exception of the last two years of COVID-19 pandemic crisis [31], human progress saw a constant increase in terms of prosperity and living standards [113].

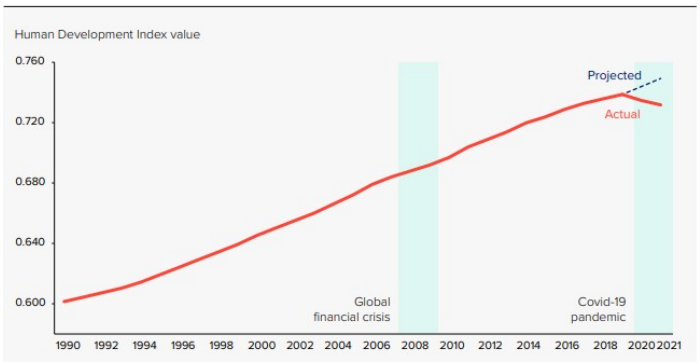

Figure 1.1: The global Human Development Index trend over the years. Note that the Index value has declined two years in a row during the pandemic period [113].

The developing countries' populations demand a better quality of life, and thus the exploitation of natural resources is getting increasingly relevant. Indeed, the change in habits and consumptions are favoring the decrease of the availability of natural resources and their degradation.
In this perspective, the circular economy and sustainable development concepts are key

role players in the maintenance of the Earth's system balances. These fragile equilibriums are endangered and already today altered by the emission of greenhouse gases (mainly CO_2, CH_4, N_2O fluorinated gasses), waste production, water and air pollution, land use (agriculture, infrastructure, buildings...) and loss of biodiversity.
Climate change is a consequence of human activities and it is happening now [112]. In order to face it, two strategies have been proposed so far. The first one is to decrease the drivers of climate change (mitigation). The second one is to cope with the impacts of climate change (adaptation).
In other words, mitigation aims to limit the uncontrollable while adaptation aims to manage the unavoidable. Following these principles, to provide solutions from a world scale, several international conferences have been held in the last decades.
The most recent and relevant was the Paris Agreement, signed by 194 states and the European Union in 2015. It is a binding international treaty on climate change which states that all the parties involved committed themselves in holding the increase in the global average temperature to well below 2°C above pre-industrial levels and to pursue efforts to limit the temperature increase to 1.5°C above pre-industrial levels [72].
The resulting framework aims to support the nations in tackling climate change and adaptation challenges, embracing the previously mentioned ambitious pledges.
However, most of the countries are falling short of achieving the targets.
The last available update indicates that almost all the nations are not doing enough to accomplish their obligations showing an insufficient effort [109]. A possible cause of this is also due to the COVID-19 pandemic crisis which represented a delay in political actions and in general, brought a switch of priorities in people's concerns, overshadowing the climate crisis [85].

It is very complex to find a unique way to measure and assess these negative effects.
In the same way it is difficult to identify a proper classification of the damages according to specific macro classes.
From this perspective, researchers and scientists, led by J. Rockström, developed the concept of planetary boundaries [123].
The nine planetary boundaries (Fig.1.2) define the environmental limits within which humanity can safely operate and thrive. Each boundary represents a sphere of the Earth's system affected by the human activity. Within every sector are settled thresholds under which humankind can develop in harmony with natural dynamics. If the human pressure overcomes these thresholds means that the anthropic action is too high, producing irreversible changes and degradation of the quality of that boundary.

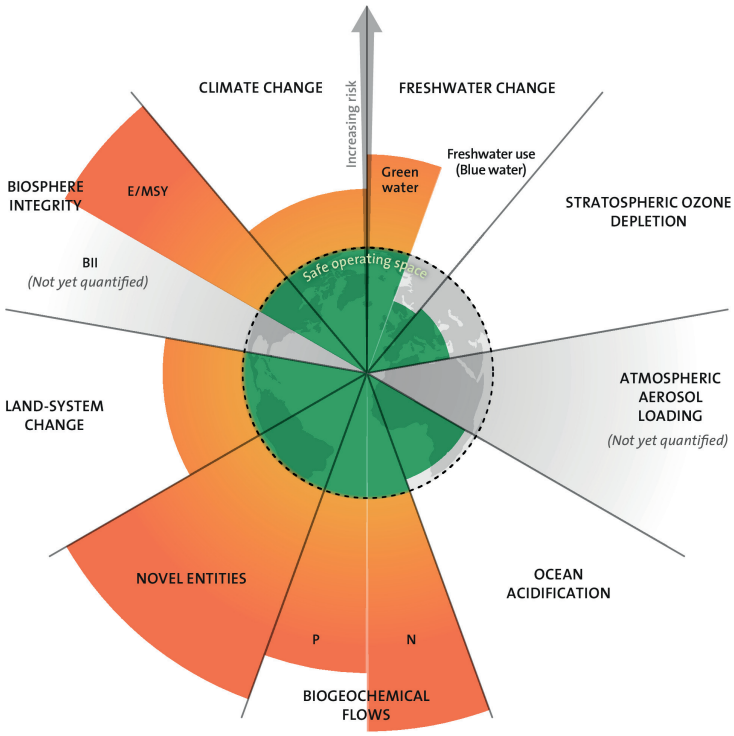

Figure 1.2: Planetary boundaries updated to 2022 [123].

As can be seen from the Fig.1.2, more than half of the boundaries safety thresholds have been already overtaken today.
Among them, we can identify the main boundaries which can be influenced directly and indirectly by the application of microalgae, the topic of the present work.
Indeed, biogeochemical flows, climate change and ocean acidification boundaries can theoretically benefit from the widespread usage of microalgae-based technologies.

Besides, the urgency to change the progress paradigm has brought to the concept of sustainable development.
The first mention of sustainable development was made in 1987 in the Brundtland Report, later institutionalized in 1992 during the Earth Summit in Rio de Janeiro.
The sustainable development concept can be divided into three different domains: the environmental, the economic, and the societal domain. Focusing on the environmental level, sustainable development drives a rational exploitation of natural resources, preventing their degradation and granting their exploitation by future generations.

Similarly, the exploitation of microalgae-based technologies can be part of the tools for achieving the 17 Sustainable Development Goals set in the UN Agenda 2030 roadmap [74].
Potentially, this kind of solution can improve all the SDGs performances, but particularly

interesting is the focus on goals n.6 (clean water and sanitation), n.7 (affordable and clean energy), n.12 (resource recovery) and n.13 (climate action to tackle global warming).

1.1. Thesis aim

The present work sets multiple objectives. The first is to provide a general overview of the current microalgae cultivation processes and uses. Then, various growth models are shown concerning the development of consortia of microalgae-bacteria and pure culture of microalgae. In particular, the last one is the main object of investigation in the experimental work done. Indeed, the most relevant goal is the calibration of three parameters included in the microalgal model developed by Viruela et al., 2021 relative to the microalgal growth rate and the free proton concentration.

Additional objectives set forth in this work are the following ones.

- Understanding and selecting the most suitable growth medium for the development of microalgae in photobioreactors, choosing between a synthetic medium and one derived from the liquid fraction of anaerobic digestate.
- Monitoring the biological composition that develops in the culture as operational parameters vary.
- Studying the response of algal growth to changing growth conditions through batch testing.
- Validation of the results obtained through both qualitative and quantitative methods, including the use of statistical techniques. Finally, a critical analysis of the validation results.

2 | State of the art

The life mechanisms of microalgae and their applications are still being researched by the scientific community today. A major focus of research is the modeling of the biological processes characterizing microalgae and microalgae-bacteria consortia. The following chapters will discuss the main biological characteristics of these phototrophic organisms, the factors influencing their survival and their most widespread applications. Finally, the main simulation models of algal-bacterial consortia as well as the reference algal model of this thesis work are explained.

2.1. Microalgae

The definition of microalgae includes a wide range of different organisms, living both in freshwater and marine ecosystems. They can be characterized by their chemical synthesis route of useful molecules, recognizing heterotrophic, autotrophic photosynthetic and mixotrophic organisms. The greatest part of microalgae are photoautotrophic organisms, since they adopt as carbon source inorganic carbon (primarily CO_2) and as energy source the light irradiance, producing oxygen and glucose. Conversely, heterotrophic algae can use organic carbon as substrate and energy sources. Finally, mixotrophic metabolism develops by exploiting organic carbon and the photosynthesis process. Mixotrophy combines both autotrophic and heterotrophic metabolisms depending on the environmental conditions such as light and substrate availability [76]. Thanks to this property, microalgae growing in mixotrophic mode are less sensitive to photo-inhibition, leading to higher biomass production [128].

These organisms show a cellular structure very diversified, ranging from unicellular to multi-cellular. Similarly, the disposition of the cells can vary, forming single-cell organisms or organized in groups or chains creating colonies and filamentous formations, as in symbiosis with other organisms, primarily bacteria. This last scenario has sparked interest in microalgae applications to wastewater treatments in the last years, developing a great number of growth-kinetic models of bacteria-microalgae consortia.

As suggested by the name itself, the microalgae size is very limited, usually between a

few micrometers to a hundred micrometers. However, under certain conditions, it is easy to observe the occurrence of algae agglomeration into flocs clearly visible. Normally this event happens in adverse growth conditions. Indeed, for what resulted during the experimental activity, floc formation is mainly due to cyanobacteria presence. These organisms occurred when the culture had not been purged regularly or when was necessary a temporary change of the feeding medium. Consequently, the prevention of floc formation is associated with selecting the most appropriate biomass retention time and feeding a medium showing a constant chemical composition in the time.
Taxonomically, the most common way to classify microalgae is based on their prevalent color, so by their light-harvesting photosynthetic pigment. In this way, they can be recognized in ten main groups: green algae (*Chlorophyceae*), greenish-blue algae (*Cyanophyceae*), brown algae (*Phaeophyceae*), diatoms (*Bacillariophyceae*), Eustigmatophyceae, dinoflagellates (*Dinophyceae*), golden algae (*Chrysophyceae*), Prasinophyceae, red algae
(*Rhodophyceae*) and yellow-green (*Xanthophyceae*) [124]. The most relevant group is represented by the green one, characterized by pigments of *chlorophyll-a* and *chlorophyll-b*.

In the present work, the presence of mainly four types of autotrophic organisms has been observed: Chlorella sp.; Scenedesmus sp.; seldom Bacillariophyceae (diatoms) and Cyanophyceae (cyanobacteria). Generally speaking, cyanobacteria are assimilated to microalgae even if this definition may be misleading. Indeed, this kind of organisms exploits light as an energy source through a photosynthetic process (autotrophic) but they present a cellular structure proper of a prokaryotic system. In the present work with the term microalgae, we assume to include also cyanobacteria. Chlorella is characterized by a simple spherical shape. Scenedesmus is typically present grouped in colonies (coenobium) of four or eight units and they can be easily recognized by the spines structure on the edges. Cyanobacteria will be focused on later. An overview of the mentioned algal strains is shown in Fig.2.1.

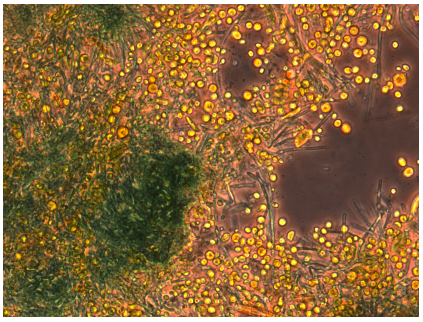

(a) Chlorella sp., 40X.

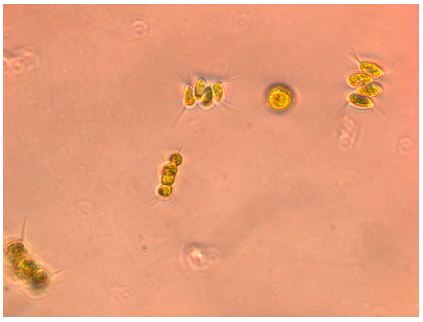

(b) Scenedesmus sp., 40X.

(c) Filamentous cyanobacteria with algae floc, 10X.

(d) Diatomea, 100X.

Figure 2.1: Main typologies of algae observed in the culture. Images obtained by fluorescence Leica DM2500 microscope.

2.1.1. Chemical composition

Microalgae are organisms based on an elemental chemical composition that varies depending on the strain and the environmental conditions. They are basically constituted of C, H, N, O and P, with variable ratios.
The uptake of minerals and micronutrients (calcium, magnesium, potassium, sodium, sulfur, copper, iron, manganese, selenium, zinc) is an important factor for effective growth. However, the mineral composition of microalgae biomass has not been deeply studied because of a lower commercial potential of biomass inorganic fraction compared to the organic one [107]. For a more complete explanation of current commercial uses of microalgae biomass see chapter 2.1.5.
Biochemically microalgae are not complex organisms and they are basically structured of macromolecules: proteins, lipids and carbohydrates [91]. Starting from these macromolecules it is possible to extract useful building blocks and chemicals with added value, as well as exploit the substances produced by the algae themselves like pigments and other growth by-products, as explained later in chapter 2.1.5. In Tab.2.1 the chemical

compositions of the main algae strains are reported.

Table 2.1: General chemical composition of different microalgae species [115].

Biomass	Carbohydrates	Proteins	Lipids	References
Chlorella vulgaris	20.99	15.67	41. 51	Wang et al. (2013)
Spirulina platensis	30.21	13.30	48.36	Jena et al. (2011)
Chlorella sorokiniana	35.67	9.90	18.81	Chen et al. (2014b)
Nannochloropsis oceanica	22.70	24.80	19.10	Cheng et al. (2014)
Scenedesmus obliquus	13.41	4.66	30.38	Chen et al. (2014c)
Dunaliella tertiolecta	21.69	2.87	61.32	Shuping et al. (2010)
Dunaliella salina	32.00	57.00	9.00	Castrillón et al. (2013)
Scenedesmus dimorphus	21 - 52	8 – 18	16 - 40	Castrillón et al. (2013)
Chlorococum humicola	32.50	-	-	Harun and Danquah (2011a)
Chlamydomonas reinhardtii	22.60	64.70	12.60	Mahdy et al. (2014)
Spirogyra sp.	33 - 64	6 - 20	11 - 21	Milano et al. (2016)
Porphyridiumcruentum	40 - 57	28 - 39	9 - 14	Milano et al. (2016)
Dunaliella salina	85.58	8.46	11.47	Pirwitz et al. (2016)

2.1.2. Metabolism

Microalgae metabolism is fundamentally based on three factors: the photosynthesis process (energy conversion), nitrogen and phosphorus assimilation, and micronutrient assimilation. In the present study, the latter is assumed to be always verified thanks to the abundant concentration of inorganic compounds in growth medium and wastewater.

Photosynthesis

Sunlight energy must be converted into useful chemical molecules in microalgae cells and photosynthesis is the process appointed to this function. Overall, photosynthesis transforms water and carbon dioxide driven by photon energy into new organic biological matter and oxygen.

Photosynthesis can be divided into two parts. The first one is dependent on the light availability in the thylakoid membranes of algae cells [61] and it is composed of a series of reactions that convert light energy to chemical one in form of adenosine triphosphate (ATP). Within this stage five main steps are recognized: light harvesting using ad-hoc antennae, photosystem II (PS II), photosystem I (PS I), cytochrome b_6f, and ATP synthase [9]. The light-harvesting antennae are pigments consisting of proteins placed in two receptors called light-harvesting complexes LHC I and LHC II, associated respectively with PS I and PS II. LHCs are made of Chlorophyll a (Chl a), Chlorophyll b (Chl b), and carotenoids [61]. Not all the photon energy can be adsorbed by the algae cells. Indeed, photosynthetically active radiation (PAR) is the only fraction of the spectral range of

solar radiation that photosynthetic organisms can exploit. PAR is defined as the interval of the solar spectrum between 400 and 700 nanometers. All the photons characterized by a lower wavelength expose the cell tissues to damage and, at the same time, higher wavelength photons do not carry enough energy to start the photosynthetic process.
Photosystems II and I are complex systems in which light is received by LHC chlorophyll respectively with a wavelength of 680 (P_{680}) and 700 (P_{700}) nanometers. The first system to be activated is PS II when exposed to PAR at 680 nanometers starting in this way a series of oxidation–reduction reactions. Without going into details, P_{680} is oxidized allowing an electron transfer process between different molecules. Among them, the most relevant ones are plastoquinone Q_B, plastoquinone Q_A, and cytochrome b_6f complex. Simultaneously light is adsorbed by LHC I in PS I at a wavelength of 700 nanometers, creating similarly an electron transport chain in which the most relevant step is the reduction of $NADP^+$ to NADPH by net oxidation of an electron donor (water to oxygen). The removal of protons from the stroma medium contributes to the formation of an electrochemical gradient across the thylakoid membrane [122].
Overall, the electron transport reactions including both PS II and PS I proceed energetically from a lower to a higher redox potential [110], generating across the thylakoid membrane the electrochemical gradient of H^+. The energy from this gradient allows the formation of ATP, the actual chemical energy carrier together with NADPH, thanks to a process defined as photophosphorylation. This process can take place according to two different pathways, non-cyclic and cyclic electron transport.
Cyclic phosphorylation consists of only PS I while the non-cyclic one involves in series both PS II and PS I. In this case, there is the production of NADPH as well as ATP, otherwise only NADPH formation by cyclic phosphorylation occurs. Generally speaking, photosynthesis and phosphorylation are considered in relation to non-cyclic electron transport chain.
Globally, light-phase photosynthesis ends up with the production of the energy chemical compound ATP and a reducing agent NADPH. These molecules are then exploited in the second photosynthesis phase, the so-called dark phase, or Calvin cycle.
In the Calvin cycle, the synthesis of new organic matter is performed starting from the fixation of carbon dioxide, according to the general expression here reported.

$$CO_2 + 4H^+ + 4e^- \xrightarrow{2\,NADPH+3ATP} (CH_2O) + H_2O$$

As mentioned, this series of reactions is not driven by the presence of light, and four main steps enclosed in the cycle are defined: carboxylation, reduction, production, and

regeneration phases [61]. Carboxylation defines the assimilation of carbon dioxide to a five-carbon compound, ribulose 1,5-bisphosphate (RuBP). This reaction leads to the formation of a molecule called 3-phosphoglycerate (PGA) using a specific enzyme, RuBisCo. Subsequently, the reduction of PGA by NADPH which acts like an electron donor, is driven by the energy supplied by ATP. Finally, in the last step of the cycle, RuBP is regenerated using the ATP energy producing different primary end-products, like simple glucids, amino acids and various organic acids [61]. Glucose molecules are also synthesized starting from one glyceraldehyde 3-phosphate (G3P) that is produced by three rounds of the cycle, fixing 3 molecules of carbon dioxide.
As seen, photosynthesis is based on a very complex series of reactions, and considering both light-dependent and light-independent steps, it can be summarized as:

$$H_2O + CO_2 + \text{photons} \rightarrow {}^{1}/_{6}\,(C_6H_{12}O_6) + O_2$$

Eventually, starting from the availability of light energy, carbon dioxide and water, are produced glucose as an energy source for cellular growth and oxygen.

2.1.3. Growth factors

Microalgae growth is very complex and depends on several parameters. The most common trend of growth and decay of a microalgal culture is shown below in Fig.2.2.

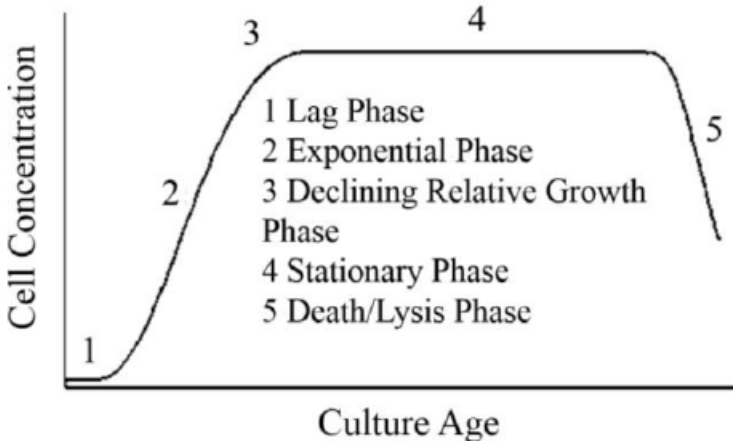

Figure 2.2: General trend of growth and decay of a microalgae culture over the time [35].

As can be seen, four main steps are distinguished. The development begins following an exponential trend (1-3), then it gets stationary (4) and eventually decreases due to lysis

phenomena (5). In order to maintain an optimal environment and a constant concentration of microalgae in the bioreactor is important to properly set up the main factors affecting the microalgae growth.
Nutrient availability in the growth medium is a fundamental factor to consider. The main macronutrients useful for algal metabolism are nitrogen and phosphorus.

Nitrogen

In order to allow the synthesis of necessary proteins, nitrogen is a fundamental element. Indeed, it is the main component of amino acids, which are the building blocks forming proteins and also it is the basis of nucleobases composing DNA and RNA. Nitrogen uptake can occur starting from different compounds, according to the type of N available in the growth medium and its oxidation state. Thus, N-assimilation can be operated from inorganic compounds like ammonium NH_4^+, nitrite NO_2^- and nitrate NO_3^-, or organic ones, like urea. The preferential way to assimilate nitrogen is from ammonium because most effective in terms of energy [13] [33]. Indeed, the other inorganic compounds, nitrite and nitrate, must be reduced intracellularly [43] before forming amino acids, while ammonium can be exploited directly in amino acid formation. Reduction is driven by specific enzymes in the chloroplast [23] [33] using as electron donor NADPH formed by photosynthesis. Organic nitrogen, primarily urea, can not be exploited immediately but only after that it is decomposed into ammonia and ammonium in the cellular cytoplasm. In nitrogen depletion conditions phenomenons that bring to the formation of triglycerides and starch in different proportions occur, depending on the environmental growth conditions [79]. This aspect can bring to interesting applications of microalgae in the production of chemical compounds. Moreover, nitrogen scarcity causes a decrease in microalgae growth and at the same time an increase in lipid productivity [114]. Normally the limiting growth nutrient is phosphorus, while it has been observed that nitrogen in excessive concentration, especially in the form of nitrite, can result as toxic, inhibiting the microalgae activity [131] [10].

Phosphorus

Phosphorus is another essential nutrient for microalgae to thrive. It is involved in several metabolic processes and it can be found in various molecules such as nucleic acids, phospholipids and ATP. Inside a single cell, the phosphorus content in percentage of dry weight can achieve 1% but in specific conditions up to 3%. This case is defined as "luxury uptake" and occurs when the phosphorus concentration in the growth medium is particularly high. In such conditions, microalgae cell adsorbs phosphorus in excess storing it

in the form of polyphosphate which can be exploited when the extracellular one becomes a limiting factor for the growth [89]. In the present work, the algae cultivation has been performed under P-replete conditions, meaning a phosphate content in the medium that never drops below 0.5 g_P/m^3 [117].
Phosphorus is present in the liquid phase in organic or inorganic form and under certain conditions tends to show precipitation reactions with other ions.
As inorganic P, the main forms depend on the medium pH and usually are $H_2PO_4^-$, HPO_4^{2-} and PO_4^{3-}. The greatest part of microalgae strains prefer to use inorganic phosphorus, especially as $H_2PO_4^-$ and HPO_4^{2-}, because they are in general the most bioavailable forms of P.
In the biological cycle of algae, inorganic phosphorus present in the liquid phase, assumed to be orthophosphate [117], can increase in concentration due to microalgae lysis and the lysis of the polyphosphate stored in the intracellular vacuoles. At the same time it is consumed and reduced by the microalgae metabolic growth and by the storage in case of luxury uptake conditions (excess of P in the feeding). As it will be explained later, in the present work, not all the dynamics previously mentioned are considered and some simplifications have been applied for complexity reasons.

In addition to nutrient uptake previously reported, other factors affect microalgal development. Among them, we can recognize the medium pH, total inorganic carbon (TIC), light intensity, dissolved oxygen (DO), temperature, and mixing.
In the next paragraphs is explained how each factor affects the development of microalgae, while the selection of the most appropriate value for each one is described in the experimental design section.

pH

The pH of the liquid solution is a relevant parameter to set up in order to guarantee a fast and constant development of the biomass.
The pH value influences several aspects of microalgae cultivation such as the carbon dioxide solubility and availability in the solution, the chemical form of nutrients and it affects significantly the microalgae metabolism [20]. The pH varies during microalgae growth and it tends to increase up to values of 9 or more due to autotrophic organisms' metabolism [39] [45] [78].
Indeed, in the dark phase of photosynthesis (Calvin cycle) carbon dioxide is adsorbed by microalgae cells in the carboxylation phase by means of RuBisCo enzyme, so its concentration in the aquatic environment decreases and subsequently the pH increases. Moreover,

in the presence of significant nitrate NO_3^- concentration, microalgae can assimilate it and increase the pH as well. The consequence of the reduction of nitrate to molecular nitrogen is the release in the liquid solution of the excess OH^- ions that tend to raise the pH. It must be highlighted that in the present thesis, the denitrification phenomenon never occurred. As a matter of fact, as explained later in the growth medium selection section, an addition to the feeding of allylthiourea is always operated, whose function is to inhibit the ammonia-oxidizing bacteria (AOB). In this way, there is no production of nitrite NO_2^- which is the one oxidized to nitrate in nitrification, and eventually, any denitrification process occurs. Moreover, high levels of COD have not been measured in the medium, so the denitrification process can not take place.
It has been observed that once high pH values are reached, the CO_2 availability in the liquid environment becomes critical. The consequence is the inhibition of the photosynthetic activity of the biomass and a slight slowdown of the cell growth [20] [130].
The pH level also influences the appearance of external organisms which can represent a threat to microalgae survival [16]. The main ones are cyanobacteria and microzooplanktonic grazers like rotifers (Fig.2.3). In the present work, these kinds of organisms have been observed only in the experimental phase concerning the modeling of cyanobacteria-microalgae culture.

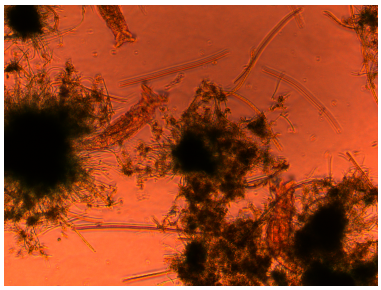

(a) Rotifer Philodinidae, 10X.

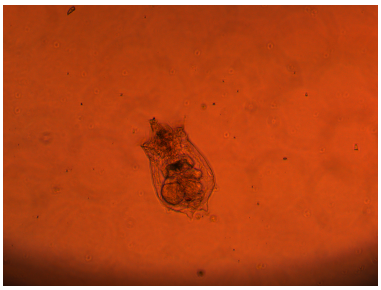

(b) Rotifer Euchlanis, 10X.

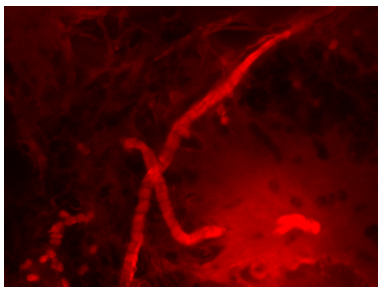

(c) Cyanobacteria, 63X.

Figure 2.3: Invading organisms observed in the culture in different environmental conditions. Images obtained by fluorescence Leica DM2500 microscope.

pH seems to influence also the chemical composition of microalgae cells, thus the potentially profitable chemicals obtainable from them. Indeed, pH around 6 seems to be more beneficial for biomass growth and lipid accumulation, while at higher pH the biomass shows a greater protein content with a lower C/N ratio [80].

Eventually, pH is a key-factor for microalgae growth and for the correct operation of the cultivation. To be noted, in the present work it is assumed that the pH value of the medium is ideally an average pH constant in all the photobioreactor volume.

For most of the microalgae strains of interest, mainly Chlorella and Scenedesmus genera, the growth is optimal in a pH range of 7.0-8.0. The exception is represented by cyanobacteria which show a good development at higher pH values, between 8.0-9.0 [25] [90]. Other studies show that for growing up Scenedesmus can fit in medium with a larger pH range, from 7.0 to 9.0 [15].
At the same time, productivity can vary within the mentioned ranges. For instance, it has been demonstrated that Chlorella productivity decreases by 22% at very basic values 8-9.1 [34] and also that photosynthetic yield worsens at higher values than the optimal ones [25].
Moreover, different microalgae studies set up pH values to perform their analysis in different scenarios, similarly to what is done in the present one. In this way, three scenarios at 7.0, 8.0 and 9.0 have been selected by Rossi et al., 2020 [88] as at 8.5 as reference value in Rossi et al., 2020 [87]. Another study concerning Chlorella cultivation performed by Renhe Qiu et al. set up five different pH levels (6.5, 7, 7.5, 8 and 8.5) [80]. As stated in the research conducted by Bartley et al., 2014, related to microalgae growth and invading organisms presence in function of the pH, pH values of 8 to 9 help to increase algae production and at the same time to minimize the presence of invading organisms such as microzooplanktonic grazers [16].

Light intensity

Light intensity is a key operating parameter to set up. Irradiance is measured as photosynthetically active radiation (PAR) which provides energy for the light reactions in the photosynthesis process and comprises wavelengths in the range of 400 - 700 nm.
Photosynthetic activity is proportional to light intensity but it shows an upper limit beyond which inhibition phenomenon occurs. This point is defined as light saturation point [86] and for irradiance levels above it the light-harvesting complexes (LHCs) can be

damaged, leading to a photoinhibition process. Practically, it results in the inhibition of photosynthesis and consequently a reduction in photosynthetic efficiency and microalgae development [70] [73]. Photoinhibition leads to photooxidative cellular stress and it is caused by a long period of exposure to light at high intensity, generating reactive oxygen species (ROS) able to damage cellular components [108].
The intensity and the type of light affect the growth rate as well as the microalgae composition. Moreover, not all microalgae strains contain the same type of pigment, so each strain can only exploit a certain wavelength of PAR. In addition to the light saturation point, the existence of a lower threshold under which LHC does not catch the photon energy properly has been reported. Below this level, the light energy is partially dissipated in the form of heat [50] without being exploited for cell growth.
The figure below (Fig.2.4) shows a general light-response curve that describes the relationship between light irradiance and photosynthetic activity.

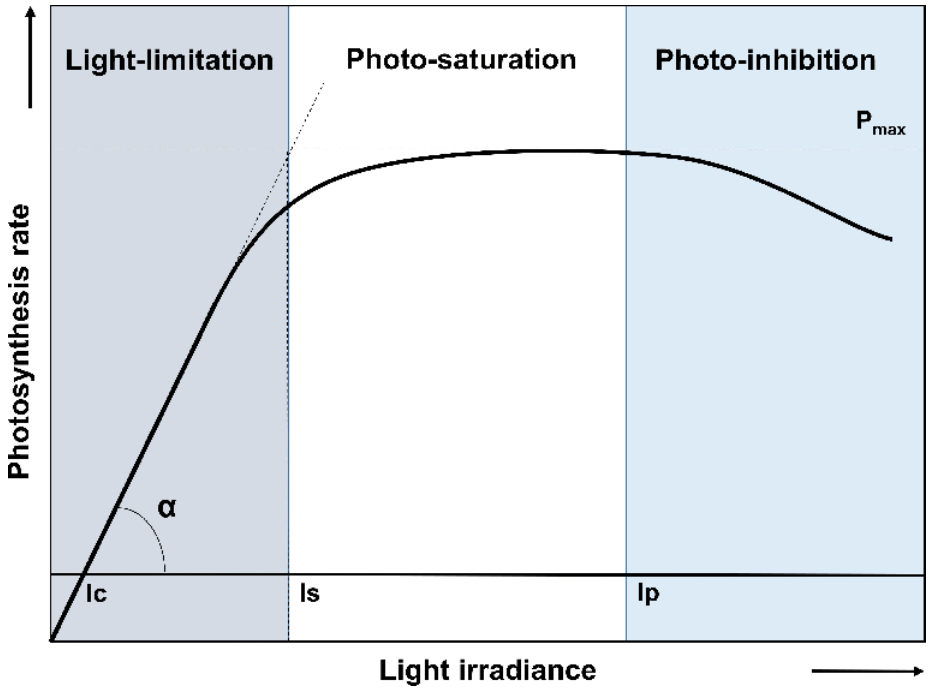

Figure 2.4: Example of light-response curve showing the relationship between photosynthetic activity and light irradiance [38]. α: curve slope representing the max light conversion efficiency; Pmax: maximal rate of photosynthesis; Ic: compensation irradiance (oxygen balance between photosynthesis and respiration); Is: saturation irradiance; Ip: photoinhibition irradiance

.

As it is visible, three zones are defined and an optimal interval of light intensity can be recognized. Low irradiance corresponds to a linear increase in the photosynthetic rate

according to a slope factor α, the ratio between photosynthesis rate and light irradiance. This area is light-limited and, for further increase of light irradiance, the linearity is gradually lost and α decreases. At higher irradiances, a photo-saturation area is defined. Here photosynthesis rate reaches a plateau equivalent to the maximal rate of photosynthesis. The last zone recognizable is the photo-inhibition one. Increasing the light irradiance beyond the saturation point causes a decline in the photosynthetic rate, eventually damaging the photosynthetic apparatus. The excess of the photon's energy is lost as heat, in the so-called non-photochemical quenching (NPQ) mechanism.
Overall, the photosynthesis rate is proportional to the microalgae growth rate, thus, it is clear that a proper selection of light intensity is a key factor in establishing the fastest and most reliable conditions for biomass development.
The biomass concentration in the reactor strongly affects the light availability for the cells located in the center of the reactor, far away from the reactor's edge. Indeed, light is adsorbed by the microalgae closer to the external wall and a self-shadowing effect among them is also generated, preventing the light from reaching the space in the middle of the reactor volume.
The light source can be both natural or artificial, by means of LED tubes. The intensity of artificial light can be regulated through the number of lamps switched on or moving closer/farther the lamp itself to the reactor.

Overall, light attenuation within the system is strongly affected by the reactor radial depth, the sunlight or lamp intensity, biomass concentration, and microalgae strain harvesting pigment [2] [50] [126]. On the other hand, microalgae close to the irradiated surface are more sensitive to high levels of irradiance, thus it is easier that they are affected by the photoinhibition phenomenon due to light levels greater than the saturation point [77]. Eventually, it is fundamental to guarantee a good mixing of the culture into the reactor in order to achieve a mean irradiance value within it, overcoming the possible generation of dark and high-irradiated zones.

Temperature

The aqueous medium temperature is a relevant characteristic that affects the biokinetics of all the microorganisms. Indeed, it influences both photoautotrophic activity and endogenous respiration. Moreover, it regulates also the chemical equilibria and the gas solubility [100].

There is not one specific range of temperature to enhance microalgal growth. Indeed, each microalgae strain is characterized by an optimal interval of temperature [18]. The growth and temperature dynamics show a trend similar to the one between the growth itself and the light intensity previously explained. In fact, two thresholds can be identified, one upper and one lower. Without going into details, temperatures below the lower value do not allow an appropriate rate of the enzymatic processes in the cells, while levels above the upper value can cause protein degradation [81] [84] [27].
A study demonstrated that for a great number of species, the suitable interval of temperature for proper development can range between 16°C and 27°C [62]. In the study, it has been reported that at a temperature lower than 16°C the growth kinetic is strongly slowed down while at temperatures above 35°C the majority of microalgal strains died.
To be more focused on the microalgal species involved in the present work, another research compared the temperature ranges suitable for the growth of Chlorella sp. and Scenedesmus sp. The first type resulted to be better tolerant to elevated temperatures [46].
In general, the optimal temperature to achieve the maximum growth for both species has been identified at around 30°C [21] [129]. Another study suggested that Chlorella sp. shows a decrease of 17% in growth rate at 35°C compared to 30°C and even at temperatures above 38°C the biomass tends to die sharply [24]. Similarly, it has been highlighted that for Scendesmus sp. growth favorable interval of temperature is between 20-40°C [106].

The present research has been carried out at a constant temperature of 25°C through the adoption of a thermostatic chamber that maintained the temperature constant in the bioreactors throughout the experimental period.

Total inorganic carbon

Carbon is the fundamental element constituting the cell biomass since it represents more than 65% of biomass dry mass weight.
In the photosynthesis process, inorganic carbon is assimilated by the microalgae and transformed into organic carbon, constituting new biomass.
With the term total inorganic carbon, the sum of carbon dioxide CO_2, bicarbonate HCO_3- and carbonate $CO_3{}^{2-}$ is conventionally defined. However, microalgae are able to assimilate only inorganic carbon in an aqueous medium as carbon dioxide and bicarbonate [66][90]. Moreover, the tendency to use one form in place of the other depends on the microalgae strain.
The proportion in the aqueous solution between the three carbon compounds is strongly

influenced by the pH value. At alkaline pH, HCO_3- and CO_3^{2-} are the predominant forms while dissolved CO_2 concentration is negligible [66] because of the pH-dependant equilibrium of inorganic carbon within aqueous solutions. For instance, it has been observed that a shift from 8.2 to 7.5 resulted in a fifty times increase in dissolved CO_2 [67] because of the carbon equilibrium. Indeed, at lower pH, the prevalent chemical form of inorganic carbon is represented by free CO_2. On the other hand, at pH around 8, it has been reported that some type of microalgae prefers to uptake bicarbonate rather than carbon dioxide [63].
The control of pH in bioreactors requires the addition of carbon dioxide or bicarbonate to balance the natural increase of pH due to photosynthetic activity. Moreover, in this way, inorganic carbon is supplied favoring the microalgae productivity.
Nevertheless, it must be noted that between the two acidification ways, the CO_2 injection is poorly applicable for large-scale commercial ponds due to the high cost and the low transfer efficiency [59]. On the opposite, bicarbonate shows a better commercially viable means of pH modulation and it is a provider of inorganic carbon. So far, it has been studied that through a bicarbonate feeding system, the microalgae optimal growth kinetics are comparable to the conventional ones with carbon dioxide systems [5].

Dissolved oxygen

Dissolved oxygen (DO) is a parameter that must be kept monitored during microalgal growth. Indeed, it is a variable that is directly indicative of the presence of good environmental conditions allowing biomass growth.
Microalgae consume the dissolved carbon dioxide during phototrophic growth and produce oxygen. The oxygen generated can easily reach high concentration values in the aqueous solution depending on certain conditions, such as the photobioreactor (PBR) geometry and the type of stirring. Under these circumstances, the global consequence is a decrease in biomass productivity because of the occurrence of different phenomena.
A good oxygen concentration in the solution should be at saturation level. It depends on multiple factors like temperature, pressure, and depth. In this study, the most important to be considered is the temperature. At 25°C, that is the reference temperature adopted in the work, dissolved oxygen concentration in balance with the atmospheric one is around 7.5±0.5 mg/l (oxygen saturation 100%)
Values of oxygen saturation higher than 100% can affect negatively the microalgal growth. For instance, it has been observed that an oxygen concentration of 30 mg/l (saturation more than 300%) leads to a decrease of 30% in biomass productivity of Chlorella vulgaris [55]. In addition, another study showed a loss of microalgal productivity in correspon-

dence to an oxygen saturation level of 250% in the solution [82].

Generally speaking, at high levels of dissolved oxygen three main processes have been reported: photorespiration, Mehler reaction (water-water cycle), and photoinhibition.
The most critical are the first and the last ones. Photorespiration is a process depending on the light availability and related to the oxygenase reaction catalyzed by RuBisCo [55] and it brings to the consumption of oxygen generating CO_2 [69] resulting in a reduction in biomass yield [56].
The second process, photoinhibition, has been already focused on previously in the light intensity section 2.1.3.

The main good practice to be adopted in order to solve the accumulation of dissolved oxygen in the reactor is stripping the excess oxygen from the aqueous system in an effective way. Enhancing the oxygen stripping is doable through a good stirring of the solution, thus increasing the gas transfer efficiency to the atmosphere [55].
At the same time, it must be noted that there is the risk to strip other fundamental gases like carbon dioxide CO_2. For this reason, it is common to use CO_2 injection systems into the culture medium to maintain a sufficient inorganic carbon concentration.
Stirring methods based on airlift techniques seem to represent the best solution to ensure good mixing of the biomass and simultaneously maintain a liquid oxygen saturation balanced with the ambient air [55].

Mixing

Mixing is an important operational parameter and it affects positively microalgal growth in different ways. First of all, it homogenizes the medium culture avoiding the generation of hydraulic dead zones, and improves the nutrient availability for biomass.
Moreover, it is necessary to prevent biomass sedimentation [50] and to enhance the mass transfer between gas and liquid phases. An effective stirring also contributes to preventing photorespiration phenomena intensifying the stripping of the excess oxygen produced by photosynthesis [6] and guarantees a homogenous exposure to light [14].
The only factor that must be kept under control is the risk that excessive turbulence can cause hydrodynamic stress to microalgae.

The stirring of the culture can be carried out in a mechanical way or through air-lifting. Mechanical stirring results to provide a stronger mixing but at the same time it does not

enhance sufficient oxygen stripping leading to oxygen accumulation.

2.1.4. Cultivation methods

There are two main methods of microalgae cultivation: open cultivation and closed cultivation. Each one adopts different types of bioreactors.

Open systems

Open systems have been used to scale up microalgae cultivation from lab-scale cultivation to large-scale applications. Among the main advantages of an open cultivation system, there are minimal investment and low operative costs [71]. However, open systems are easily subjected to uncontrolled contamination and fluctuations of external environmental factors. For instance, contamination can be caused by bacterial loads from animal sources or microalgal grazers like rotifers. Biological contamination of the cultures is probably the main disadvantage for large-scale plants because it is almost unavoidable and it brings to slower growth rates and possibly to the crash of the biomass system [28] [120].
Adverse environmental conditions can be caused by the local weather and climate, and they influence mostly the light intensity and the evaporation rate. Finally, in open cultivations, the overall control of the operative growth parameters (temperature, light intensity, pH, DO, TIC) is more complex due to the larger areas to be monitored and uncontrollable phenomena such as evaporation and weather conditions.
Open systems are generally divided into two typologies, natural ponds such as lakes and lagoons, and artificial ponds (Fig.2.5). The most investigated one among the artificial types is for sure the high-rate algal pond (HRAP) configuration, known also as raceway pond (RW). This technique was the first one widely adopted for scaling up microalgae cultivation [54].
Despite the difficulties of properly setting up and regulating all the growth parameters, open systems have been proven to be suitable to treat wastewater and they are reliable for microalgae production and their by-products like lipids on industrial and commercial scale.

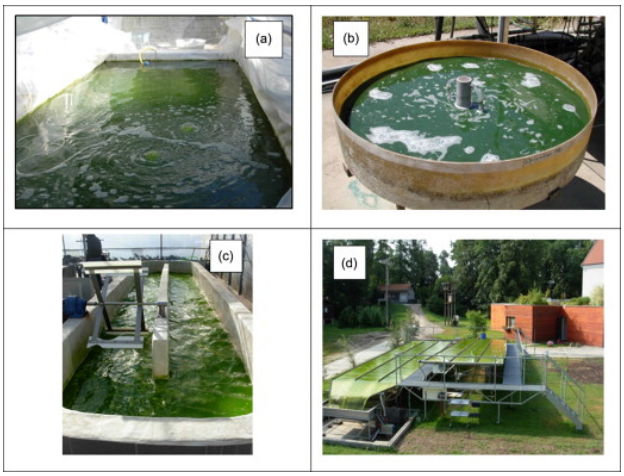

Figure 2.5: Examples of different configurations of open systems. (a) A walled pond lined with a plastic foil and mixed by air; (b) a circular pond; (c) a raceway pond with paddle-wheel mixer; (d) an inclined-surface system of sloping planes arranged in cascades [60].

Closed systems

Closed systems are generally defined as photobioreactors (PBRs) and they can be commonly adopted in lab-scale investigations where there is the necessity to set and maintain very specific parameter values. PBRs show more expensive installation and operative costs [22] and they are suitable for producing high-value products with better-controlled growth conditions. Moreover, they can be designed and set up focusing precisely on the concerning microalgal strain characteristics, allowing faster growth and achieving higher biomass concentrations.

The greatest advantages compared to open systems are the absence of external undesired sources of contamination and the relatively small space required for their installation. On the other hand, closed systems present some drawbacks like biological fouling on the reactor's wall, cleaning issues depending mainly on the reactor geometry, limited volumes, and possible accumulation of excess oxygen in case of ineffective stirring [36]. In Fig.2.6 the main closed systems are reported.

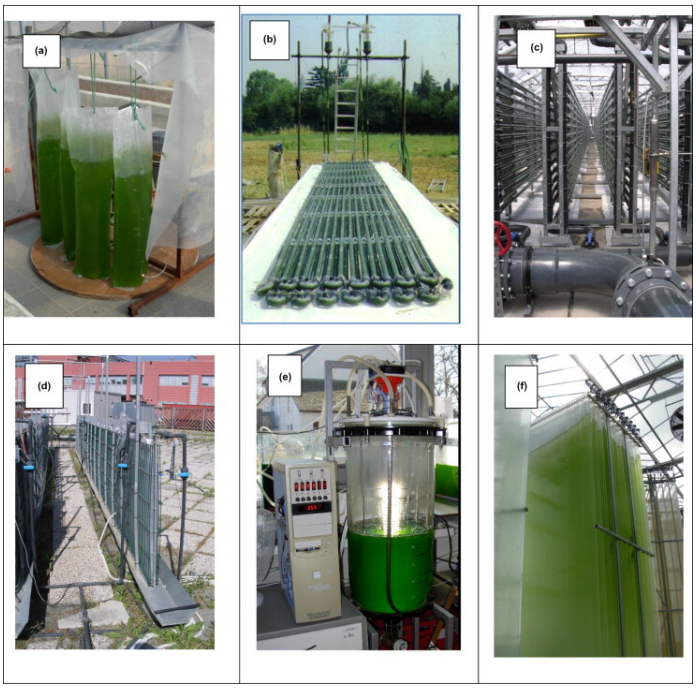

Figure 2.6: Examples of different configurations of closed systems. (a) Hanging plastic bags mixed by air; (b) a two-plane, horizontal tubular photobioreactor; (c) vertically stacked tubular photobioreactor mounted in a greenhouse; (d) a vertical flat-panel photobioreactor; (e) annular column photobioreactor consisting of two glass cylinders placed one inside the other to form the culture chamber; (f) flat-plate photobioreactor [60].

Two-stage hybrid systems

Two-stage hybrid systems have been studied recently and they aim to overcome the limits shown by the other microalgae production typologies. They resulted advantageous for microalgae cultivation since they allow to maintain separated biomass growth from the lipid accumulation phase [92] [104].

Basically, this method is based on two consecutive stages. The first one is the cultivation of the microalgae in a closed reactor like a PBR, followed by an open system. In the closed one, microalgae grow in an environment characterized by controlled parameters and conditions, thus achieving high biomass concentrations and reliable continuous production.

In the second stage, microalgae are cultivated for the intended application (like wastewater treatment and harvesting) in an open system working under nutrient stress. It has been demonstrated by a life cycle assessment study that hybrid systems are a promising technique that can reduce the overall environmental impact compared to the classical open and closed typologies alone [4]. From an economic point of view, hybrid systems are a good option too. They can provide a continuous microalgae inoculum to short-period batch open ponds preventing biological crashes compared to longer-term open systems

[51]. In Tab.2.2 the main features of each configuration previously mentioned are summarized.

Table 2.2: Summary of the advantages and disadvantages of the three main types of cultivation methods [71].

Factor	Photobioreactor	Raceway pond	Hybrid system
Space required	Moderate	High	High
Evaporation loss	Low	High	Moderate
CO_2 sparging efficiency	High	Low	Moderate
Maintenance	Difficult	Easy	Moderate
Contamination risk	Low	High	Low
Biomass quality	Reproducible	Variable	Reproducible
Energy input for mixing	High	Low	Moderate
Operation type	Batch	Batch	Continuous
Setup cost	High	Low	Moderate
Maintaining continuous exponential phase	Difficult	Difficult	Easy

(Borowitzka, 1999; Barbosa et al., 2003; Moheimani and Borowitzka, 2006; Chisti, 2007; Huntley and Redalje, 2007; Eriksen, 2008; Ugwu et al., 2008; Brennan and Owende, 2010; Harun et al., 2010; Mata et al., 2010).

2.1.5. Current uses and perspectives

Microalgae are organisms that show different commercial purposes. They can be harvested and then exploited in a wide range of applications. Below the main application fields of microalgae biomass besides wastewater application are reported.

Human consumption

The food market is recently opening to new alternative products according to a more sustainable vision. Microalgae-based products have been already proven to be a valid solution thanks to their nutritional properties. Indeed, microalgae represent a rich source of nutrients like carbohydrates, proteins, vitamins, minerals, and fibers. Moreover, specific strains can be used for the extraction of natural edible dyes such as carotene [83].
The main species cultivated for nutritional purposes are Spirulina Platensis, a strain of cyanobacteria, and Chlorella, green algae. In particular, the first one shows a dry weight composition with a protein content reaching 60% (51–71%) and about 15-25% of carbohydrates [119]. Normally, microalgae-based products are composed of biomass powder or in the form of tablets for nutritive supplements.

Cosmetic and pharmaceutical

The cosmetic and pharmaceutical sectors can take advantage of the chemicals developed by microalgae during their growth replacing conventional substances whose synthesis is

environmentally unfriendly. This is a way through which green chemistry can help to make the production of goods in the cosmetic and pharmaceutical industries safer and less impactful.
During their development microalgae produce a lot of useful and essential bioactive primary and secondary metabolites through the photosynthesis process. These metabolites represent a valid alternative for the compounds of interest in the pharmaceutical industry. Some specific uses of microalgal metabolites are for instance as thickening agents, water-binding agents, and antioxidants. Among the most relevant bioactive compounds are proteins, carbohydrates, vitamins, pigments, minerals, polysaccharides, exopolysaccharides, and essential oils. In cosmetic formulations, typical applications take place in anti-aging, sunscreen, and skin whitening [134]. However, it is still necessary to investigate the harvesting process and components extraction in order to improve profitability and environmental friendliness [57].

Energy

In the last few years, the energy sector has faced several innovations in the pathway toward decarbonization. In this view, microalgae can find a valuable application in biofuel production thanks to their chemical composition. One type of biofuel obtainable from biomass is the biodiesel. It has been proven that not all the microalgal strains are suitable for this purpose but only the ones that show an elevated content of lipids like Chlorella and Scenedesmus sp. (in general around 30% d.w.) [37]. Without going into details, biodiesel can be produced by a transesterification process of the fat with methanol, producing fatty acid methyl ester (FAME) which is the main molecule of biodiesel. The initial lipidic material can be both the microalgae biomass or the essential oil extracted from it by the hydrocracking process. To exploit the biomass in the most efficient way it is usual to integrate lipid extraction with the processing of the remaining lipid-free material to obtain products rich in proteins [41].
Another option is the generation of biogas (a mixture of methane, carbon dioxide, hydrogen, and other gases) starting from the microalgae biomass valorized by anaerobic digestion. Moreover, another advantage is that the digestate generated by the anaerobic treatment is particularly rich in nutrients like nitrogen and phosphorus assimilated during the cell growth, opening interesting scenarios for the usage of this material in the agronomic field.
Research projects are also focusing on the generation from microalgae of valuable fuels, like the production of hydrocarbon or crude oil-like substances by gasification and pyrolysis techniques [105].

Nowadays, biofuels are mainly produced by biomass like corn, sunflower or palm. There are two main disadvantages, strictly connected, concerning these predominant cultures. The first one is the occupation of arable land. Indeed, in order to produce a profitable quantity of biofuel, it is necessary a certain amount of fresh raw material. This means a consumption of land for plant cultivation. Microalgae cultivation has been observed as the species less impactful and land-demanding. As it can be seen in the table below (Tab.2.3), the biodiesel yield and land occupation by the implementation of microalgae cultures is by far the most efficient solution.

Table 2.3: Comparison of the performances of different types of vegetable cultures [133].

Plant name	Lipid content (%)	Lipid yield (L/ha·year)	Land use (m^2 year/kg ·biodiesel)	Biodiesel yield (kg/ha·year)
Corn	44	172	66	152
Cannabis	33	363	31	321
Soybeans	18	636	18	562
Jatropha	28	741	15	656
Camelina	42	915	12	809
Canola	41	974	12	862
Sunflower	40	1,070	11	946
Castor	48	1,307	9	1,156
Palm	36	5,366	2	4,747
Microalgae (low lipid content)	30	58,700	0.2	51,927
Microalgae (medium lipid content)	50	97,800	0.1	86,515
Microalgae (high lipid content)	70	126,900	0.1	121,104

The second aspect to be considered is that the current main cultures for biofuel production are human food crops (corn, sunflower, palm). Thus, the production of biofuel from them presents the major drawback that they can not be harvested for food production, generating competition between biofuel-food crops.
In order not to enhance land consumption and not to interfere with the food sector, new alternatives for the production of biofuels are needed. Overall, microalgae culture is a very valid solution thanks to the limited demand for land and the fact that they do not affect the traditional agricultural market.

Fertilizers and aquaculture feeding

Nowadays, global human population growth leads to a greater need for food, thereby, to a higher demand for fertilizers and soil conditioners. The main fertilizers, nitrogen and phosphorus, show several issues. For instance, phosphorus has mainly mineral origin and nowadays it is extracted in politically unstable countries, like Russia, China, and Marocco.

On the environmental side, the problems caused by the usage of chemical fertilizers are arid soil, groundwater and surface water pollution, and eutrophication of areas.
In view of circularity, fertilizers must be replaced by biofertilizers, in order to increase crop yield while minimizing the agricultural environmental footprint. A contribution to this boost toward bio-based agricultural chemicals can be represented by microalgae, recovering the nutrients from secondary sources such as wastewater. Indeed, for the greatest part of microalgae strains, the assimilation of nitrogen and phosphorus from the aqueous medium in the biomass is operated, especially in luxury uptake conditions. In this sense, there are already studies concerning the exploitation of Chlorella sp. and Scenedesmus sp. [26]. Moreover, cyanobacteria (Spirulina) are studied as well, since they are able to fix atmospheric nitrogen and improve soil fertility [99].

In the aquaculture field, microalgae-based products are also an alternative to traditional animal feedings. In nature, the food chain of the aquatic environment is based on microalgae usage as the primary source of nutrients. The greatest part of invertebrates feeds on microalgae since they are utilized as live feed for bivalve mollusks, crustaceans, zooplankton, for early juvenile stages of abalone, and even for some fish species. Thus, the cultivation of microalgae along with mollusk and fish farming is an economically and environmentally effective solution. Below, a schematic representation summarizing the main applications of microalgae is reported(Fig.2.7).

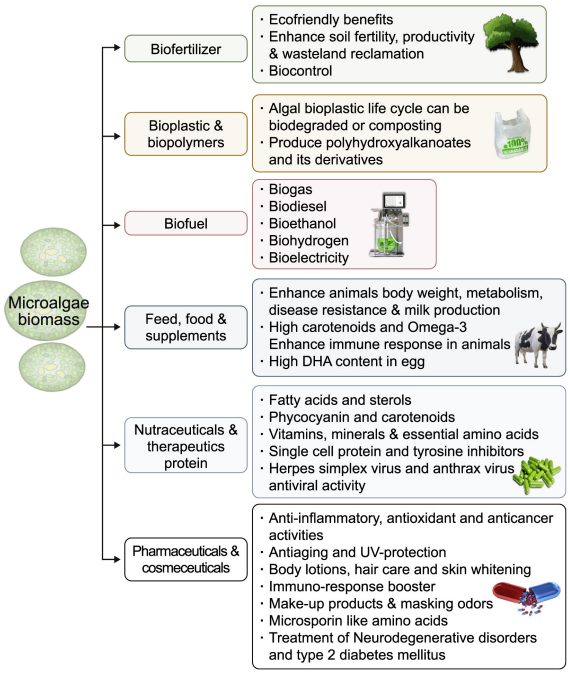

Figure 2.7: Wide schematic graphics of the general routes of microalgae applications after the harvesting phase [1].

2.2. Wastewater modeling

The wastewater sector is facing a fundamental shift toward a new paradigm in the perspective of the circular economy. In this sense, wastewater treatment plant acquires new functions, becoming a facility conceptually closer to a biorefinery. Moreover, the investments of the private sector are moving in this direction, demonstrating that is a profit-making route, as can be an example the innovative biorefinery project of GRUPPO CAP in Sesto San Giovanni, Milan, Italy. In this project, the construction of a wastewater sludge line treatment is planned. The fate of the sludge is divided into two routes. 75% of the total tons yearly produced are delivered to thermal recovery for district heating, while, at the same time, the rest is treated to produce fertilizer.

This new trend redefines traditional WWTPs as sustainable water resource recovery facilities (WRRFs) [93], which are plants able to remove water pollutants and, at the same time, recover nutrients and energy from the treatment products.

Microalgae application in wastewater treatment is a very valid option to integrate the conventional remediation goals of wastewater treatments with the innovative wide range of applications characteristic of a WRRF.

In recent years, wastewater scientific research has focused on modeling the dynamics of the processes involved within the conventional wastewater treatment plant, a necessary step in designing or revamping in the best way possible water resource recovery facilities. The modeling of the processes and of phenomena occurring in wastewater treatments are objects of investigation by several scientific groups and a great variety of models have been proposed so far.

The implementation of microalgae within a WRRF is still an object of study and the general idea is the creation of a stable and reliable biological ecosystem constituted by consortia of bacteria and microalgae. However, the modeling of the co-existence of the two kinds of microorganisms is very complex. Deeper in detail, models generally include biological processes by bacteria/microalgae activity and chemical/physical phenomena like precipitation. The ecological interactions that are established in consortia of microalgae and bacteria are highly dependent on the strains involved and do not always end up in a positive way. Moreover, the abiotic conditions of the growth environment deeply affect the development of the consortium and they must be taken into account as well [40].
A good model is supposed to provide a reliable prediction of the performance of the plant. The advantages of an effective model are the reduction of the costs of field tests and pilot plant operations, the assessment of the resource recovery, and the evaluation of the environmental and economic costs. In this sense, the most significant operative cost of a WWTP is associated with external aeration provided during the nitrification phase [3] [8] that can represent almost the 50% of the total costs of the plant operations. Thus, the exploitation of natural photosynthetic oxygenation by microalgal activity reduces the economic expenditure. Moreover, a model describing the action of bacteria interacting with microalgae can be interesting not only for wastewater treatment applications. Indeed, it can be useful to predict the algal behavior in microalgae cultivation in case of accidental or unavoidable contamination by bacteria in outdoor open systems.
In order to obtain a well-grounded model that integrates biochemistry dynamics along with chemical/physical processes, a well-done data collection is necessary, followed by a calibration and a validation of the results.
In the following paragraphs will be provided a general presentation of the modeling of bacteria-microalgae consortia and of microalgae pure culture, focusing deeper on the most recent models developed in CALAGUA group.

2.2.1. Bacteria-microalgae consortium

The integration of microalgae in the biological phase of wastewater treatment leads to a major modeling complexity in comparison to the traditional processes operated only by bacteria. Indeed, the establishment of new biological interactions and the dependence on external abiotic parameters like pH, temperature and light intensity, are very difficult to model for both biological communities. Moreover, simulation complexity also increases for other physical-chemical processes associated with pH variations, such as chemical equilibria or chemical precipitations.
It is recognized that the greatest challenge is represented by the lack of reliable microalgae models [97]. On the contrary, models dedicated only to bacteria are well consolidated and used, such as the Activated Sludge Models (ASMs) [48] and the Anaerobic Digestion Model (ADM) [17]. This is due to the diffuse utilization of bacteria on industrial-scale applications and, thus, the large availability of operational and experimental data. In this sense, a microalgae pure culture model [118] has been developing in the CALAGUA group and it will be described in the following chapter.

Generally speaking, a WRRF can be modeled according to two alternative philosophies. The first one is to aggregate different models relative to the single-unit processes present in the plant, while the second one is to generate a global model of the plant that considers all the processes occurring in it. CALAGUA investigation group has adopted this second approach.

In the last twenty years, several models have been proposed trying to describe the interactions occurring in consortia of bacteria and microalgae, the physical and chemical phenomena, and the influence of the abiotic parameters on the ecological community. A synthetic overview of the main well-established models is now presented.
The first effective model that describes the dynamics in a bacteria-microalgae consortium was developed in the early 2000s and it is the River Water Quality Model No. 1 (**RWQM1**) [96]. In this model, the main components are included such as carbon, nitrogen, and phosphorus (evaluated by chemical equilibrium) and the particulate organic matter sedimentation. RWQM1 was developed with the aim of assessing the water quality of rivers, however, it also demonstrated to fit well for the evaluation of wastewater treatment.
Another reference model is the **ASM-A** [127] built up as an extension of the ASM-2d [47]. This model was developed starting from a bacterial model, the Activate Sludge

Model, and it describes microalgae metabolism in waste stabilization ponds, high-rate algal ponds and closed photobioreactors. It comprises 6 processes and 11 components of interest among particulate and soluble ones. The major characteristic introduced in this model is that within the particulate fractions, the internal cell content of nitrogen and, especially, of phosphorus, stored in the form of polyphosphates, are considered. The model predicts microalgal growth, nutrient uptake removal, and storage. It is considered also the light dependence for the biomass using the Steele equation [102].
Thanks to the coupling of the RWQM1 with the modified ASM3 [52] the **BIO_ALGAE 2** model has been generated [101]. This model is quite complex since it includes 25 processes and 19 components. It describes the microalgal growth in waste stabilization ponds, high-rate algal ponds, and photobioreactors. The model also includes the influence on microalgal and bacterial communities of pH and temperature by means of pH and cardinal temperature sub-models. Furthermore, the effect of light intensity on photosynthesis for microalgae growth and photoinhibition phenomenon is taken into account using the dynamic model of Eilers and Peters [32]. Moreover, the model also includes an equation for pH control by on-demand injection of carbon dioxide.
Finally, the **ALBA** model [19] was developed in an outdoor raceway system of microalgae-bacteria consortia treating synthetic wastewater. This mathematical model includes 19 processes and 17 components among solubles and particulates and it is intended to be a reference model for microalga-bacteria consortia. Indeed, ALBA predicts the microalgal growth and describes the dynamics among microalgae, heterotrophic, and nitrifying bacteria, as well as taking into consideration the carbon, nitrogen, and phosphorous balances. It also considers chemical/physical processes like gas transfers, dissociation of weak acids and bases, and phosphorus precipitation due to alkaline pH achieved by photosynthesis that can constitute the main phosphorus removal mechanism [121]. The model shows good robustness due to the calibration and validation that took place over a wide range of time, comprising all four seasons.
A limitation of ALBA model is that it does not include the luxury uptake of phosphorus and the utilization of intracellular polyphosphate as a phosphorus source in P-deplete conditions. Like BIO_ALGAE 2 model, also ALBA includes the influence of pH and temperature using sub-models and of light dependence by a Haldane-type function [18].

The modeling of microalgae-bacteria consortia has been a research topic also for the CALAGUA group. The basic idea is to couple a wastewater treatment model by means of bacteria, the Biological Nutrient Removal No.2 (BNRM2) [12], with the microalgae model developed by Viruela et al. [118]. The final model resulting from the integration

of the previous two is the Biological Nutrient Removal No.2 Algae (BNRM2A) model developed by Aparicio et al. [11] and it takes into consideration a bacteria-microalgae consortium. This model is described more in-depth in the next section.
For the sake of brevity, bacterial model BNRM2 is not detailed in this report as it is not directly concerned with this investigation. A general overview of the integrated model is now introduced, while in the next section the algal model, which is the actual object of the present work, will be described in detail. For a more detailed explanation of the integrated model BNRM2A, the reader is referred to [11].

BNRM2A

The model takes into account the processes involved in a full-scale plant and it couples the previously mentioned bacterial-microalgal models. It aims to describe the interactions between different bacteria strains and microalgae by including the main biological, chemical, and physical processes occurring in the consortium.
The major novelties of the proposed model are the inclusion of chemical precipitation processes and the inhibition of the photosynthetic process due to nitrite accumulation at high pH values. P-precipitation is a relevant phenomenon at high pH as it leads to a lower concentration of phosphorus in the liquid medium, so it decreases the P availability for microalgae metabolism.
In addition, nitrite inhibition is another phenomenon that influences microalgae activity. Indeed, the inhibition mechanism affects photosynthesis, reducing light absorption and hampering the electron transport chain. In particular, plastoquinone Q_A is not able to transfer electrons to plastoquinone Q_B, so the primary photosynthetic process presents a strong limitation, consequently, the maximum electron transfer yield is decreased [10].
The conceptual scheme of the model can be divided between the two biological systems, microalgal and bacterial ones.
The former is carried on by photosynthesis in light conditions and it consumes nutrients (N, P) dissolved in the growth medium while producing oxygen by fixation of inorganic carbon. The oxygenation of the culture medium promotes the symbiosis with heterotrophic bacteria which are able to oxidize biodegradable organic matter during the nitrification phase.
The latter is based on the presence of ammonium-oxidizing bacteria (AOB), nitrite-oxidizing bacteria (NOB), and heterotrophic bacteria. Microalgae can assimilate N in the form of ammonium or nitrate $NO_3{}^-$. However, the preferred way is in the form of $NH_4{}^+$, energetically more convenient. The bacterial mechanism is the conventional one, consisting of denitrification during which the biodegradable organic matter is degraded

by heterotrophic bacteria and nitrification. Nitrification is operated in two steps. In the first one, AOB oxidize ammonium to nitrite, then, by NOB activity, nitrite is oxidized to nitrate.
The abundance of micronutrients in the culture medium is considered high enough to assume micronutrients as non-limiting for biomass development.

The model considers two categories of components, soluble and particulate. Among the soluble ones the total ammonia nitrogen NH_X (NH_4^++NH_3), nitrite, nitrate, total soluble inorganic phosphorus PO_4^{3-}, total inorganic carbon (CO_2+HCO_3^-+CO_3^{2-}), total proton concentration (free protons+those associated with acidic components), magnesium, potassium, calcium, iron, aluminum, readily biodegradable soluble organic matter, inert soluble organic matter, nitrogen, are present. Among the particulate components, the most relevant are: microalgae biomass stoichiometrically considered as $C_{106}H_{181}O_{45}N_{17}P$ [75], heterotrophic bacteria, AOB, NOB, intracellular polyphosphates stored in the algal cell (luxury uptake), TSS.

Concerning the processes included in BNRM2A model, they are subdivided among the different microorganism typologies, for a total of 19 biological processes. In particular, three macro-groups of processes are considered: 8 relatives to microalgae, 7 to heterotrophic bacteria, and 4 to nitrifying bacteria. In addition to them, 19 processes of stripping phenomena and chemical precipitation of compounds are included. The microalgal processes group is focused on in the next section concerning the microalgal model by Viruela et al. For heterotrophic bacteria, the processes related to growth, hydrolysis and lysis are included, while for the nitrifying ones the growth and lysis, all of them in different environmental conditions in terms of oxygen concentration (aerobic, anaerobic, and anoxic).
Gas/liquid transfer processes are described by the general expression $K_{La,j} \cdot (S_j - S_j^*)$.

In this expression $K_{La,j}$ is the specific mass transfer coefficient of the j gas (d^{-1}), S_j is the gas concentration of j gas in the liquid phase ($g \cdot m^{-3}$), S_j^* is the saturation concentration of j gas in the liquid phase ($g \cdot m^{-3}$). The chemical compounds affected by stripping phenomena are CO_2, O_2, N_2 and free ammonia NH_3.
Dissolution processes come along with precipitation processes and they are related to mineral compounds present in the medium such as struvite, varscite, and others.
In conclusion, the bioprocess kinetics account for the effect of nutrient concentration (limitation or inhibition) and the abiotic factors influencing microalgae-bacteria cultivation (light intensity, pH, and temperature). In this section, the kinetics are not detailed because the relevant ones are described in the next chapter relative to the microalgal model.

2.2.2. Microalgae model

The model proposed by Viruela et al. [118] has been developed to study the microalgae growth in a pure microalgal culture and it represents the microalgae model compartment in the integrated model BNRM2A. The main aim of the model is to predict the abundance of microalgae in terms of concentration, the removal from the liquid phase of nitrogen and phosphorus, polyphosphate storage and consumption, and the release and accumulation of soluble and particulate organic matter.
The microalgae model described is structured similarly to the intended coupled bacterial model BNRM2, whose full explanation can be found here [12], and now it is briefly explained. Basically, it is based on two integrated sub-models. The first one is the biological model that comprises the kinetic processes. The second one is the chemical model which contains the chemical equilibria. Computationally, the solutions of the chemical model are gained by Visual MINTEQ code, working on the basis of acid-base, ion-pairing, and redox reactions. In the present work, the code reported in Appendix B.2 includes both the sub-models. Below in Fig.2.8 is reported a schematic diagram of the simulation procedure for each component of Viruela's model, showing as an example S_{PO4}.

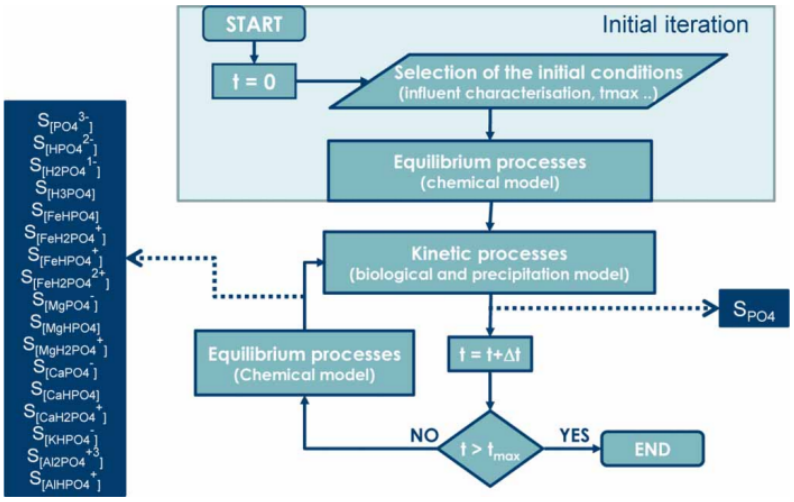

Figure 2.8: Graphic representation of the iterative simulation procedure of the microalgae model, picture taken from BNRM2 [12]. To be noted that in the present microalgal model, the precipitation is not included in the kinetic processes block.

In Fig.2.8 the two sub-models can be recognized. Moreover, the simulation is run continuously and it needs initial conditions known such as abiotic factors and basic chemical compounds. In the same way, the model components (see Petersen matrix in Tab.2.6)

comprised in the biological model have to start from specific initial values. The chemical species involved in MINTEQ are not reported in this work, but they can be found in Appendix B of the BNRM2 model description [12].
The model was calibrated and validated by using experimental data from a pilot-scale membrane photobioreactor (MPBR) fed with the permeate obtained from an anaerobic membrane bioreactor (AnMBR) pilot plant fed with the effluent from the pre-treatment step of the 'Barranco del Carraixet' WWTP (Valencia, Spain).
AnMBR is a configuration that couples anaerobic digestion (AD) with a membrane system. The digestate produced in the bioreactor is circulated to the membrane (with a pore-size of microfiltration 0.4 µm or ultrafiltration 0.03 µm) and the resulting permeate is then sent to the MPBR. The main advantages of this technology are the production of biogas by AD and the generation of an effluent rich in nitrogen and phosphorus, so very suitable for microalgae cultivation [94].
Concerning the MPBR pilot plant section, two parts can be distinguished. Firstly, the influent flow is fed to a two flat-panel PBR where occur the biomass growth. Then the stream extracted from the bioreactor is treated in a membrane tank. At this point, the purified permeate is extracted while the concentrate flow is in part discharged and in part recirculated to the PBR in order to maintain the desired biomass retention time (BRT) decoupling it from the HRT. For further details on the AnMBR and MPBR plant sections see [93] and [116].

Theoretical background and assumptions

Before providing the description of the components and processes comprising the model, a short explanation of the conceptual functioning of the model (Fig.2.9) and of the simplifying assumptions made are offered.

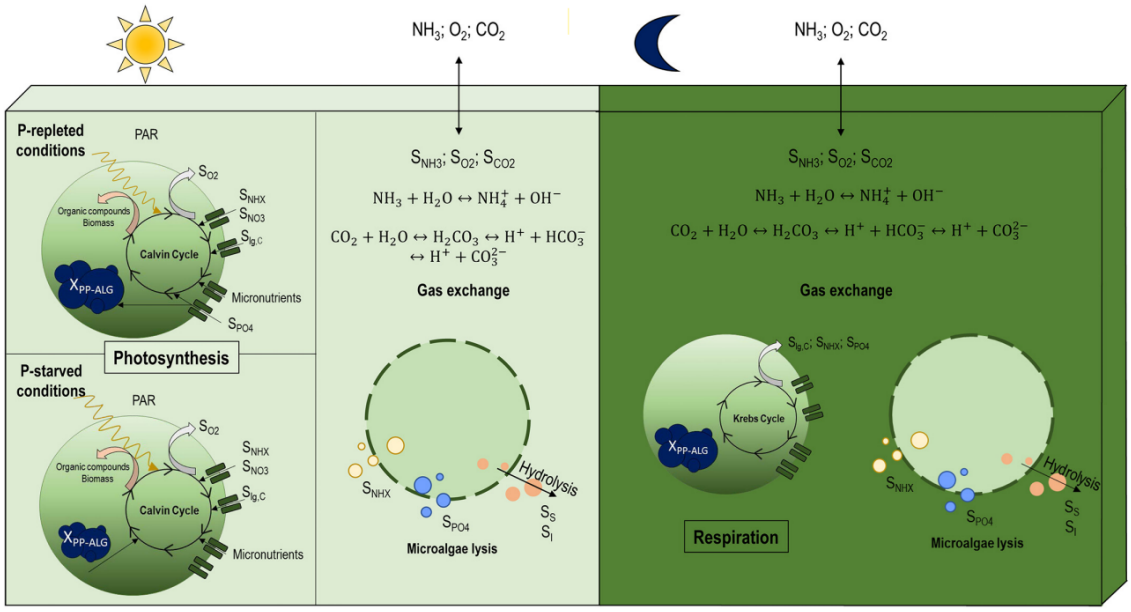

Figure 2.9: Schematic representation of the most relevant dynamics occurring in the conceptual model both in light conditions (left) and dark conditions (right) [118].

The photosynthetic activity of the microalgae is based on two cycles, the light-dependent one and the dark one (Calvin cycle), as explained in chapter 2.1.2. Moreover, the model takes into account also the respiration phase in night conditions.
First of all, the most relevant feature of the model is the phosphorus concentration in the growth medium that leads to the two scenarios of P-repleted and P-starved conditions. Indeed, in terms of phosphorus assimilation, the luxury uptake concept was applied and a threshold of 0.5 mg_P/l is set as the condition above which the storage of phosphorus is established in the algal cell as polyphosphate.
During microalgal photosynthesis pH increases and the bicarbonate-carbonate equilibrium shifts towards the formation of carbonate (Fig.2.10) boosting the stripping of free ammonia nitrogen (FAN) and simultaneously the phosphorus precipitation.

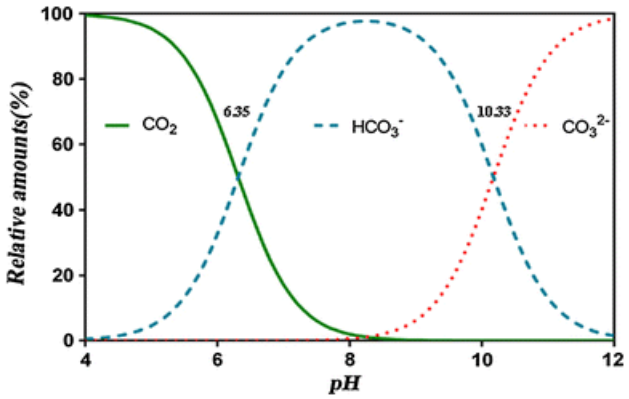

Figure 2.10: General equilibrium relationship between bicarbonate-carbonate in function of pH [42]. The relative percentage abundances are shown.

In the night period, photosynthesis is disabled, and endogenous respiration (Krebs Cycle) takes place whose effect is the release into the medium of carbon dioxide. This affects the carbon equilibrium bringing to lower pH values (fig.2.10) and the carbonate is turned again into bicarbonate,
Cell lysis generates organic matter and phosphate release into the culture medium and, at the same time, the hydrolysis of organic compounds to readily biodegradable organic matter occurs.

A series of assumptions have been made in order to simplify the dynamics involved in the natural processes present in the model.

- From a biological point of view, the model is not strain-dependent, meaning that it describes the behavior of a general algal culture. Nevertheless, it has been calibrated and validated with a community constituted of *Chlorella sp.* and *Scenedesmus sp.*
- Among the possible inhibition phenomena affecting microalgae growth (photoinhibition, excess of nitrogen, high oversaturation of dissolved oxygen) only the photoinhibition effect is taken into consideration in the modeling. Indeed, in the MPBR pilot plant adopted to calibrate/validate the model, oxygen conditions close to saturation were guaranteed, as well as a free ammonia concentration low enough not to represent a toxic excess.
- Heterotrophic bacteria are responsible for the hydrolysis of biodegradable particulate organic matter (X_S) to biodegradable soluble one (S_S). However, the model does not include heterotrophic bacteria presence (microalgae pure culture). Thus, the bioprocesses were simplified assuming that operating and environmental conditions

allow a complete and direct hydrolysis of particulates organic matter to soluble one.

- The developed model assumes that microalgae are characterized only by a photoautotrophic metabolism, excluding any mixotrophic or heterotrophic growth, thus biodegradable particulate organic matter S_S is not assimilated.
- Micronutrient concentrations are not a limiting factor for any biological process.
- The photobioreactor is considered as CSTR, thus the concentration of all the compounds taken into account in the model are constant in the volume, with no evidence of hydraulic dead zones and accumulation zones.

An important assumption and limitation of the microalgal model is the exclusion of chemical precipitation phenomena, that are only present in the integrated model BNRM2A.

Model components

The variables of the model can be divided between soluble and particulate components. In general terms, the soluble ones are illustrated as "S" and the particulate as "X". In the actual model, 10 soluble and 4 suspended variables are included. Below in Tab.2.4 a brief summary of all of them is shown.

Table 2.4: Variables comprised in the microalgae model.

Variable	Description	Unit of measure
S_{O_2}	Dissolved oxygen conc.	g_{O2}/m^3
S_{NH_X}	Ammonium + free ammonia nitrogen conc.	g_N/m^3
S_{NO_3}	Nitrate conc.	g_N/m^3
S_{PO_4}	Total soluble inorganic phosphorus conc.	g_P/m^3
$S_{ig,C}$	Total inorganic carbon, CO_2+HCO_3^-+CO_3^{2-}	mol_C/m^3
$S_{H_{TOT}}$	Total proton conc.	mol_H/m^3
S_{Mg}	Total soluble inorganic magnesium conc.	g_{Mg}/m^3
S_K	Total soluble inorganic potassium conc.	g_K/m^3
S_S	Readily biodegradable soluble organic matter	g_{COD}/m^3
S_I	Inert soluble organic matter	g_{COD}/m^3
X_{ALG}	Microalgal conc.	g_{COD}/m^3
X_I	Inert particulate organic matter	g_{COD}/m^3
X_{PP-ALG}	Polyphosphates stored by X_{ALG}	g_P/m^3
X_{NVSS}	Non-volatile suspended solids	g_{TSS}/m^3

Total proton concentration is computed as the sum of all the chemical species where H^+ component participates: H^+-HCO_3^-+$2H_2CO_3$+HPO_4^{2-}+$2H_2PO_4^-$+$3H_3PO_4$-NH_3-OH^-. Basically, it represents the total acidity (or titratable acidity) of the solution and it is complementary to the alkalinity. The concentration of H^+ is S_H and it is directly related

to pH, not to be confused with total proton concentration variable $S_{H_{TOT}}$.
Regarding the TSS, X_{TSS} is the sum of microalgal component X_{ALG}, the inert particulate organic matter X_I and the polyphosphate components X_{PP-ALG}.

Model processes

Now that the variables have been explained, the 11 processes kinetics included in the model are shown in Tab.2.5, while process stoichiometry is in Tab.2.6.
Microalgal growth is considered in four different processes. The changing variables that differentiate each scenario are the nitrogen and phosphorus sources. In this sense, nitrogen can be assimilated starting from ammonium or from nitrate. Nevertheless, the ammonium route is privileged for energetic reasons as seen in section 2.1.3.
Regarding the phosphorus uptake, it is applied the luxury uptake concept. In this way, P can be consumed by algal metabolism in the form of polyphosphate stored in the cell, in case of P-deplete conditions, or directly from the liquid phase as orthophosphate $PO_4{}^{3-}$ (S_{PO_4}) in P-replete conditions. S_{PO_4} concentration increases due to endogenous respiration and lysis of microalgae biomass as well as of intracellular phosphorus (polyphosphate), while it is reduced by microalgae growth and phosphorus storage.
Various dynamics are then considered: the phosphorus storage in the algal biomass, the microalgae endogenous respiration, the lysis of microalgae biomass and of the stored polyphosphate, and eventually the gas/liquid transfer of the gaseous components CO_2, O_2, NH_3. These last processes are not fully detailed since they are not direct objects of study in this work, with the exception of the CO_2, O_2, and NH_3 stripping. Ammonia gas-liquid transfer is particularly relevant at alkaline pH, where the phenomenon is enhanced. For further information on these processes not detailed see [118].

Table 2.5: Processes involved in the model dynamics [118].

Processes	Processes rate [M L^{-3} T^{-1}]
1. X_{ALG} growth on S_{NHX} and S_{PO4}	$\mu_{ALG} \cdot \frac{S_{Ig,C}}{K_{Ig,C}+S_{Ig,C}} \cdot \frac{S_{NHX}}{K_{NHX}+S_{NHX}} \cdot \frac{S_{PO4}}{K_{PO4}+S_{PO4}} \cdot X_{ALG} \cdot f_L \cdot f_{pH} \cdot f_T$
2. X_{ALG} growth on S_{NO3} and S_{PO4}	$\mu_{ALG} \cdot \eta_{NO3} \cdot \frac{S_{Ig,C}}{K_{Ig,C}+S_{Ig,C}} \cdot \frac{K_{NHX}}{K_{NHX}+S_{NHX}} \cdot \frac{S_{PO4}}{K_{PO4}+S_{PO4}} \cdot \frac{S_{NO3}}{K_{NO3}+S_{NO3}} \cdot X_{ALG} \cdot f_L \cdot f_{pH} \cdot f_T$
3. X_{ALG} growth on S_{NHX} and X_{PP-ALG}	$\mu_{ALG} \cdot \frac{S_{Ig,C}}{K_{Ig,C}+S_{Ig,C}} \cdot \frac{S_{NHX}}{K_{NHX-qXPP}+S_{NHX}} \cdot \frac{K_{LPO4}}{K_{LPO4}+S_{PO4}} \cdot \frac{\frac{X_{PP-ALG}}{X_{ALG}}}{K_{XPP-ALG}+\frac{X_{PP-ALG}}{X_{ALG}}} \cdot X_{ALG} \cdot f_L \cdot f_{pH} \cdot f_T$
4. X_{ALG} growth on S_{NO3} on X_{PP-ALG}	$\mu_{ALG} \cdot \eta_{NO3} \cdot \frac{S_{Ig,C}}{K_{Ig,C}+S_{Ig,C}} \cdot \frac{K_{NHX}}{K_{NHX-qXPP}+S_{NHX}} \cdot \frac{K_{LPO4}}{K_{LPO4}+S_{PO4}} \cdot \frac{S_{NO3}}{K_{NO3}+S_{NO3}} \cdot \frac{\frac{X_{PP-ALG}}{X_{ALG}}}{K_{XPP-ALG}+\frac{X_{PP-ALG}}{X_{ALG}}} \cdot X_{ALG} \cdot f_L \cdot f_{pH} \cdot f_T$
5. X_{PP-ALG} storage	$q_{PP-ALG} \cdot \frac{S_{PO4}}{K_{PO4}+S_{PO4}} \cdot \frac{S_{Mg}}{K_{Mg}+S_{Mg}} \cdot \frac{S_K}{K_K+S_K} \cdot \frac{K_{XPP-qXPP}{}^n}{K_{XPP-qXPP}{}^n+\left(\frac{X_{PP-ALG}}{X_{ALG}}\right)^n} \cdot X_{ALG} \cdot f_L \cdot f_{pH} \cdot f_T$
6. X_{ALG} endogenous respiration	$b_{ALG,\,1} \cdot X_{ALG} \cdot f_T$
7. X_{ALG} lysis	$b_{ALG,\,2} \cdot X_{ALG} \cdot f_T$
8. X_{PP-ALG} lysis	$b_{ALG,\,2} \cdot X_{PP-ALG} \cdot f_T$
9. $S_{[CO2]}$ stripping	$K_{La,\,CO2} \cdot (S_{[CO2]} - S_{[\hat{C}O2]})$
10. S_{O2} stripping	$K_{La,\,O2} \cdot (S_{O2} - S_{\hat{O}2})$
11. $S_{[NH3]}$ stripping	$K_{La,\,NH3} \cdot (S_{[NH3]} - S_{[\hat{N}H3]})$

Process kinetics

The kinetics of the previously mentioned processes depend on the environmental abiotic conditions of the medium culture influencing microalgae development. In the model light intensity, pH, and temperature are considered and they are illustrated through the factors f_L, f_{pH}, f_T, respectively. The values of all the parameters not reported in this section are provided in Appendix A.
The Monod kinetic is used to relate microalgal growth rate to the concentration of the limiting substrates such as nitrogen, phosphorus and inorganic carbon compounds.

Light intensity is measured in µmol/m^2/s as photosynthetically active radiation (PAR) that comprises wavelength in the range of 400 to 700 nm. The modeling of light intensity is operated by use of Steele's equation [102] since it has been proved to describe in the best way the photoinhibition:

$$f_L = \frac{I_{av}}{I_{opt}} \cdot e^{\left(1-\frac{I_{av}}{I_{opt}}\right)}$$

where I_{opt} [µmol/m^2/s] is the optimal light intensity for microalgae growth and I_{av} [µmol/m^2/s] is the average light intensity available for microalgal growth. The average light intensity is a function of the measured incident light intensity $I_{0,S}$, of the TSS assumed to be represented only by microalgae biomass (generation of shadowing effect), and the PBR depth d [m]. This relationship is expressed by the Lambert-Beers Law according to:

$$I_{av} = \frac{I_{0,s} \cdot \left(1-e^{-(k_w+K_I \cdot Xtss)\cdot d}\right)}{(k_w + K_I \cdot X_{TSS}) \cdot d}$$

where k_W [m^{-3}] and K_I [m^2/g_{TSS}] are the extinction coefficient associated to water and particulate components, respectively.

Multiple variables and biokinetics are influenced by the pH value of the culture medium. In order to integrate pH influence into the model configuration by means of the factor f_{pH}, the following formulation has been chosen:

$$f_{pH} = \frac{\frac{S_H}{S_H+K_{S,H}} \cdot \frac{K_{I,H}}{S_H+K_{I,H}}}{\frac{S_{H,opt}}{S_{H,opt}+K_{S,H}} \cdot \frac{K_{I,H}}{S_{H,opt}+K_{I,H}}}$$

This expression is a synthesis of a pH non-competitive inhibition switching function formulated in [95] combined with a Monod kinetic. The inhibition is related to the phosphorus precipitation occurring at high pH values, making it unavailable for algal absorption. Overall, dissolved phosphorus limitation in the medium is related to the Monod expression in the kinetic function and to the pH in f_{pH}. In f_{pH} expression, S_H [mol_H/l] represents the free proton concentration directly associated with pH, $K_{S,H}$ the half-saturation constant for S_H, $K_{I,H}$ the inhibition constant for S_H, $S_{H,opt}$ represents the optimum S_H concentration obtained as the square root of the product between $K_{I,H}$ and $K_{S,H}$. $S_{H,opt}$ is used to remove the pH inhibition effect when performing under optimal pH growth conditions.
The kinetics involved in the model processes are dependent on water temperature. This influence is expressed by the parameter f_T, which was modeled by a Ratkowski thermic factor:

$$f_T = (b \cdot (T_0 - T_{MIN}))^2 \cdot \left(1 - e^{c \cdot (T_0 - T_{MAX})}\right)$$

where T_0 [°C] is the temperature of the culture medium, T_{MIN} [°C] and T_{MAX} [°C] are the lower and upper limits below and above which the growth rate is expected to be zero, b is a parameter of the model that is defined as the square root regression coefficient of the rate versus the suboptimal temperature, c is a parameter that enables the model to fit data at a temperature near and above the optimal temperature for growth.

A consortium of microalgae-bacteria as well as a pure microalgae community represents a complex biological system and, in order to be properly described, must follow the standard of the IWA ("*International Water Association*"). In this sense, a Petersen matrix is the tool by which it is expressed. Petersen matrix is an exhaustive description of the model forming a system based on biochemical reactions. It couples each process with each component by means of stoichiometric coefficients. In Tab.2.6 is reported the Petersen matrix of Viruela's microalgal model.

All the stoichiometric coefficient values are reported in Appendix A.

Table 2.6: Stoichiometry of the processes considered in the microalgae model by Petersen matrix [118].

Components → i	S_{O2}	S_{NHX}	S_{NO3}	S_{PO4}	S_{IC}	S_H	S_{Mg}	S_K	S_S	S_I	X_{ALG}	X_I	X_{PP-ALG}
Processes ↓ j	g O_2 m^{-3}	g N m^{-3}	g N m^{-3}	g P m^{-3}	mol C m^{-3}	mol H m^{-3}	g Mg m^{-3}	g K m^{-3}	g COD m^{-3}	g COD m^{-3}	g COD m^{-3}	g COD m^{-3}	g P m^{-3}
1. X_{ALG} growth on S_{NHX} and S_{PO4}	$v_{1,1}$	$v_{2,1}$		$v_{4,1}$	$v_{5,1}$	$v_{6,1}$					$v_{11,1}$		
2. X_{ALG} growth on S_{NO3} and S_{PO4}	$v_{1,2}$		$v_{3,2}$	$v_{4,2}$	$v_{5,2}$	$v_{6,2}$					$v_{11,2}$		
3. X_{ALG} growth on S_{NHX} and X_{PP-ALG}	$v_{1,3}$	$v_{2,3}$			$v_{5,3}$	$v_{6,3}$	$v_{7,3}$	$v_{8,3}$			$v_{11,3}$		$v_{13,3}$
4. X_{ALG} growth on S_{NO3} on X_{PP-ALG}	$v_{1,4}$		$v_{3,4}$		$v_{5,4}$	$v_{6,4}$	$v_{7,4}$	$v_{8,4}$			$v_{11,4}$		$v_{13,4}$
5. X_{PP-ALG} storage				$v_{4,5}$		$v_{6,5}$	$v_{7,5}$	$v_{8,5}$					$v_{13,5}$
6. X_{ALG} endogenous respiration	$v_{1,6}$	$v_{2,6}$		$v_{4,6}$	$v_{5,6}$	$v_{6,6}$					$v_{11,6}$		
7. X_{ALG} lysis		$v_{2,7}$		$v_{4,7}$	$v_{5,7}$	$v_{6,7}$			$v_{9,7}$	$v_{10,7}$	$v_{11,7}$	$v_{12,7}$	
8. X_{PP-ALG} lysis				$v_{4,8}$		$v_{6,8}$	$v_{7,8}$	$v_{8,8}$					$v_{13,8}$
9. $S_{[CO2]}$ stripping					$v_{5,9}$	$v_{6,9}$							
10. S_{O2} stripping	$v_{1,10}$												
11. $S_{[NH3]}$ stripping		$v_{2,11}$											

3 | Materials and methods

In the next sections, the theoretical methodologies adopted for the performing of the experimental activity will be explained.
In addition, the experimental equipment and the assumptions made on the values of the key parameters in the experimental design are described, as well as the explanation of the microalgae growth medium used.

3.1. Analytical methods

The setting of appropriate experimental procedures and the usage of adequate equipment is fundamental to avoid systematic and random errors and to perform in the best possible conditions the research investigation.
In the next sections, the experimental equipment used and the characteristics of two possible growth mediums taken into consideration for the algae cultivation are described.
The equipment adopted during the experimental activity is described. For each instrument, its objective is explained synthetically. Moreover, the techniques and standard procedures adopted are reported as well.

The nutrient analysis performed to assess the nutrient concentrations in the bioreactor where conducted by a SMARTCHEM 200 - AMS FRANCE. This instrument provides the concentrations in terms of total nitrogen and total phosphorus. It is utilized when there is the necessity for a fast evaluation and, in addition, it can supply the concentrations of NO_2^-, NO_3^-, and SO_4^{2-}. Ammonium, nitrite, nitrate, and phosphate concentrations are analyzed according to Standard Methods [7]: Methods 4500-NH3-G, 4500-NO2-B, 4500-NO3-H, and 4500-P-F, respectively.
The ionic composition is obtained through the ion-exchange chromatography technique, by the utilization of an ion chromatograph (IC) (883 Basic IC Plus, Metrohm, Switzerland). This device provides the concentrations in ppm of the following ionic compounds: Na^+, NH_4^+, K^+, Mg^{2+}, Ca^{2+}, Cl^-, NO_2^-, NO_3^-, PO_4^{3-}, SO_4^{2-}, $S_2O_3^{2-}$. The standards adopted are DIN EN ISO 10304-1 / 10304-3 / 10304-4 relative to water quality.

The evaluation of the total suspended solids (TSS) has been operated according to the method 2540D Total Suspended Solids by gravimetric determination from "Standard Methods for the Examination of Water and Wastewater". In order to carry out the procedure, a hydrophilic glass fiber prefilter characterized by a pore size of 0.7 µm (Merck Millipore Ltd.) and a cellulose nitrate membrane filter with 0.45 µm pore size (Cytiva Whatman) have been used.
During the test campaign, for the determination of ionic composition a filtration is required, thus filters with 0.45 µm pore size (SFMC-245-100 Branchia) are adopted.

Light intensity is evaluated in PAR on the external surface of the flask and of the bioreactor. An Apogee quantum sensor model SQ-222 connected with a PicoLog 1216 data logger is used. As it is explained later in section 3.2.2, in the calibration and validation phase five conditions of light irradiance on the flask are selected, depending on the number and position of lamps used. In order to characterize each condition with a unique representative value of light irradiance on the external surface, the irradiance on different points of the flask is measured (section 3.1.1).

The light is provided by the use of white-light LED lamps (T8 LED-Tube AC85-265 V, 9 W). Each reactor, and also the flasks used in the calibration and validation periods of the experimental activity, are surrounded by a variable number of LED lamps. The number is variable since it is not possible to set a proper light intensity a priori to guarantee proper growth while avoiding the photoinhibition effect. In Fig.3.1 and in Fig.3.2 the experimental equipment adopted is shown, with photos and a schematic representation, respectively. The description of the equipment is detailed in the following paragraphs.

(a) Control computer and relay area

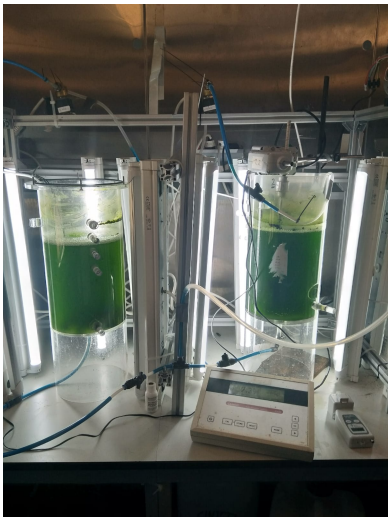

(b) Photobioreactors area

(c) Flasks test area

Figure 3.1: Experimental area in the room at controlled temperature.

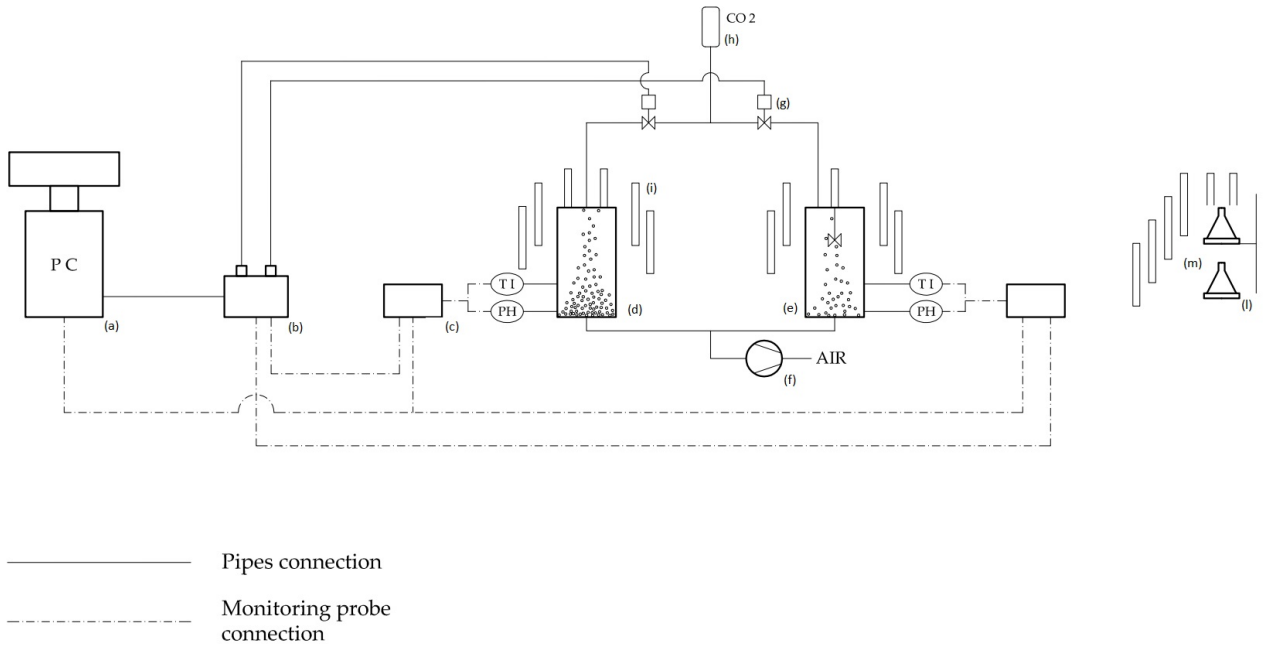

Figure 3.2: Schematic representation of the installation used. (a) Control computer station; (b) Electrical relay; (c) Consort multi-parameter controller for continuous monitoring of pH and temperature; (d) PBR1 (shortly R1); (e) PBR2 (shortly R2); (f) Air pump; (g) Automatic electrovalve; (h) Carbon dioxide tank; (i) LED lamps; (l) Magnetic stirrer; (m) Glass flasks.

The monitoring of the living conditions and health status of the microalgae is performed by means of the fluorometer AquaPen-C AP-C 100 (Photon Systems Instruments). AquaPen measures quickly and in a reliable way photosynthetic parameters both in algal and cyanobacterial suspensions.

In the initial phase relative to the growth medium selection, the evaluation of the TSS is performed following the method "2540D Total Suspended Solids by gravimetric determination from Standard Methods for the Examination of Water and Wastewater". In the rest of the experimental activity, after having chosen the most ideal growth medium, the TSS assessment is done using AquaPen-C AP-C 100 by measuring the optical density

since it is faster and more practical. This device, which records optical density, is actually related to the microalgae component X_{ALG} rather than TSS, which includes also the inert components. In order to simplify the experimental procedure, it is neglected the contribution to TSS of polyphosphates (X_{PP-ALG}) and of the inert particulate organic matter (X_I), assuming that the only TSS contribution is due to algae concentration.
So, optical density (OD) is a parameter that is directly proportional to the solids concentration represented only by microalgae presence. To be more specific about the functioning of the device, optical density is measured at 680 nm and it represents the light scattering and chlorophyll-a absorption by the algal biomass. In this sense, higher concentrations of total suspended solids bring more consistent light adsorption. This type of measurement is considerably faster than manual TSS determination and to guarantee a reliable result it is necessary to determine a robust calibration curve. In this way, it is generated the calibration curve that relates the TSS with the optical density evaluated by the device (Fig.3.3). The assessments of TSS by the 2540D method are related to the values acquired from AquaPen.

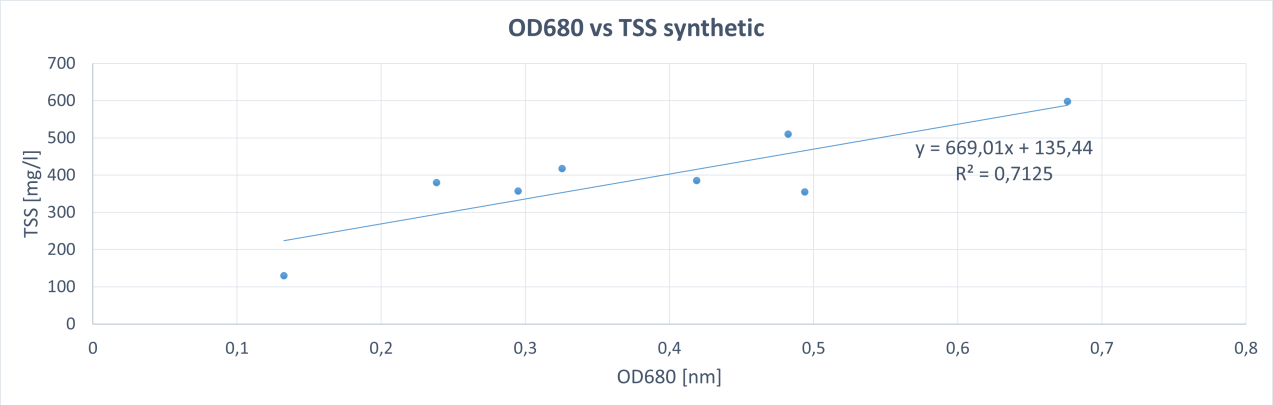

(a) Calibration curve TSS-OD for synthetic wastewater

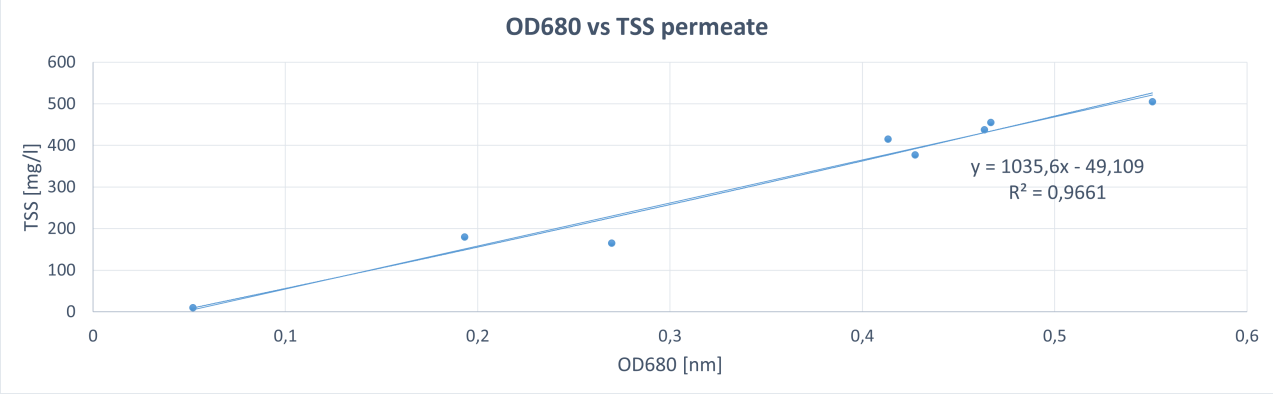

(b) Calibration curve TSS-OD for permeate

Figure 3.3: In (a) the calibration curve between biomass concentration in terms of TSS and optical density for the scenario with synthetic wastewater is shown. In (b) the calibration curve TSS-OD for the permeate is represented. The relative equations of the linear regression curve are visualized. The adjusted R^2 are shown as well.

The equations of the linear regression lines are adopted to calculate the biomass concentration in TSS following the optical density measurement.

Some periodical checks of dissolved oxygen (DO) levels are done by using the oxygen probe OxiCal-SL - WTW. The main concern is to not go into an oxygen oversaturation condition. To be noted that oxygen has not been monitored continuously since it is not a relevant parameter studied in the present work. Indeed, the main purpose was to provide the PBRs with an aeration system aiming to avoid O_2 oversaturation.

A single experimental assay lasts for a total of 5 hours and the sampling times are five, occurring at 10.00h, 11.00h, 12.00h, 14.00h, 15.00h for the first flask, 10.30h, 11.30h, 12.30h, 14.30h, 15.30h for the replica flask. At each sampling around 150ml of solution is

extracted from the flask and analyzed.

Alkalinity is determined following the 5 pH Point Titration Method proposed by R. E. Moosbrugger [68]. The advantages of this method are the cheap cost and the relative simplicity of the technique. However, systematic error on all pH observations must be noted since it is strongly dependent on the pH meter calibration and user confidence in performing the procedure. The titration is performed using a water solution with 0.7% of hydrochloric acid.
Moosbrugger's method is then elaborated in the software "Valora" (see section 3.3).

The monitoring of biomass health is important to understand which factors can lead the microalgal community to death and to guarantee a good health status throughout the experimental phases.
A proxy variable that measures the algal biomass quality is the efficiency of the photosynthesis process. Photosynthetic energy conversion is evaluated by chlorophyll fluorescence which is used as an indicator showing the re-emitted light by chlorophyll a (Chl a) molecules during the passage from excited to non-excited condition.
It is recognized that Chl a fluorescence screening provides plenty of information about the photosystem II (PS II) performance and electron transport chain [103]. The fluorescence is assessed by means of AquaPen-C AP-C 100 device. There are several protocols to analyze the fluorescence response. In the present work have been assessed the Quantum Yield (QY) of the photosystem II and Chlorophyll Fluorescence Induction Kinetics (OJIP curve).
Photon's energy absorbed by chlorophyll molecules can undergo two routes: it can drive photosynthesis (photochemical quenching) or excess energy can be dissipated as heat or it can be re-emitted as light—chlorophyll fluorescence (non-photochemical quenching). These two alternative endings are complementary, so an efficiency increase of one will result in a decrease of the other. Thus, measuring the yield of chlorophyll fluorescence provides information about the efficiency of photosynthesis and heat dissipation [64].
The parameters adopted in the fluorescence evaluation are F_v and F_m:

- F_0, minimal fluorescence level of dark-adapted sample.
- F_m, maximal fluorescence level of dark-adapted sample when a fast and high-intensity pulse is applied.
- F_v, difference between F_m and F_0, variable fluorescence values.

In addition to the technical instrumental measurements, a visual inspection represents

a useful way to evaluate quickly and easily the culture conditions and cyanobacteria presence. The most visible characteristics adopted to evaluate the algal status are flocs formation and the color change from brilliant green to dark-yellowish.
In general, the drawback is that these phenomena are clear when they are already consolidated, leading to the death of the microalgae. For sure, the most effective way to verify cyanobacteria presence is by use of a microscope, checking their presence directly in the observed sample.

Quantum yield
Quantum yield (QY) is equivalent to the ratio F_v/F_m and it measures the maximum efficiency of PS II photochemistry. Generally, the effective quantum yield of photosynthesis shows an output value ranging from 0.68-0.75 in good-healthy conditions [10] [53]. If microalgae are stressed or negatively affected by cyanobacteria in the culture, photosystem II is inhibited and its working is compromised, resulting in a QY lower than the previously mentioned values.

OJIP curve
OJIP methodology assesses the transient chlorophyll fluorescence induction in dark-adapted samples of algal culture. Four florescence points are evaluated in sequence after 50 µs (O), 2 ms (J), 60 ms (I) and at the maximum recorded fluorescence intensity (P). Each fluorescence point is defined respectively as O-J-I-P. During the exposure of photosynthesizing organisms to high-level irradiance, photochemical quenching is recorded. The fluorescence transients are higher in the case of effective photochemical quenching, so with an algal culture in good health status. On the contrary, if photosynthesis is compromised, the curve trend falls.
The algal culture is negatively affected mainly by the cyanobacteria as previously mentioned. Indeed, it has been observed that reduced photosynthetic activity is recorded when cyanobacteria are abundantly present in the medium, enhancing the non-photochemical quenching (heat dissipation) by the biomass in the culture.

3.1.1. Photobioreactor

The setting up of two photobioreactors (PBRs), defined as R1 and R2, has been made at a controlled room temperature that is maintained thermostatically at around 25°C. Each PBR has dimensions of 19.5cm diameter and 35cm high, showing a volume of around 10

liters. They are made of transparent plastic and the volume filled with the culture is 7 liters.
Two ways of mixing the cultures are chosen, diversifying and making safer the cultivation. R1 is mixed by air bubbling from the bottom of the reactor, while R2 is mechanically stirred and lightly mixed by air bubbling. The airflow rate was regulated by specific manual valves placed on the input pipes to the reactors. It has been tested that the advantage of air bubbling is to avoid completely the risk of oxygen oversaturation, not avoidable with only mechanical stirring. On the other hand, mechanical stirring results in a cleaner surface of the reactor since the mixing is more powerful and the generation of biofilms is hindered. Biofilm on the reactor wall must be avoided because it causes a shading effect. Moreover, biofilm tends to generate a stagnant habitat that can lead to thriving microorganisms negatively affecting the culture like cyanobacteria and rotifers. Anyway, biofilm built up is avoided in both the reactors by daily manual cleaning of the inner walls. For the pH control and continuous monitoring in the PBRs a couple of multi-parameter analyzers 3010/3050 (Consort) have been used, monitoring also the temperature value. The medium pH is controlled by assembling a CO_2 bubbling system for both reactors. This system is composed of a CO_2 tank set at 1 bar, pipe connections, an electrical relay, and automatic electrovalves. The activation of the electrovalve is operated automatically by a software running in Microsoft Visual Studio environment. The bubbling is switched on only when the measured pH reaches a level above the value set in the software. The addition of carbon dioxide brings a pH decrease according to carbonate-bicarbonate equilibrium boosting the formation of carbonic acid. Light irradiance is provided by five lamps for both reactors.
Moreover, the relay is connected to the Consort consoles to allow their restarting remotely in case of temporary failure of the monitoring equipment.

Incidence light on the PBR external surface has been calculated taking into account four sides of the cylinder (front/back, left/right). As can be seen in Fig.3.1, LED lamps are placed on three sides of the reactor. Average light intensity is computed as the weighted average of the light intensities measured on the four sides. The weights are defined as the ratio between the measured light of a single side over the total incident light of all four sides. Both the PBRs are irradiated with a final average intensity of 300 µmol/m^2/s using five LED lamps each. The present work does not investigate the dynamics of the biomass during the dark phase, thus the illumination is maintained continuously on the PBRs.

The bioreactors can be ideally considered as CSTR to simplify the monitoring operations such as the evaluation of total suspended solids, nutrient concentration, pH and temperature, and dissolved oxygen.

The selection of appropriate hydraulic retention time (HRT) and biomass retention time (BRT) is reported in section 3.2.1.

Flask

Experimental assays are carried out in a pyrex glass flask of 1 liter. The base diameter measures 13cm, and the top diameter is 4cm. The assays are performed in different light conditions, so it is necessary to set various levels of light intensity by switching on/off the lamps. An adequate number of lamps is required. Eventually for the flask six lamps were set up, and placed in an L-shape around the flask itself (Fig.3.1). The experimental measurements are performed in replica so two flasks working in parallel are placed vertically. In order to guarantee the mixing of the flask culture in the test operations avoiding sedimentation, each flask is provided with a magnetic stirrer.

The incident light intensity is measured on the external surface of the flask used during the experimental phase. It depends both on the number of LED lamps switched on and their position with respect to the flask itself. The light inside the culture flask is not a measured parameter since it is already included in the algal model by light attenuation according to the Lambert-Beers Law by the term d (depth). Even if the flask geometry does not allow an accurate measurement of depth factor d, it is approximated to the average radius along the vertical section of the flask, resulting in 0.0425m (see Appendix A for numerical explanation).

Each light condition is obtained as the weighted average of the light intensities measured at different points of the flask covering the external flask area, as shown in Fig.3.4.

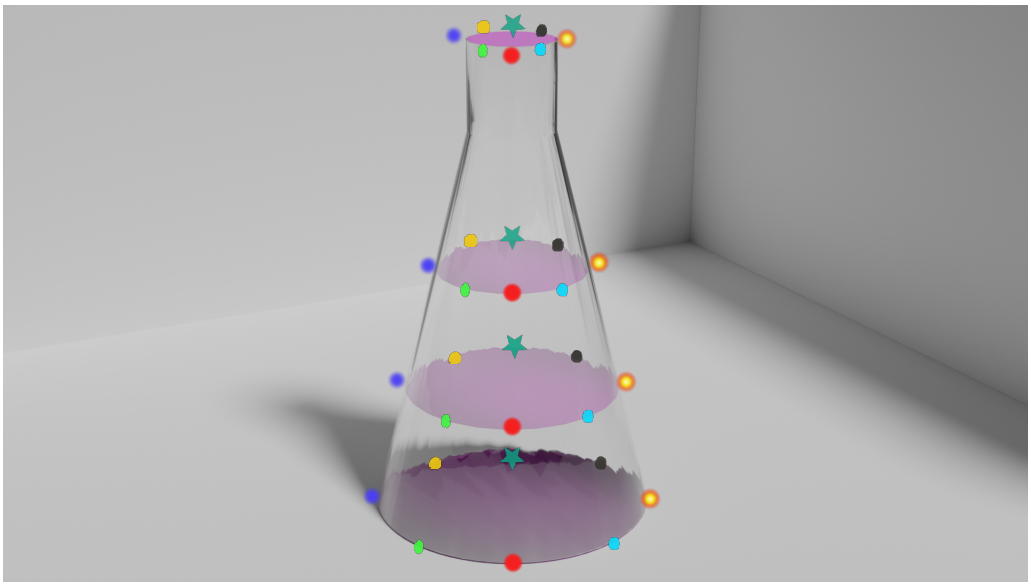

Figure 3.4: Measurement points of the incidence light on the external surface of the experimental flask.

Eight vertical sections can be recognized (characterized by different point colors), each one divided into four measurement points. The average light intensity of the four points for each section is calculated, thus obtaining eight light intensities representative of the eight sections. In order to define a unique irradiance value it is not correct to assign the same weight to all the eight intensities.
The weights assigned to each section are relative to the average intensity measured in that vertical section compared with the total intensity reaching ideally one single microalga in a full rotation along the surface of the flask. The total intensity is the sum of all the eight intensities around the flask. It can be easier to understand visually by the following picture (Fig.3.5):

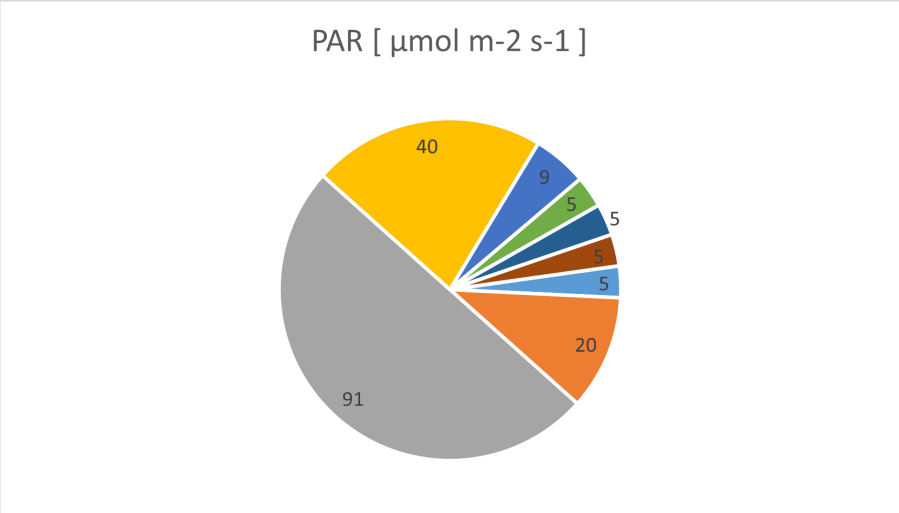

Figure 3.5: Average incident light intensities along the circular flask surface for each vertical section. Example taken from the two lamps experimental condition.

Due to the disposition of the LED lamps in the flask experimental area, shaped like "L", the light irradiance is not equally distributed around the flask. In the example in Fig.3.5, taking into consideration a microalga rotating at constant speed along the flask surface, it would be subjected for most of the time to a light irradiance of 90 µmol/m^2/s and 40 µmol/m^2/s, while just for a shorter time to lower values. Giving the same weight to all the sections would bring misleading values, usually showing a lower intensity with respect to the real one. For this reason, each intensity is weighted according to the actual exposure time to that intensity, evaluated as the ratio between the single one and the total sum of the irradiances along all the rotation period. A numerical example is provided in Tab.3.1, referring to the 2 lamps condition (all the measurements are in µmol/m^2/s).

Eventually, for the experimental phase, five light scenarios are obtained: 60, 110, 140, 195, 250 µmol/m^2/s.

Table 3.1: Eight vertical sections (columns) and four horizontal sections (Top-Base) can be recognized. The total light irradiated is the sum of the average light calculated for the eight vertical sections. Weight factors are the ratio between each average light and the total one. The average light condition corresponding to 2 lamps condition is 60 µmol/m^2/s, measured as the sum of the products between the average light on the vertical section and the relative weight.

#lamps-side	2-red	2-green point	2-blue point	2-yellow	2-green star	2-black	2-orange	2-light blue
Top	4,54	26,81	80,44	45,38	12,38	4,54	4,54	4,54
1000ml	4,95	22,69	99,00	41,25	8,25	4,95	4,95	4,95
700ml	5,78	18,56	103,13	43,31	8,66	5,78	5,78	5,78
Base	6,60	11,14	82,50	30,94	8,25	6,60	6,60	6,60
Aver. light, vert.	5,47	19,80	91,27	40,22	9,38	5,47	5,47	5,5
Total light	183							
Weights	0,030	0,108	0,500	0,220	0,051	0,030	0,030	0,030
Av.light	60,00							

3.1.2. Growth medium

The selection of a suitable growth medium is fundamental in order to guarantee a correct and fast development of the microalgae culture. The growth medium is, by definition, the aqueous solution in which the biomass suspension thrives thanks to the presence of the nutrients required for its development.
In the research field at lab-scale, different types of mediums are adopted. They can be created synthetically in the laboratory according to a desired chemical composition. Alternatively, flows extracted from different sections of the treatment line of a real wastewater treatment plant can be used.

In the present work, two types of medium have been tested in order to establish which one allows the fastest and most reliable growth of biomass. The first medium tested is synthetic wastewater, whose recipe is taken from [9] adapting the test No. 201: Alga, Growth Inhibition Test, 2006, OECD guidelines. The resulting macronutrients have been measured by Smartchem 200 and their values are shown in Tab.3.2. The resulting concentrations are coherent to the expected ones.

For what concerns to the presence of micronutrients, the mentioned recipe already accounts for them in the following concentrations [9]: $CaCl_2 \cdot 2H_20$, 37.67 g/m^3; $FeCl_3 \cdot 6H_2O$, 17.16 g/m^3; H_3BO_3, 1.72 g/m^3; $CuSO_4 \cdot 5H_2O$, 0.15 g/m^3; KI, 0.25 g/m^3; $MnCl_2 \cdot 4H_2O$, 1.02 g/m^3; $Na_2MoO_4 \cdot 2H_2O$, 1.07 g/m^3; $ZnSO_4 \cdot 7H_2O$, 4.21 g/m^3 and $CoCl_2 \cdot 6H_2O$, 0.66 g/m^3.

Table 3.2: Macronutrient composition of synthetic wastewater.

Substance	Concentration
NH4 mgN/l	22.9
PO4 mgP/l	5.61
NO3 mgN/l	1.92
NO2 mgN/l	0
SO4 mgSO4/l	296

It is assumed that there is no presence of suspended solids in the synthetic wastewater and a negligible level of biodegradable organic matter. Thus, heterotrophic bacteria can not survive. Moreover, in the medium is added allylthiourea (ATU) with a concentration of 10 mg/l inhibiting ammonia-oxidizing bacteria (AOB) formation. So, there is no need for inhibition of nitrite-oxidizing bacteria (NOB) by $KClO_3$ since the feeding synthetic wastewater does not contain nitrite.

The second medium tested is permeate from the anaerobic membrane bioreactor (An-MBR) pilot plant in "Cuenca del Carraixet" Waste Water Treatment Plant (WWTP), Valencia, Spain.
The permeate extracted from the membrane has origin from a digestate of an anaerobic digestion, for this reason, it is rich in nitrogen and phosphorus but also in hydrogen sulfide.

The first action to be taken is to operate aeration for some hours of the collected permeate in order to oxidize hydrogen sulfide to sulfate. Indeed dissolved H_2S is recognized to be an inhibitor to oxygenic photosynthesis [65] and must be removed through oxidation to ${SO_4}^{2-}$.
The chemical analysis conducted to characterize the permeate reported a complete absence of total suspended solids (0 g_{TSS}/l) following the membrane. Moreover, the results indicated a very low concentration of organic matter both in terms of chemical oxygen demand (94 g_{COD}/l) and of biodegradable oxygen demand (68.4 g_{BOD}/l) thanks to the previous anaerobic digestion. The alkalinity is around 540 mg_{CaCO_3}/l. The micronutrients are assumed to be always abundant and they do not constitute a limiting factor for the microalgae growth.
Concerning the nutrient concentration, the medium is rich in terms of nitrogen and phosphorus. In order to maintain in the feeding permeate a minimum constant concentration of N and P during the experimental and maintenance operations, minimum concentration levels are set. In this way, even if the feed shows variability of nutrient abundance during

the time, it can be guaranteed always a minimum concentration. The nitrogen value is set at 40 mg_N/l, and the phosphorus one at 6 mg_P/l. These wanted concentrations of N and P are reached by the addition of NH_4Cl and KH_2PO_4, respectively.
As made with the synthetic wastewater, ATU (10 mg/l) is added in the solution in order to avoid the growth of AOB, and consequently of NOB as the nitrite NO_2^- concentration already present in the permeate is negligible (always around 0.012 mg/l). The chemical composition of the permeate feeding the bioreactors is shown in Tab.3.3.

Table 3.3: Macronutrient composition of AnMBR permeate.

Substance	**Concentration**
NH4 mgNH4/l	13
PO4 mgPO4/l	1.8
NO3 mgNO3/l	1.9
NO2 mgN02/l	0
SO4 mgSO4/l	296
TSS mg/l	0
COD mgCOD/l	94
BOD mgBOD/l	68.4

3.2. Experimental design

The experimental design is a fundamental step in the research activity. It aims to set the values of the different input parameters involved in the microalgal model. In the present work, the input variables that can be regulated in the experimental tests influencing the system response through the model are pH, light intensity and biomass concentration.
The number of values associated with each variable defines the total number of combinations that are tested. For this reason, it is important to choose the values not only with a theoretical logic but also considering the time-resources consumption needed for performing the tests. As a rule of thumb, the selection of the variable levels is based on the literature review and on practical experience.
In the following sections, the choices made for each variable in PBR and flask configurations are explained. The initialization of the PBRs is explained. Moreover, the experimental procedure adopted during the calibration and validation phases in the flask is described, together with the model assumptions made.

3.2.1. PBR operation

The pH values that are investigated must be chosen in order to cover a reasonable range of values of interest. In this way, they have been selected according to the evidence from the literature (see section 2.1.3) and three levels have been chosen: 7.0, 8.0, 9.0. This range of values appears to be adequate to analyze the microalgae dynamics so that the final response model can fit in their predominant growth conditions.
It is fundamental to note that the mentioned values are only ideally the starting pH value for the tests performed in the calibration. Indeed, during the practical work, it is complex to maintain a very stable pH value as the starting value of the test. The oscillation can derive from the carbon dioxide injection that acidifies the solution or from the difference between the pH meter used continuously in the reactor and the one adopted during the alkalinity determination operation.

The artificial light is provided by five lamps for each PBR. The light intensity has been calculated around 300 µmol/m^2/s.

The biomass concentration is assessed in terms of TSS and it influences the light irradiance of the culture due to the shading effect. Unlike the pH, the setting of biomass concentration values is less related to technical aspects and optimal literature levels.

As a matter of fact, the selection of appropriate levels of values is dependent on the maximum value of concentration that the reactor can achieve in the long term. This value is considered the one that is measured when the microalgae culture reaches stationary conditions in the reactor.
As explained more in detail later in the results section 4.1, steady-state conditions are reached when the concentration of total suspended solids daily measured shows a variation lower than 10% for at least 3 consecutive days [30], taking into account a certain tolerance toward the unavoidable experimental and casual errors.
The result of the experimental activity that aims to determine the optimal growth medium between permeate and synthetic wastewater is anticipated, resulting the permeate one. With this medium feeding and the reactor operating at a constant pH of 7.5, the maximum concentration reaches almost 500 mg_{TSS}/l. In order to obtain concentrations easily achievable in the reactor in real operating conditions, three levels are set: 300, 200, 100 mg_{TSS}/l.
The biomass during the experimental phase most of the time presents a concentration of total suspended solids higher than 100 or 200 mg/l, sometimes even 300 mg/l (Fig.4.7b). In these conditions, a reduction by dilution of the suspension is needed to match the assay concentration. The dilution is made by adding a certain volume of permeate to the original tested culture. The dilution changes the initial chemical composition of the tested culture in terms of nutrients and alkalinity, but this aspect is not relevant since the relevant factors for the assay are the biomass concentration and the initial pH. The pH value of the added permeate is modified to the bioreactor level before the addition. If it needs to be acidified, CO_2 injection is made, in case it is basified, NaOH is dosed.

Once the equipment has been set up, it is started the actual cultivation phase. Microalgal inoculum is taken from WWTP in Cuenca del Carraixet, Valencia, Spain. Specifically, the sample of water with the presence of microalgae is extracted from a section between secondary settlement and tertiary treatment.
The carbon dioxide intake is provided by switching on the electrovalve when the monitored pH is below the desired value set in the control software.

After that the algal inoculation is placed, the start-up of the PBR is done. This step is a transient phase in which the reactor is operated in batch for a week in order to increase the biomass concentration. Following this first phase, the reactors are operated in fed-batch mode according to a specific biomass retention time (BRT). In the scenario here presented the BRT is equivalent to the hydraulic retention time (HRT) since there are no systems for decoupling the two times. In this operative mode, a constant and reliable

daily supply of new clean feed is required.
The hydraulic retention time selection is based both on the literature review and on the practical limitations of feeding medium supply frequency. In the section 4.1 two options of medium to be adopted are described. From the literature review, it has been observed that shorter BRTs boost the growth of the fastest microorganisms [125], which can favor bacteria growth over microalgae [44]. Microalgae have been found to be favored over NOB at mid-range BRT values comprised into a range of 2-4.5 days for an outdoor flat-panel MPBR system treating AnMBR effluent [44]. Anyway, in the present work bacterial presence is avoided by the inhibition by ATU in the medium. It has been noted that permeate after a couple of days starts to degrade, forming particulate suspension and losing nutrients. Furthermore, the supply from the WWTP where is placed the AnMBR pilot plant can not be ensured on a daily basis. As a result of the mentioned reasons, it is chosen a BRT (HRT) of 4.5 days over a week. From this value, knowing that the chemostat solution volume is 7 liters, the daily flow purge rate can be calculated, corresponding to 1.45 l/d.
However, the previous HRT takes into consideration seven days of operations, while the actual working days in a week are only five. Thus, the purging flow rate is then corrected by a factor that is the ratio between the week days (7) and the operative ones (5), resulting in a purge volume of 2 l/d.
As a rule of thumb, the acclimatization time required for the biomass to thrive is around three times the HRT value [29]. Then, it is possible to start the test experimental phase once the PBR achieves steady-state conditions. The principle adopted to define when steady-state conditions are reached states that the biomass concentration in TSS must show a variation lower than 10% for at least three consecutive days [30].

In order to assess the most suitable growth medium, the measurements of TSS and optical density (OD) are performed two times per day, at the beginning and at the end of the day, for each reactor. For the first three days after the feeding of 7 liters in the chemostat, purging is not operated. Then, a weekend of no operations is included, so the reactors operate in batch for five days. For the next five days, the purge and feed of 2 l/d according to the selected HRT is operated. In the next chapter, the procedure and the results of the selection of the growth medium fed to the chemostats are described.

The ecological composition of the culture is the same in both reactors at any time of the experimental activity but some variations are observed by changing the operating conditions. At controlled pH values between 7 and 8, the algal community shows a predominance of Chlorella sp. over Scenedesmus sp. The opposite occurs when the tests

at higher pH are performed, around 9. Indeed, when the pH is not limited by CO_2 and it is let increase to higher values, it has been observed a switch of proportion with a greater abundance of Scenedesmus sp. than Chlorella sp. (Fig.3.6). At pH around 8.7, after two days of no CO_2 insufflation but only operating purging/alimentation, a replacement of Chlorella sp. with Scenedesmus sp. occurred, with a proportion around 1:4. This result is valorized in other studies conducted at laboratory scale, where it has been observed that at higher pH, around 9, Scenedemsus sp. fits better than Chlorella sp. [132]. However, the reasons for a shift in the culture's ecological composition are not confirmed, and a unique cause that can explain the phenomenon has not been identified. According to what has been observed in the experimental activity, other causes could be constituted by a change in the chemical composition of the feeding permeate or a rapid switch of feeding medium representing a shock for a strain of algae but not for the other one.

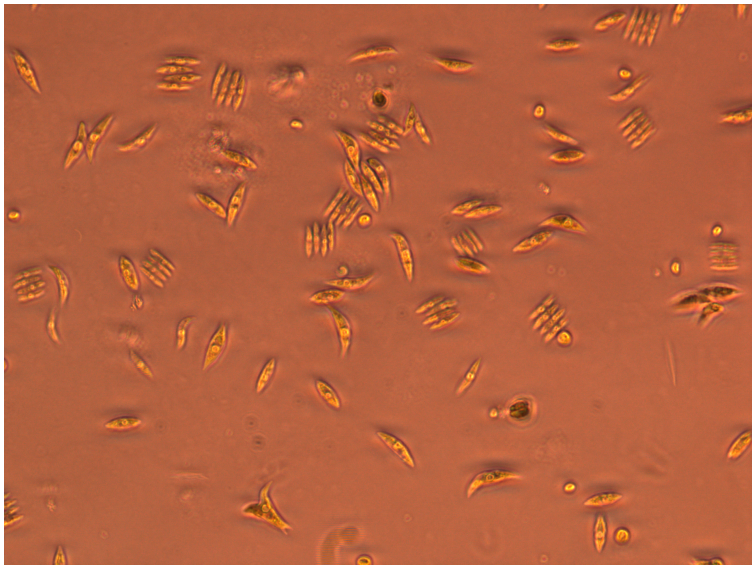

Figure 3.6: Ecological abundance in the culture at alkaline pH, showing a majority of Scenedesmus over Chlorella. Image obtained by fluorescence Leica DM2500 microscope, 40X.

3.2.2. Batch tests operation

In this section, the operations operated during the batch tests are explained.

In the calibration and validation phases, the flasks are placed under five PAR conditions: 60, 110, 140, 195, 250 µmol/m^2/s, equivalent to 2, 3, 4, 5, 6 LED lamps switched on, respectively.

The model components to be experimentally determined are $S_{Ig,C}$, $S_{H_{TOT}}$, S_{NH_X}, S_{PO_4} and S_{O_2}.
The determination of these variables is based on an experimental procedure composed of different steps. The procedure is the same for all the tests performed, in calibration, for the replicas and in the validation phases.

The desired pH level in the reactor is set by means of the Microsoft Visual Studio control software regulating the electrovalve switching on/off for CO_2 bubbling. From R1 is extracted a certain quantity of culture and it is used to fill the test flask. If the biomass concentration (assessed by the permeate curve TSS-OD) is already equivalent to the one set in the test boundary conditions, 1 liter of culture is extracted. Otherwise, if the concentration is higher, a dilution of the solution is operated by the addition of feeding permeate characterized by the absence of solids (section 3.2.1). In this case, the culture quantity utilized is less than 1 liter, since the permeate addition is calibrated depending on the reaching of the desired TSS value in 1 liter of solution. The flask characterized by the desired pH and TSS is then stirred magnetically and placed under the wanted light intensity regulating the number of lamps switched on.

Once the flask is filled, the first step is the measurement of the pH value in the flask sample. Then a pre-filtration of fine solid particles from liquid solution with a paper filter is operated in order to guarantee easier filtration later. So, 20ml of pre-filtrate is again filtrated through a filter with 0.45 µm pore size (SFMC-245-100 Branchia) and this sample is then analyzed by ion-exchange chromatography. It is determined the ionic composition in terms of Na^+, $NH_4{}^+$, K^+, Mg^{2+}, Ca^{2+}, Cl^-, $NO_2{}^-$, $NO_3{}^-$, $PO_4{}^{3-}$, $SO_4{}^{2-}$, $S_2O_3{}^{2-}$ [ppm].
From the pre-filtrate solution, a volume of 50ml is extracted in order to evaluate the alkalinity of the sample by titration method.

The remaining pre-filtrate is stored as a backup in case of any failure in the chromatography operations or in the alkalinity method, in case of repeating the procedures. If the results are considered good, the backup is then thrown.
Each test point is now characterized by an ionic composition, a pH value, and an alkalinity value. Following the simulation procedure described in Fig.2.8, the ionic composition, pH, and alkalinity are input parameters to Visual MINTEQ 3.1, obtaining the chemical species such as S_{CO_2}, S_{O_2} and free ammonia nitrogen S_{NH_3}. Then the biological model is run, giving the model components of interest $S_{Ig,C}$, $S_{H_{TOT}}$, S_{NH_X}, S_{PO_4} and S_{O_2}. S_{PO_4} and S_{NH_4} are directly measured from the chromatography while S_{NH_X} is the sum of am-

monium and free ammonia nitrogen. The oxygen component is the same computed by the chemical model.

The main aim of the present work is to identify updated values of three model parameters present in the microalgae model published by Viruela et al. [117].
These three parameters are:

- μ_{ALG} maximum growth rate of microalgal biomass
- $K_{S,H}$ half-saturation constant for free proton concentration S_H
- $K_{I,H}$ inhibition constant for free proton concentration S_H

The first parameter μ_{ALG} is present in the kinetic process 1 relative to the growth rate of microalgae in a phosphorus-replete medium. $K_{S,H}$ and $K_{I,H}$ are constants related to the pH factor f_{pH} developed as a combination of a Monod kinetic and an inhibition function as explained in section 2.2.2.

$$\mu_{ALG} \cdot \frac{S_{Ig,C}}{K_{Ig,C}+S_{Ig,C}} \cdot \frac{S_{NHX}}{K_{NHX}+S_{NHX}} \cdot \frac{S_{,PO4}}{K_{PO4}+S_{PO4}} \cdot X_{ALG} \cdot f_L \cdot f_{pH} \cdot f_T$$

$$f_{pH} = \frac{\frac{S_H}{S_H+K_{S,H}} \cdot \frac{K_{I,H}}{S_H+K_{I,H}}}{\frac{S_{H,opt}}{S_{H,opt}+K_{S,H}} \cdot \frac{K_{I,H}}{S_{H,opt}+K_{I,H}}}$$

In order to simplify the study, some assumptions have been made about the model processes and components.
Within the algal model, recalling the model processes reported in Tab.2.5, only some of them are considered during the experimental phase.
The variables involved in the actual research are $S_{Ig,C}$, $S_{H_{TOT}}$, S_{CO_2}, S_{NH_X}, S_{PO_4}. In particular, S_{CO_2} and S_{NH_3} (that is in equilibrium with measured S_{NH_4}) are input variables in the processes that involve $S_{Ig,C}$ and $S_{H_{TOT}}$. The biomass concentration value (X_{ALG}) set as the boundary condition of the assay is considered constant throughout the experimental assay, due to the relatively short assay period.
Moreover, reasonable simplifying assumptions can be done and the following processes are neglected in the microalgal model:

- Process 2 and process 4: nitrate NO_3^- concentration is considered negligible (always around 1 mg/l) and ammonium NH_4^+ is assumed to be the only nitrogen source for microalgae.

- Process 3 and process 5: the phosphorus source is represented only by orthophosphate from the liquid phase since luxury uptake conditions are considered and the cultivation is performed with an excess of phosphorus concentration (>0.5 mg_P/l). Since the medium conditions are always P-replete, microalgae do not consume accumulated polyphosphate.
- Process 7 and process 8: lysis of algal cells does not occur because of the relatively short time needed during the assay execution.

Eventually, the processes that are taken into account in the present work are processes 1, 6, 9, 10, 11.

Calibration design

A dynamic calibration is performed by adjusting the simulated data of pH, alkalinity and S_{NH_X} to the experimental ones. A global constrained optimization was conducted using a genetic algorithm in MATLAB R2021a (Appendix B.1). The objective function to be minimized by the standardized residuals technique is shown below, where X_{SIM} and X_{EXP} are the simulated and experimentally three variables, and i is the index of the measured data.

$$\sum_{i=1}^{n}\left(\sum \frac{|X_{SIM\,i} - X_{EXP\,i}|}{\sqrt{\text{std}(X_{EXP\,i})}}\right)$$

Ponderation factors were not applied in the calibration phase. As mentioned before, the variables chosen in the objective function are the alkalinity, pH and S_{NH_X}. Their choice has been made because pH and alkalinity are directly measured experimentally so we can assume that they embed a lower error than other experimental model components derived from the simulation of the chemical or biological models. S_{NH_X} is an experimental variable as well as a model component, so it suits good to be used as an optimization factor. Another variable directly measured is S_{PO_4}. However, phosphorus is not included because the measure of total P has not been done (only dissolved orthophosphate) and Viruela algae model does not consider phosphorus precipitation.

For the calibration phase, all the parameter values within the processes are the ones reported in Fig.A.1 in Appendix A but the value of $K_{La,CO2}$, that is experimentally obtained. Moreover in the optimization operation, as first attempt values for the three target parameters (μ_{ALG}, $K_{S,H}$, $K_{I,H}$) the values in Fig.A.1 have been adopted.

The determination of the specific mass transfer coefficient $K_{La,CO2}$ has started from the assessment of $K_{La,O2}$. As a first step, it has been performed a continuous measurement of the dissolved oxygen (DO) in the experimental flask filled with deionized water with magnetic stirring at 200 RPM in order to evaluate the oxygen decreasing in one day. It is assumed that oxygen consumption is due to only stripping phenomena since adding allylthiourea to the water avoids nitrifying bacteria presence in the liquid phase. From the linearization of the experimental DO trend in the time, $K_{La,O2}$ is determined as the slope. To determine the carbon dioxide coefficient, $K_{La,O2}$ is related to the ratio between the gas diffusivities of carbon dioxide and oxygen in the reference conditions (temperature and viscosity).

$$(K_{\mathrm{L}}a)_{\mathrm{CO_2}} = (K_{\mathrm{L}}a)_{\mathrm{O_2}} \sqrt{\frac{D_{\mathrm{CO_2}}}{D_{\mathrm{O_2}}}}$$

According to what is described in chapter 3.2, the external conditions set for every assay are pH, light intensity and biomass concentration. In the calibration process, each variable assumes different values (Tab.3.4):

- selected pH values are around 7.0; 8.0; 9.0
- selected light intensities are 60; 110; 195; 250 µmol/m^2/s
- selected algal concentrations are 100; 200; 300 mg_{TSS}/l

Table 3.4: Boundary conditions of every experimental test performed in flask during the calibration phase.

pH	Biomass concentration [mg/l]	Light intensity [PAR]
7	300	60
		110
		195
	200	60
		110
		195
	100	60
		110
		195
8	300	60
		110
		250
	200	60
		110
		250
	100	60
		110
		250
9	300	60
		110
		250
	200	60
		110
		250
	100	60
		110
		250

The total number of experiments in the calibration phase is 27, working with replica 54

assays are totally performed.
Regarding the pH, the three values are only indicative since it is complex to maintain the initial pH value of each assay so close to the reference value, as explained previously in section 3.2.1.

Validation design

The validation procedure is necessary to evaluate the goodness of the calibrated parameter values. By comparing the simulated and experimental variables, it is possible to assess the quality of the model parameters obtained.
Similarly to what was done in the calibration phase, the validation procedure takes into account the three variables pH, alkalinity and S_{NH_X}, each one for the five-time sampling points, using them to study the validation performance.
In order to guarantee optimal conditions of validation, the assays are performed under boundary conditions different from the calibration ones. Moreover, the tests are not done with replicas, except one with the presence of cyanobacteria. A total of eight tests are executed, showing as boundary conditions different levels. As biomass concentrations are set levels of 100, 125, 225, 300, 400, 475, 550 mg_{TSS}/l; the pH values are 7, 7.5, 8, 9; the incidence light values are 140 and 195 µmol/m^2/s. Overall, 40 observed pairs for each variable are obtained.
In order to speed up the workings, the validation process has been performed using both bioreactors in parallel, neglecting the backup reactor precaution. The purging is not performed for the last assays so that the higher biomass concentrations can be achieved. The carbon dioxide system for pH regulation is switched off for R1, increasing the pH up to 9, while R2 is still controlled at the desired pH level by providing carbon dioxide. Validation experiments have been done entirely after the calibration phase, so the algal strain composition of the culture is prevalently composed of Scenedesmus rather than Chlorella (Fig.3.7).

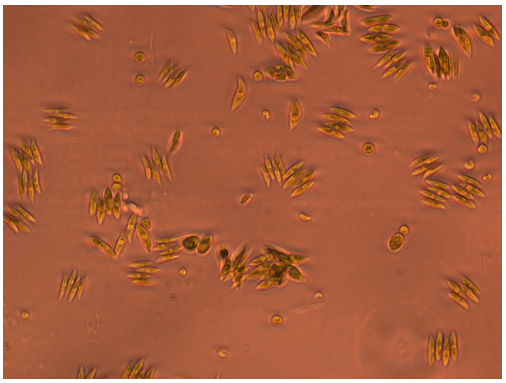

Figure 3.7: Ecological composition of the culture observed in the validation period, showing a prevalence of Scenedesmus over Chlorella sp. Image obtained by fluorescence Leica DM2500 microscope, 40X.

As done previously in the calibration, computationally the simulation of the modeled results is operated using the MATLAB code developed for the microalgal modeling (B.2), adopting the calibrated parameters.

3.3. Data processing

In this section the software, the codes and the procedures used to process the experimental collected data are described.

The Valora software has been developed within CALAGUA group and it computes the alkalinity. It needs as input the N-ammonium concentration, P-orthophosphate concentration, temperature, and the cumulated volumes of acid solution associated to the five titration pH values. The program elaborates alkalinity as the sum of the inorganic carbon species (bicarbonate, carbonate), hydroxyl ions, ammonia, and weak acid ions (phosphate, borate, sulphide...). Eventually, the alkalinity of the sample is determined in the form of mg_{CaCO_3}/l.

The speciation model used in the microalgal model is Visual MINTEQ 3.1 and it is integrated into the MATLAB code reported in Appendix B.2. By its running the chemical species are computed by working on the chemical equilibria, taking into account charge balances, acid-base and redox reactions, and mass balances. The total set of chemical species considered in MINTEQ software can be found in Appendix B of the BNRM2 model description [12]. Starting from the computed chemical species, the ionic composition, pH, and alkalinity, the calibration is performed.

Calibration process

The variables that must be experimentally determined ($S_{Ig,C}$, $S_{H_{TOT}}$, S_{CO_2}, S_{NH_X}, S_{PO_4}) are calculated according to the experimental procedure already exposed in section 3.2.2. Differently, the model components are $S_{Ig,C}$, $S_{H_{TOT}}$, S_{NH_X}, S_{PO_4} and S_{O_2}. From the tables reported in Tab.2.5 and Tab.2.6 and the stochiometric coefficients reported in Appendix A, the differential equations relative to the five modeled variables (3.1) can be found:

$$\begin{cases} \dfrac{\partial S_{H_{tot}}}{\partial t} = p_1 v_{6,1} + p_6 v_{6,6} + p_9 v_{6,9} \\ \dfrac{\partial S_{ig,C}}{\partial t} = p_1 v_{5,1} + p_6 v_{5,6} + p_9 v_{5,9} \\ \dfrac{\partial S_{NH_X}}{\partial t} = p_1 v_{2,1} + p_6 v_{2,6} + p_{11} v_{2,11} \\ \dfrac{\partial S_{PO_4}}{\partial t} = p_1 v_{4,1} + p_6 v_{4,6} \\ \dfrac{\partial S_{O_2}}{\partial t} = p_{10} v_{1,10} \end{cases} \tag{3.1}$$

where p_j and $v_{i,j}$ are the general process and stoichiometric coefficient, and j is relative to the process while i to the model component (see Tab.2.6). Solving discreetly the equations reported above determines the value of each variable in every time instant in which the experimental period is divided. The time discretization is operated according to a time instant set long 0.001 days (0.024h). Recalling the simulation procedure in Fig.2.8, the model components are calculated starting from their initial values at t=0 measured in the experimental phase for each assay. At the same time, the three parameters to be calibrated assume as initial values the old ones indicated in the table in Appendix A.1. The code operating the simulation of the model components and of the three variables in the optimization function (pH, alkalinity, S_{NH_X}) is entirely reported in Appendix B.2, solving both the chemical equilibria (MINTEQ) and the kinetic processes iteratively. Thus, from the simulation of the speciation and biological models, the model components of interest are obtained, as well as the simulated values of pH and alkalinity.
Finally, for each assay, are selected the simulated variable values associated with the five times at which have been obtained the experimental results, namely at t=0.0d; 0.041d; 0.083d; 0.166d; 0.208d. For every pair of experimental and simulated variables, is then calculated the standardized residuals. Finally, the previously described objective function to be minimized is defined (calibration design section 3.2.2), and it is run by the code in Appendix B.1.

Before going on with the calibration process, a focus on the experimental calibration dataset is done. In this way, a cleaning of the data is performed. The criteria adopted is to exclude all the assays that qualitatively show strong anomalies in their trends compared to the expected ones. In total, four tests have been removed, passing from 27 to 23 tests. The uncertainty of the experimental results can be explained by experimental errors related to manual and equipment operations. In particular, the Moosbrugger titration method shows criticalities due to the use of two different pH meters and the manual operation itself. Moreover, ionic chromatography happened to fail to provide non-reliable data, especially on phosphate content, so a re-analysis of the sample is needed with the backup sample. Finally, it has been decided not to consider in the calibration dataset the tests performed in the presence of cyanobacteria. Indeed, this type of culture is too different from the reference one adopted in this experimental work, which is composed of autotrophic green microalgae. The biological dynamics involved with cyanobacteria are completely different, showing experimental results not expected, so the model here studied is not suitable to describe their behavior.

The MATLAB genetic algorithm used to calibrate the parameters operates a multi-parametric optimization working similarly to an ordinary least squares method. The main difference between the two methods is that the genetic algorithm finds the global minimum point of the objective function to be minimized reported in section 3.2.2. This code is fully reported in Appendix B.1 whose theoretical description is here shortly reported.
Without going into details, the genetic algorithm function needs in input an objective function and a certain number of design variables. The selected experimental and simulated variables are pH, alkalinity and S_{NHx}. The objective function to be minimized is defined as the sum of the summation of standardized residuals of the variables involved, below reported.

$$\sum \frac{|pH_{sim} - pH_{exp}|}{\sqrt{std(pH_{exp})}} + \sum \frac{|Alk_{sim} - Alk_{exp}|}{\sqrt{std(Alk_{exp})}} + \sum \frac{|S_{sim,NHx} - S_{exp,NHx}|}{\sqrt{std(S_{exp,NHx})}}$$

From the minimizing of the objective function the three parameters of interest are calibrated.

Validation process

First of all, is operated a data cleaning of the experimental results of the validation. Indeed, like what was done in the calibration, from the useful dataset all the assays showing an untypical trend and the presence of cyanobacteria have been removed. Thus, from the previous 40 pairs of observations for each variable, the dataset is reduced to 25. Considering the three variables used to validate (pH, alkalinity, S_{NH_X}), totally are available 75 paired samples.
Once the 25 pairs of experimental-simulated variables are obtained, a statistical analysis of the results is carried out.
Two-sample t-test, paired t-test and scatter plot are used to assess the goodness of the final calibrated parameters. All the tools are performed in R v.4.3.1 environment and the relative code is reported in Appendix B.3.
The two-sample t-test (or independent samples t-test) is a method used to test whether the sample means of two groups are significantly equal or not. It is a rough method to assess if two populations can be statistically similar since it does not focus on the close relationship between the two samples in terms of a single data pair. To solve this lack is adopted also a paired t-test.
The paired samples t-test is a parametric test whose purpose is to determine whether

there is statistical evidence that the mean differences between the paired observations is significantly different from zero.
This type of test can be applied only if a series of assumptions concerning the datasets are satisfied.

1. Are related samples (dependent observations)? Yes, since the subject variables in each group are the same.
2. Are the two groups samples actually paired? Yes, the data are paired since the two variable values are collected at the same boundary conditions both in the experimental and simulated ones.
3. Is a large sample? The numerousness of the dataset is important to assess the next hypothesis regarding the differences normal distribution. Since the sample size is 75, it is large enough (i.e. n>35) and we would not need to check whether the differences between the pairs follow a normal distribution, we could assume they do. Anyway, this check is operated.
4. The differences between the paired values must show approximately a normal distribution.

In order to check the rough normality of the paired data differences, graphic instruments such as the Q-Q plot and the boxplot are used.

Like all the statistical tests, paired t-test defines a null hypothesis and an alternative one. The null hypothesis states that the difference between the paired group means is equal to 0, while the alternative one is that the difference between the paired dataset means is not 0. It is assumed a confidence interval at 95% (complementary an $\alpha = 0.05$). If from the test results a p-value > 0.05, it implies that the null hypothesis is verified, so the samples are significantly similar and the parameters are well calibrated.
T-test provides several informations. First of all, it finds the experimental data mean and the modeled one. This test also constructs confidence intervals for each mean and the difference between means. The confidence interval of the difference between the means is of particular interest because it indicates if there is a significant difference between the means of the two data samples, with a confidence level of 95%. The closer it results to 0, the more similar are the two data samples.

It is very important to note that boxplots and QQ-plots adopted to check the normality

of the differences, as well as the scatter plot of the paired observations, are expressed in normalized values. The data both experimental and simulated have been normalized with respect to each variable. Consequently, the differences result normalized. Basically, the analysis is operated on two datasets (experimental and simulated) composed of three subgroups equivalent to the three variables. This step is necessary because the three considered variables are very different from a magnitude perspective. Alkalinity is expressed as hundreds, NHx as tens, and pH as units. Thus, it is necessary to standardize to make the three datasets homogenous and avoid the formation of three data clusters characterized by different magnitudes.

4 | Results

In this chapter the results derived from the operations of the photobioreactors and of the flask tests are described.

4.1. PBR operation results

In this section, the results of the operations made on the PBRs are presented. The observed trends of different parameters are shown, as well as the results of the growth medium selection and of the biological composition of the culture.

Recalling section 3.1, the culture mixing method influences the oxygen saturation in the reactor. Indeed, it is tested that with only air mixing (R1) DO is around 7,5 mg/l.
This value at 25°C is equivalent to an oxygen saturation level of 100% (there is equilibrium with ambient air). Differently, only mechanical stirring leads to a DO measured of 24±2 mg/l, equivalent to an oxygen oversaturation level of 300±30%. For this reason, it has been chosen to aerate also R2 to avoid oxygen oversaturation.

pH analysis
The pH value during the PBR maintenance is continuously monitored. The typical pH trend observed during the operations of the PBR is shown below in Fig.4.1.

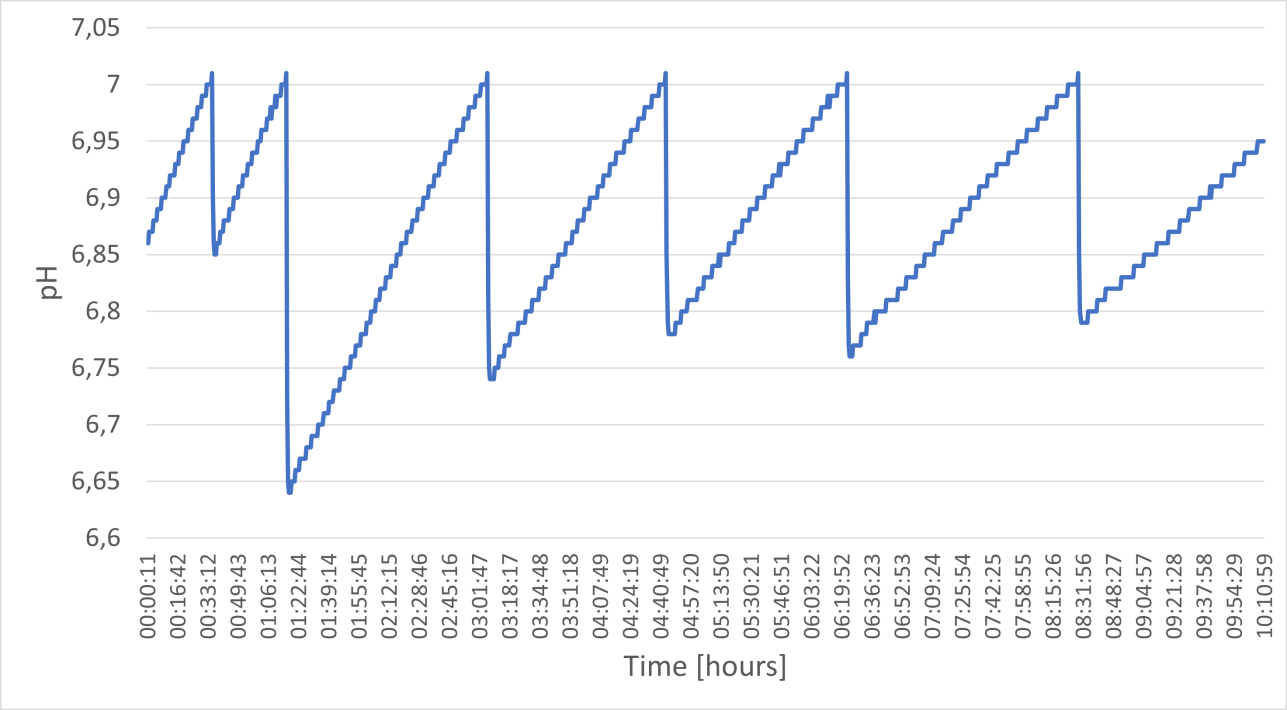

Figure 4.1: pH trend during the daily maintenance of the bioreactor. The reported scenario considers a period of approximately ten hours.

This trend describes the natural fluctuation of the pH since it increases due to the algal photosynthetic activity and it is lowered by CO_2 bubbling. Carbon dioxide injection is activated by the control software (see section 3.3) when the pH overcomes the set value in the software. In Fig.4.1 this value is 7.
As mentioned in section 3.2.1, the initial pH values set as assay boundary conditions are ideally 7, 8, and 9. However, in the actual test operations, the initial values are only close to these levels. Possible reasons are the natural increase of pH and the switching from the pH meter monitoring in continuous the PBR to the punctual one used in the titration procedure, which are instruments showing different measurement accuracy. Below in Fig.4.2 a scatter graph of the pH initial points is reported, in which can be recognized the three areas corresponding to the three pH set values.

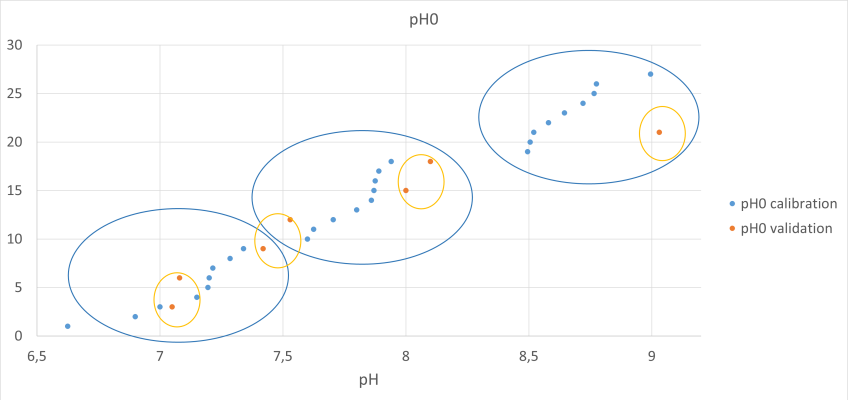

Figure 4.2: Scatter graph of the starting pH values. Blue circles correspond to the three pH clusters in calibration, the orange ones in validation.

As can be seen from Fig.4.2, pH values of 9 or above are very rare. Indeed, during the operations of the PBR without the addition of CO_2 to decrease the pH, the values almost never reach a level of 9. This aspect is unusual since with no control it is common that pH can be higher than 10 in some cases. An observed drawback is that at uncontrolled pH around 9, the formation of cyanobacteria colonies in the culture is enhanced (Fig.4.3). This aspect is coherent with the literature observations reported in section 2.1.3 where cyanobacteria thrive at high pH levels. The generation of cyanobacteria colonies must be avoided since tends to negatively affect all the microalgal community in the culture.

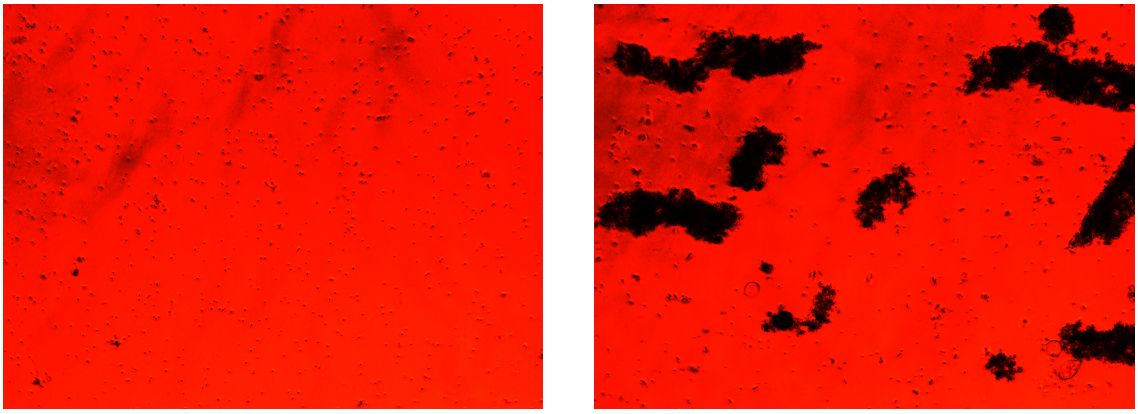

(a) At ph around 7, prevalence of Chlorella and Scenedesmus sp.

(b) At high pH around 9, cyanobacteria cause flocs formation.

Figure 4.3: Predominant algal strains in different pH conditions. Images obtained by fluorescence Leica DM2500 microscope, 10X.

Growth medium selection

The selection of the most appropriate growth medium is a key parameter for the successful cultivation of the microalgal culture. The main goal of the selection is to identify the solution that can offer the fastest growth of biomass and, at the same time, achieve a steady-state condition in terms of TSS, assumed represented only by the algal biomass.

R1 is tested using synthetic wastewater while R2 with the AnMBR permeate, maintaining a constant pH value at 7.5.

Recalling the method reported in section 3.2.1, the results of the comparison between the two growth media are now explained. Moreover, the calibration curve relating TSS-OD has been already presented in Fig.3.3., where the adjusted R^2 are reported too. It can be noted that the R^2 associated with the permeate scenario is higher than the synthetic one (0.97/0.71), thus providing a more accurate evaluation of the TSS by OD measurement.

The biomass response to the two media is evaluated, whose results are shown below in Fig.4.4.

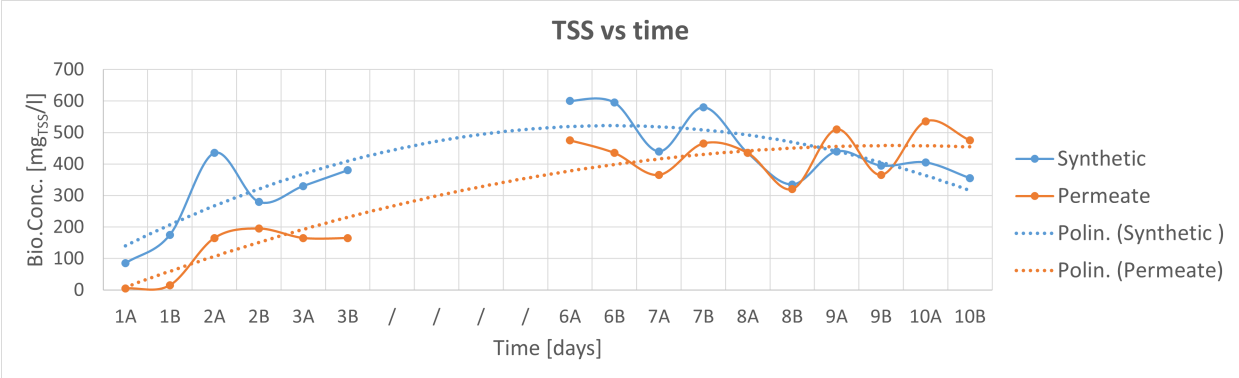

(a) TSS concentration trend in the time

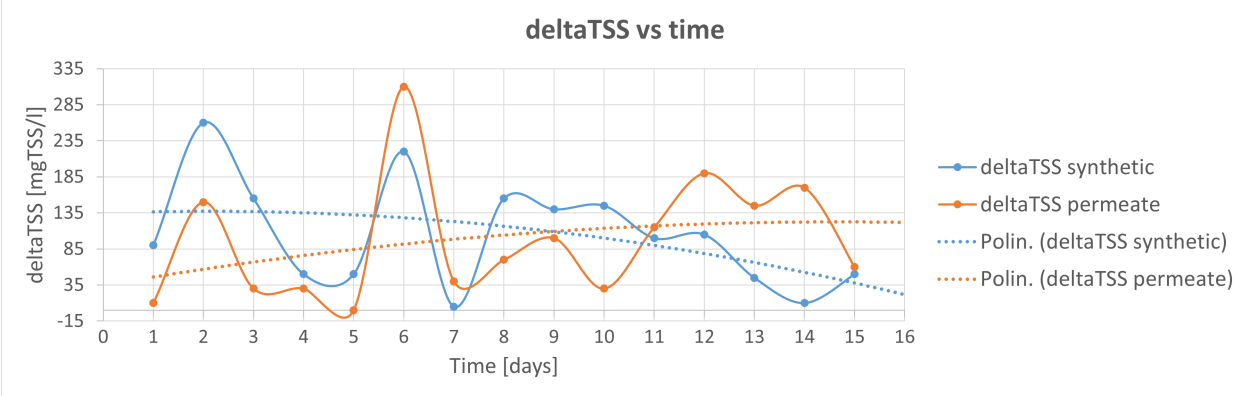

(b) TSS variation trend during the time

Figure 4.4: (a). The biomass concentration measured twice a day (A/B) over the time is shown. Time points on X axis signed with "/" correspond to a weekend where analysis is not done. (b). The variation of biomass concentration over the time is represented. Each point is calculated as the difference between the concentrations measured at t+1 and t, neglecting the weekend gap. Synthetic wastewater is in blue, permeate in orange. The polynomial trend lines are shown too.

In Fig.4.4a it can be seen that over the time the TSS concentration tends to a steady state condition for the PBR fed with permeate, while the one with synthetic wastewater presents a decrease although it reaches a higher maximum level of TSS. The TSS variation over the time shown in Fig.4.4b suggests that the permeate option guarantees a less steep trend of growth while constantly increasing up to a plateau. Instead, the synthetic option, after an initial period of no significant variation, shows a strong drop.
For the data previously described, the most reliable and performing growth medium is the permeate from the AnMBR pilot plant. Thus, this medium is adopted for microalgae cultivation from this point on.
There are two main drawbacks connected with the selected permeate. The first one is a

logistic one, concerning the frequency of supply of the material that depends on third-party availability. The second one is the dependence on the correct operations of the pilot plant. Indeed, if this equipment fails, the permeate output can not be guaranteed or the chemical quality can be negatively affected.

Biological composition

Regarding the biological composition of the culture, for most of the time, there was a prevalence of Scenedesmus and Chlorella strains. However, cyanobacteria formation occurred too.

Generally speaking, the formation of cyanobacteria colonies is an event that must be avoided since they tend to negatively affect all the microalgal community in the culture. Indeed, the main drawback is the formation of flocs based on the aggregation of microalgae around the filamentous structure of the bacteria. This results in a shadowing effect of the internal algae in the floc leading to their death. Moreover, flocculation tends to enhance the sedimentation of the biomass, hindering the light irradiance and promoting the appearance of grazers in the precipitated stagnant algal biomass. Eventually, a nitrogen accumulation can occur in the liquid medium which results toxic to algae. The causes of the accumulation are the reduced photosynthesis in the absence of proper light availability [131] (so reduced NH_4^+ consumption) and the simultaneous presence of cyanobacteria. Indeed, cyanobacteria's nitrogen sources are both the dissolved ones in the medium (nitrate, ammonium, urea) and the atmospheric nitrogen [49]. Thus, in part, they can fix atmospheric nitrogen in place of assimilating the dissolved one in the water medium, resulting in a slighter decrease in the NH_4^+ concentration measured in the solution, as can be seen in Fig.4.5.

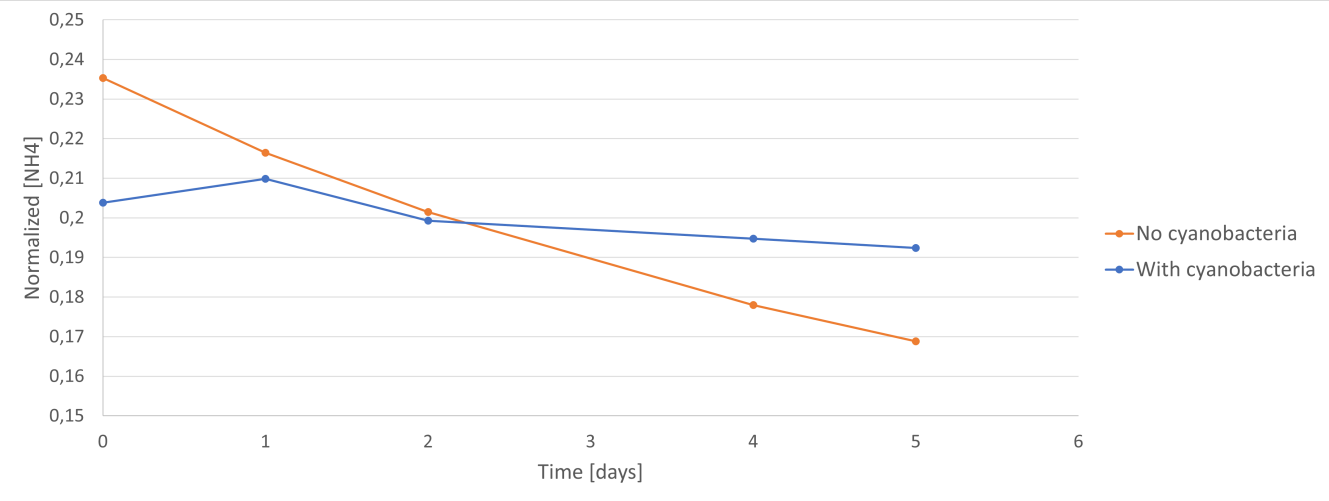

Figure 4.5: Normalized trend of nitrogen concentrations in two different assays with and without cyanobacteria during an assay period duration.

Cyanobacteria's negative influence on the culture is evaluated also by monitoring the efficiency of photosystem II in terms of chlorophyll fluorescence of a microalgae sample by means of AquaPen-C AP-C 100 device (section 3.1).
Cyanobacteria flocs affecting the microalgal community can be indirectly measured by assessing the quantum yield (QY) and the OJIP curve. In the presence of cyanobacteria in the culture, QY always resulted around 0.45. Normally, in a good-health microalgal culture, the recorded QY is 0.68-0.75. In Fig.4.6 different OJIP curves are reported.

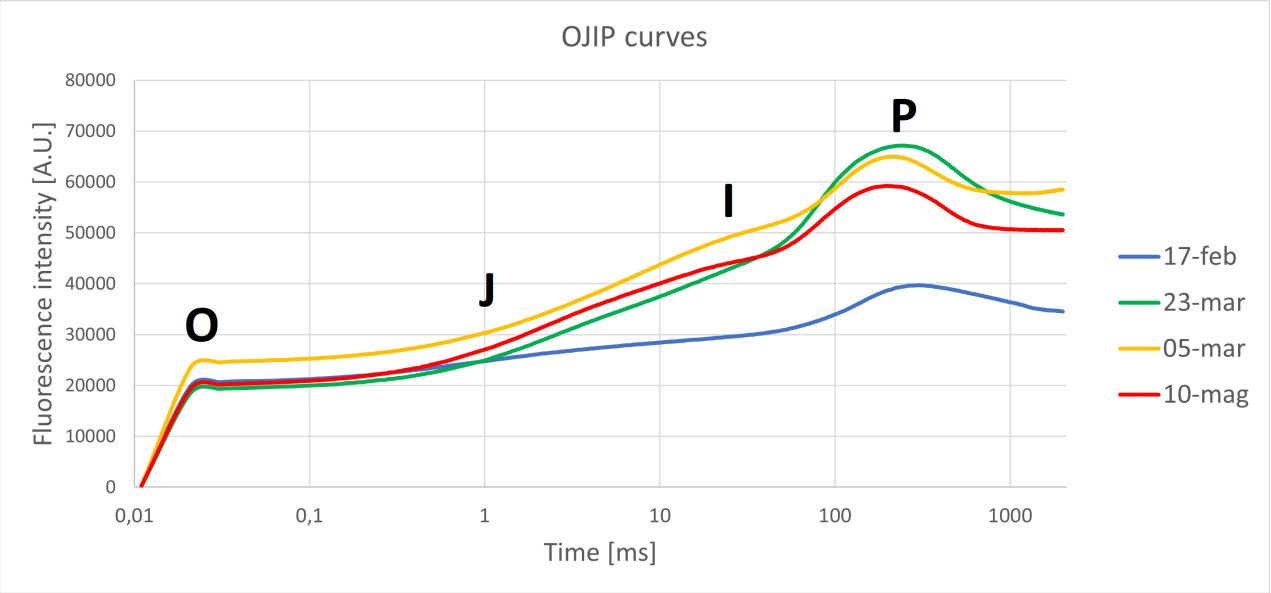

Figure 4.6: Different OJIP kinetic curves in different dates of sampling. The blue one performed on 17/02 is in the presence of cyanobacteria, while the others with only green microalgae.

In Fig.4.6 it is observed that the raw transients show a fall in the presence of cyanobacteria compared to the ones in their absence. Recalling what was said in section 3.1, cyanobacteria negatively affect the microalgal culture, enhancing the non-photochemical quenching (heat dissipation) and so decreasing the algal fluorescence intensity.

Nutrients and TSS

Nutrients and TSS concentrations over the time are important elements in the operations of PBRs.

Nutrients and TSS typical trends during the operation of the PBRs are below reported in Fig.4.5.

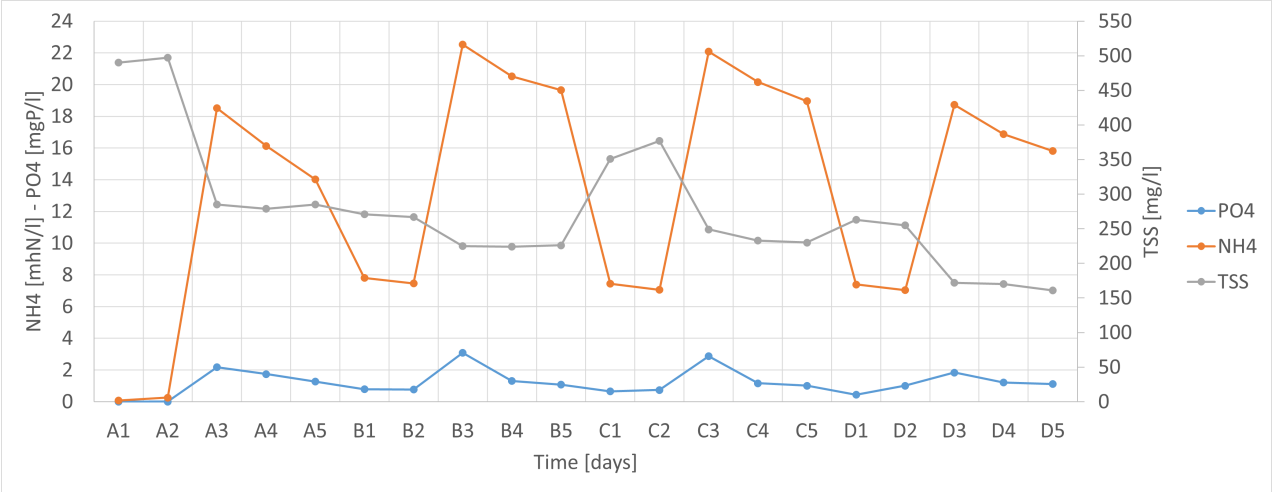

(a) Nutrients-TSS concentration trends

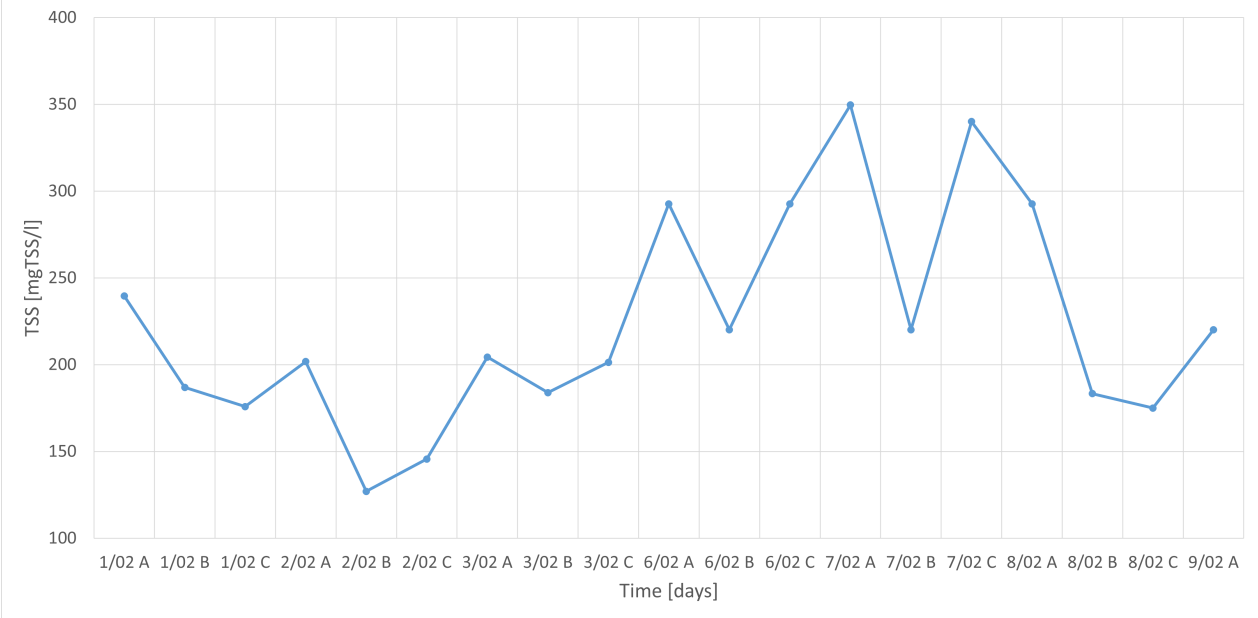

(b) TSS concentration trend

Figure 4.7: (a). In the figure, the trends over time of the nutrients (NH_4^+ and PO_4^{3-}) and of total suspended solids are represented. The scenario presented is relative to PBR1. On the X axis, four consecutive days after the weekend are marked as A, B, C, D, while the number indicates the hour of the sampling. 1 and 2 are samplings performed in the morning of the day, before the purging. 3, 4, 5 are the samplings done in the afternoon after the alimentation with fresh permeate. Purging/alimentation is done around 12:00h every day. 1 and 2 are analyzed at 10:00 and 11:00 respectively. 3, 4, 5 at 12:00, 14:00, 15:00, respectively. A1 corresponds to the first sampling performed after the weekend. (b). TSS trend over time in PBR2 in the period 1/02/2023 - 9/02/2023, including a weekend of no purging/alimentation (4/02 - 5/02, not reported in the graph). Purging/alimentation is done around 12:00h of the days reported. In each day three samplings are performed (A, B, C). A is done before purging at 11:00, B and C after the alimentation at 12:00 and 16:00, respectively.

The trends in Fig.4.7 follow a general recurring shape that reflects the daily purging/alimentation of the reactor. After the alimentation, nutrient concentrations increase thanks to the fresh rich-nutrient permeate while TSS concentration decreases because of the removal from the culture by purging and the dilution with the fresh TSS-free feeding.
In Fig.4.7a in X=A1;A2 it can be observed that after the weekend the maximum algal concentration in terms of TSS is reached. At the same time, the minimum levels of nutrients are present in the culture. Indeed, during the weekend purging/alimentation procedure is not done. Thus, there is an increase in TSS since they are not removed and diluted with fresh permeate. While the microalgae grow up they consume nutrients that are not replaced by new ones in alimentation, so nutrients are significantly lowered.
In Fig.4.7b, the total suspended solids concentration trend comprising a weekend with no operations of feeding and purging is shown. It is visible that after the weekend, between 3/02 and 6/02, TSS increase reaching higher values. However, during the working week, the daily purging/alimentation is performed and TSS tends to decrease on a daily base, as suggested also by the polynomial trend-line which decreases over the time.

4.2. Batch tests results

In this section, the results of the batch assays are described.

Recalling the operations explained in section 3.2.2, the final value determined of $K_{La,CO2}$ is 5.844 h^{-1}. The light intensity factor (f_L) and the temperature factor (f_T) are then determined. The temperature factor is calculated and it is a unique value for all the experimental activity since the temperature is fixed at 25°C. Differently, the light factor is dependent on the test boundary conditions, so it varies according to the test conditions combinations in terms of light intensity $I_{0,S}$ and microalgal concentration X_{TSS}. The depth factor d, defined as the average radius of the flask, is calculated as an average value along the vertical section of the flask, resulting 0.0425m. See Appendix A for the numerical explanation.

An example of assay results is reported in Tab.4.1, showing the results after the titration procedure.

Every test varies according to the boundary conditions. The pH is measured directly from the flask and alkalinity is assessed by the 5-point titration method by Valora software.

Table 4.1: General flask test results. The five sampling times are represented as columns. Each sampling is characterized by a pH value, an alkalinity, and an ionic composition.

	t0-10.00	t1-11.00	t2-12.00	t3-14.00	t4-15.00
pH	7	7.16	7.42	7.93	8.17
AlK [mg_{CaCO3}/l]	261.49	255.62	258.55	251.97	247.36
Na [mg/l]	174.40	174.00	173.50	174.60	175.40
NH4 [mg/l]	13.45	12.63	11.91	10.80	9.98
NH4-N [mg_N/l]	10.46	9.82	9.26	8.40	7.77
K [mg/l]	27.70	27.14	27.20	27.50	27.65
Mg [mg/l]	50.80	50.98	50.44	50.70	50.80
Ca [mg/l]	191.80	191.50	192.10	192.50	194.10
Cl [mg/l]	380.70	373.00	392.00	374.80	399.00
NO2 [mg/l]	1.99	1.88	1.80	1.81	1.68
NO3 [mg/l]	3.59	3.73	1.05	3.69	1.00
PO4 [mg/l]	7.78	7.58	7.03	6.79	6.27
PO4-P [mg_P/l]	2.54	2.47	2.29	2.21	2.04
SO4 [mg/l]	433.00	431.00	433.00	445.60	440.10
S2O3 [mg/l]	1.09	1.09	1.10	1.09	1.14

Typical trends of pH and alkalinity are reported in Fig.4.8.

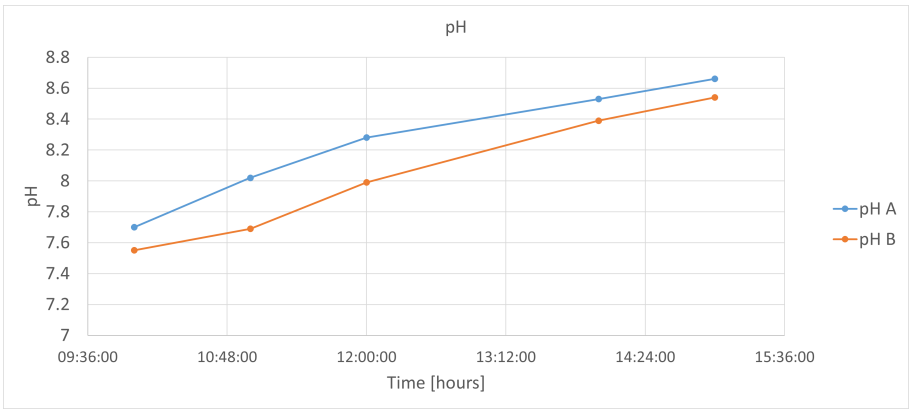

(a) pH flask test trend

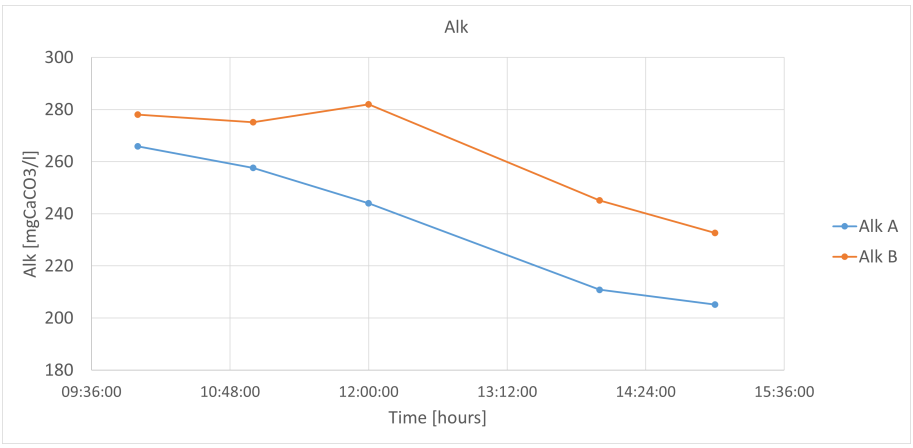

(b) Alkalinity flask test trend

Figure 4.8: (a). pH trend measured in a test period. Both the first sample and the replica are represented, in blu-A and in orange-B, respectively. (b). Alkalinity trend measured in a test period. Both the first sample and the replica are represented, in blu-A and in orange-B, respectively.

In Fig.4.8 as expected, pH values tend to increase during the assay period because of the photosynthesis results. On the opposite, alkalinity tends to decrease due to the ammonium and phosphate uptake by microalgae. It must be noted the difference between the values of the sampling points of the first sample and the replica ones. Indeed, the replica's samplings are not performed exactly at the same times as in the first assay, but with a delay of 30 minutes as explained in section 3.1. Thus, some differences in the measurements of the variables are naturally present.

Recalling what is described in section 3.2.2, the simulation procedure operates with inputs to MINTEQ software the ionic composition, pH and alkalinity. Then the biological model

is run, obtaining the model components. In Tab.4.2 a typical output of the flask tests after the model simulation is shown.

Table 4.2: Model test results. The five sampling times are represented in rows. Each sampling is characterized by a pH value, an alkalinity, an ionic composition. In orange, the results of the biological model simulation $S_{ig,C}$ and $S_{H_{TOT}}$. Model components S_{NH_X} and S_{PO_4} are represented as well. The ions showing null concentrations are not measured during the assay.

Time	Sa	Snh4	Spo4	Spro	StotH	Salk	Sca	SMg	SK	Sfe	Sal	Sno2	Sso4	Sh2s	pH	totC	totH	[H+]
(h)	mg COD/L	mg N/L	mg P/L	mg COD/L	mol/L	mg CaCO3/L	mg/L	mg/L	mg/L	mg/L	mg/L	mg N/L	mg S/L	mg S/L	un. pH	mol/m3	mol/m3	mol/m3
0	0	29.52	3.79	0	0	327.2	213.5	54.28	28.78	0	0	0.31	167.9	0	7.0	0.0077	0.00909	0.0001
1	0	29.08	3.71	0	0	321.1	214.1	54.28	28.88	0	0	0.35	175.5	0	7.3	0.0070	0.00778	5E-05
2	0	27.77	3.58	0	0	316.3	214.2	54.39	28.80	0	0	0.32	167.1	0	7.6	0.0065	0.00684	2E-05
4	0	25.30	2.87	0	0	302.5	212.0	54.07	29.38	0	0	0.34	165.3	0	8.4	0.0058	0.00544	4E-06
5	0	25.11	2.00	0	0	275.0	210.2	53.85	31.00	0	0	0.30	170.4	0	8.7	0.0050	0.00437	2E-06

In Fig.4.9 the typical trends of $S_{ig,C}$ and $S_{H_{TOT}}$ are reported. Total inorganic carbon tends to decrease because of CO_2 uptake by microalgae, as well as total protons decrease due to the basification of the medium during algal growth.

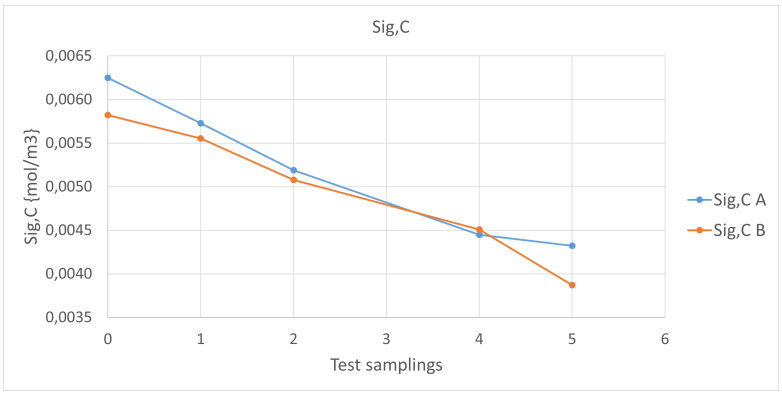

(a) $S_{ig,C}$ flask test trend

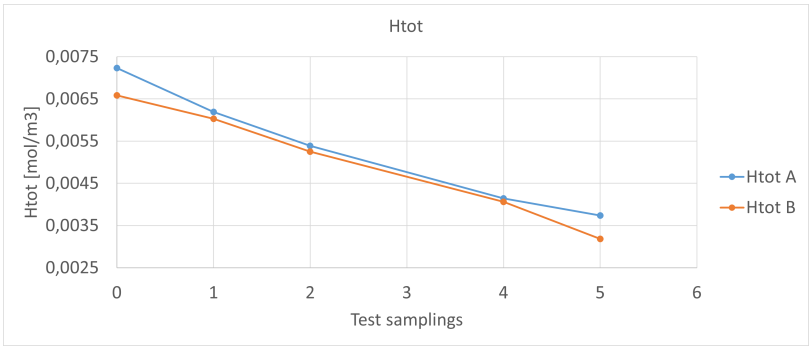

(b) $S_{H_{TOT}}$ flask test trend

Figure 4.9: (a). $S_{ig,C}$ trend measured in a test period. Both the first sample and the replica are represented, in blu-A and in orange-B, respectively. (b). $S_{H_{TOT}}$ trend measured in a test period. Both the first sample and the replica are represented, in blu-A and in orange-B, respectively.

The speciation model operated by MINTEQ software gives as results chemical species, such as S_{CO_2}, S_{NH_3}, and pH, whose typical trends are reported below in Fig.4.10.

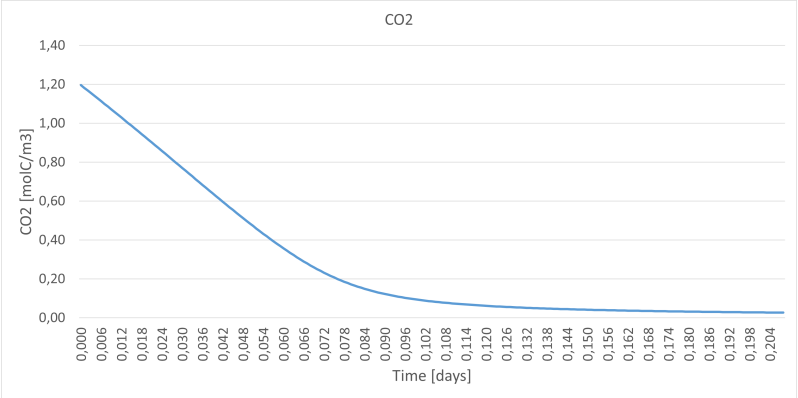

(a) CO_2 MINTEQ output trend

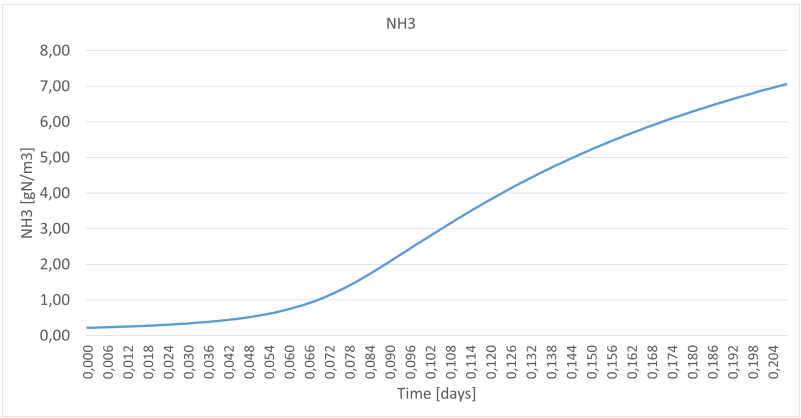

(b) NH_3 MINTEQ output trend

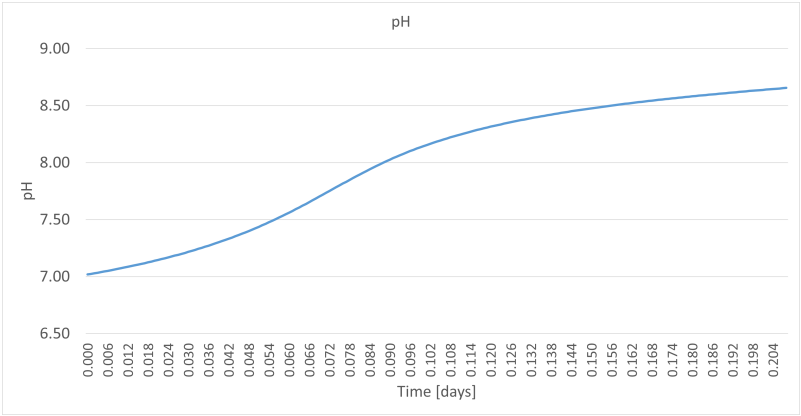

(c) pH MINTEQ output trend

Figure 4.10: (a). CO_2 trend simulated by MINTEQ during an experimental test period (5 hours) expressed in days. Software output values are computed in a continuous way. (b). NH_3 simulated by MINTEQ during an experimental test period expressed in days. Software output values are computed in a continuous way. (c). pH simulated by MINTEQ during an experimental test period expressed in days. Software output values are computed in a continuous way.

In Fig.4.10a the dissolved CO_2 trend decreases over time, because of the photosynthetic activity of the microalgae that use carbon dioxide as the carbon source for their metabolism. In Fig.4.10b ammonia concentration in the aqueous medium shows an increase over time. Indeed, this dynamic is coherent with the pH variation during an assay. Indeed, the ammonia stripping is enhanced at higher pH values of the medium (Fig.4.10c), due to the shifting in the chemical equilibrium with dissolved ammonium as seen in Fig.4.11.

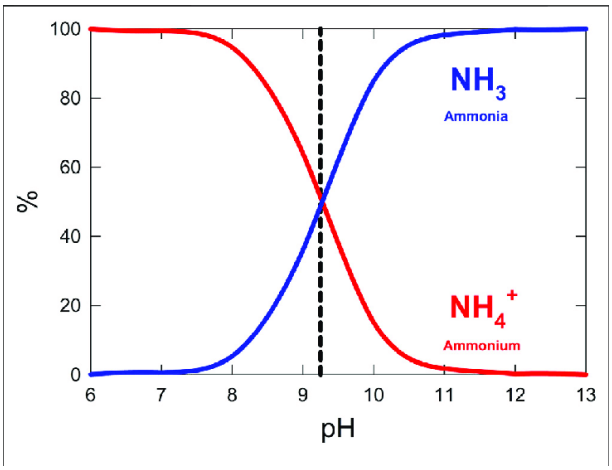

Figure 4.11: The relative percent abundances of NH_3 and NH_4^+ across a range of pH values [58].

4.3. Calibration and validation

In this section, the calibration and validation results are reported. Eventually, the statistical results and considerations on the goodness of the calibrated model are described.

Calibration results

The parameter optimization results in a set of values for the three objective parameters equal to:

μ_{ALG}(@20°C) = 1.8339 d^{-1}
$K_{S,H}$ = 0.0062978 mol_{H+}/l
$K_{I,H}$ = 3.8156e-06 mol_{H+}/l

Once the parameters have been determined, a visual analysis of some experimental points compared to the expected trend of the simulated values is done. The selected dataset

adopted is reported in Tab.4.3, including six assays in different boundary conditions.

Table 4.3: Dataset used to compare the experimental and model calibrated data. NH_X and pH are the two variables adopted. The dataset comprises six assays performed in different conditions. In orange the pH, in green NHx [gN/m^3].

	NHx - EXP (g_N/m3)	NHx - SIM (g_N/m3)	pH - EXP	pH - SIM
1	44.0	44.0	7	7.02
2	43.8	43.7	7.26	7.32
3	42.1	43.3	7.61	7.93
4	39.2	41.3	8.28	8.54
5	39.9	39.8	8.52	8.65
6	15.0	15.0	7	7.02
7	14.4	14.7	7.27	7.35
8	13.5	14.5	7.64	8.02
9	11.4	13.7	8.48	8.63
10	10.3	13.2	8.78	8.74
11	31.1	31.1	8.03	8.03
12	30.0	30.6	8.13	8.25
13	29.3	30.0	8.24	8.39
14	26.7	29.2	8.38	8.50
15	26.6	27.5	8.45	8.62
16	11.5	11.5	8	8.01
17	10.1	11.4	8.1	8.35
18	8.7	11.3	8.27	8.50
19	7.6	10.8	8.2	8.65
20	7.5	10.5	8.17	8.69
21	9.1	9.1	8.98	8.98
22	9.0	8.6	9.05	8.95
23	8.9	8.1	9.07	8.92
24	9.6	7.4	8.73	8.86
25	9.2	7.1	8.77	8.83
26	8.1	8.1	9.01	9.01
27	8.1	7.7	9.02	8.98
28	8.1	7.3	9.05	8.95
29	8.1	6.6	8.92	8.89
30	8.4	6.4	8.87	8.86

In Fig.4.12, the trends of the experimental and simulated data reported in Tab.4.3 are shown.

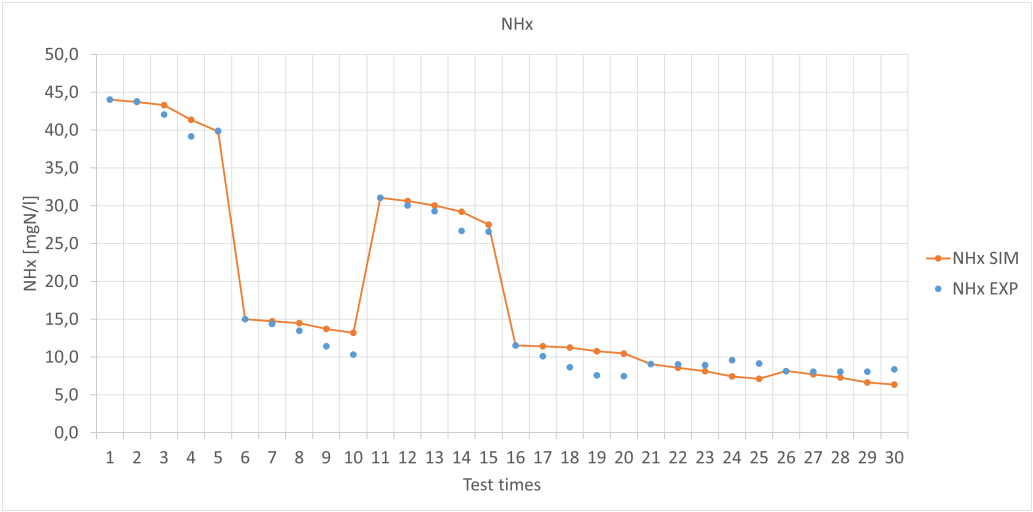

(a) Experimental-simulated NHx

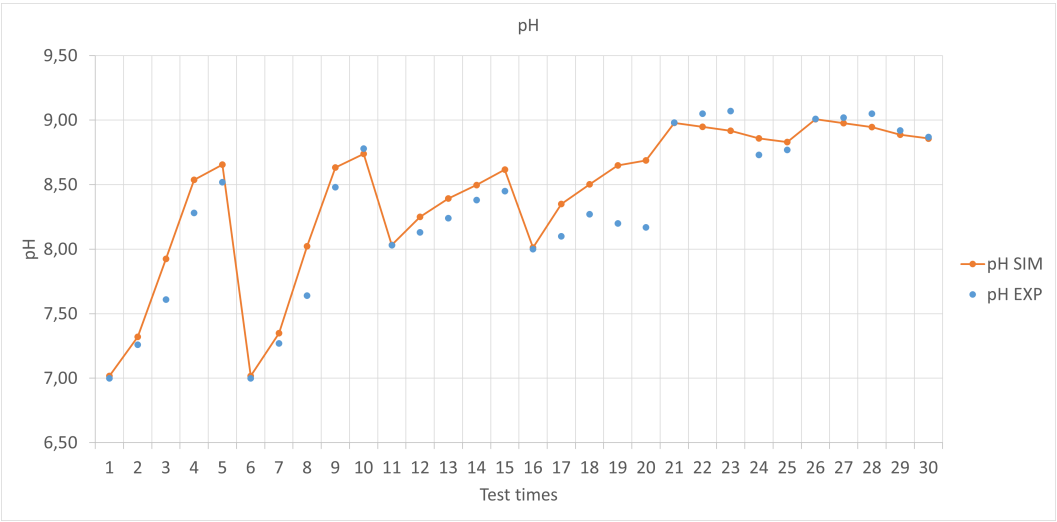

(b) Experimental-simulated pH

Figure 4.12: (a). NHx simulated trend compared to experimental sampling data. (b). pH simulated trend compared to experimental sampling data. Time axis X is numerically divided among the six assays referring to the test enumeration reported in Tab.4.3

After a first qualitative analysis, it appears that the model output tends to overestimate the experimental results. In particular, the assays characterized by a starting pH of 9 show a pH decrease during the experiment, not detected by the simulation. Nevertheless, simulated results fit the experimental data quite well. To assess deeper and quantitatively the goodness of the calibrated model, the validation of the results achieved is performed

in the next section.

Validation results

The paired observations are composed of two groups (experimental/simulated), each group comprehensive of 75 observations (25 observations for each variable multiplied for the three variables involved). The data are below reported in Tab.4.4.

Table 4.4: Complete validation dataset, showing the experimental and simulated values. In blue the alkalinity [mg_{CaCO3}/l], in orange the pH, and in green NH_X [mg_N/l].

	Alk_EXP	Alk_SIM	pH_EXP	pH_SIM	NHx_EXP	NHx_SIM
1	259.32	247.71	8.10	8.10	0.00	0.00
2	272.03	249.06	8.51	8.26	0.00	0.25
3	265.80	249.88	8.66	8.50	0.00	0.46
4	260.93	252.09	8.78	8.69	0.00	0.91
5	252.52	253.59	8.85	8.73	0.00	1.13
6	399.77	383.44	8.00	8.00	19.60	19.60
7	340.55	382.08	8.29	8.47	18.63	19.15
8	331.16	380.08	8.45	8.65	17.65	18.52
9	347.68	378.45	8.64	8.84	15.93	16.86
10	334.19	378.41	8.84	8.89	14.95	15.97
11	393.62	384.19	7.42	7.44	19.18	19.18
12	386.34	395.02	7.87	8.28	17.70	18.81
13	348.00	392.66	8.22	8.62	16.23	18.27
14	335.08	391.32	8.63	8.85	13.88	16.75
15	322.00	391.70	8.83	8.91	12.50	15.89
16	531.08	513.20	7.53	7.54	51.11	51.11
17	506.39	513.57	7.65	7.73	50.37	50.73
18	486.42	513.27	7.75	7.97	49.01	50.21
19	461.37	508.37	8.09	8.32	44.07	48.46
20	498.21	505.68	8.22	8.43	41.96	47.24
21	496.22	483.56	7.08	7.09	42.60	42.60
22	493.96	482.09	7.26	7.25	41.43	42.27
23	479.25	488.22	7.44	7.51	39.53	41.93
24	506.57	491.54	8.01	8.29	33.70	40.72
25	508.37	487.77	8.21	8.48	31.60	39.64

The paired t-test was used to compare the means of the experimental and simulated data.

The approximate normal distribution of the differences between the paired observations is evaluated by boxplot and QQ-plot. In Fig.4.13 the resulting graphs are reported.

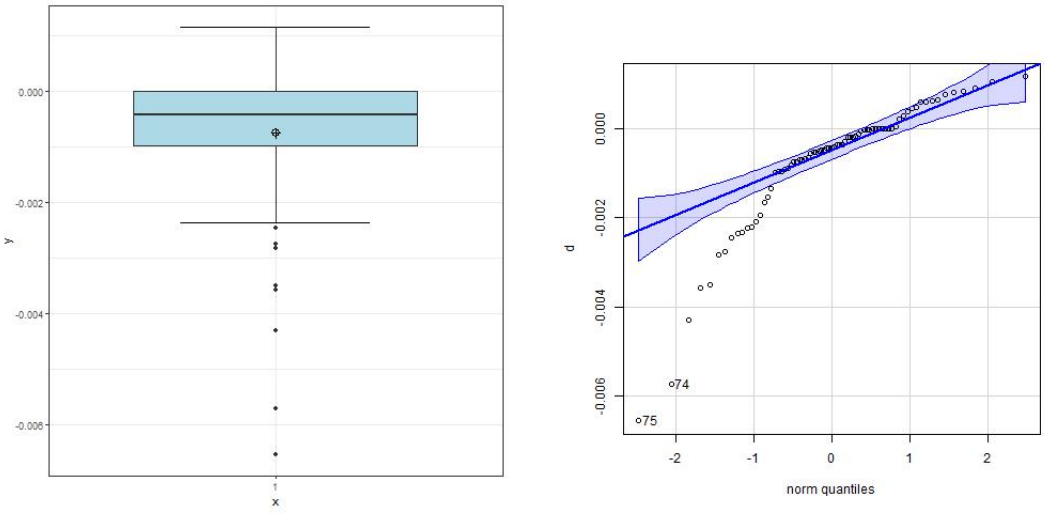

(a) Boxplot (b) QQ-plot

Figure 4.13: Boxplot and QQ-plot to check the normality of the differences of the complete validation dataset.

From Fig.4.13a can be highlighted that the boxplot is visually approximately symmetric, proving that the data distribution is close to a normal distribution. Moreover, the previous conclusion is confirmed by the QQ-plot (Fig.4.13b) since the greatest part of the points lies on a straight diagonal line area.
Now that the approximate normality assumption is verified, the two-sample and paired t-test can be performed.

The two-sample t-test performed gives an experimental mean of 141.5 and a simulated mean of 145.8, while the paired test shows a confidence interval of the difference between the means of (-8.3;-0.43). The mean difference results -4.36, indicating no significant difference between the means of the two data samples.
The significance level of the t-test is represented by the p-value, equal to 0.89 for the two-sample t-test, and 0.03 for the paired one. These results are interpreted in comparison with the significance level $\alpha = 0.05$. The p-value according to the two-sample test is greater than α, so we can reject the alternative hypothesis and conclude that the average

of experimental data is significantly similar to the simulated one. However, the opposite is true for the paired test. The quality of the paired t-test results is affected by the degree of deviation from the assumption of normality of the differences, not completely guaranteed as previously seen.

In addition to the tests, a scatter plot relating the total normalized pairs of experimental and simulated values is made (Fig.4.14).

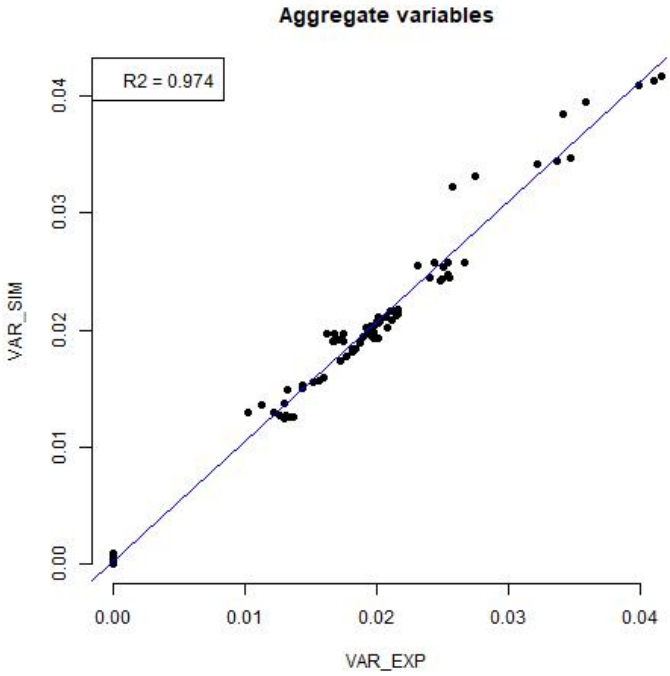

Figure 4.14: Scatter plot of complete validation dataset (experimental/simulated) including all the three variables with regression line and adjusted R^2.

A linear regression of the points is operated. The regression performed on the data shows a satisfactory adjusted R^2, equal to 0.97.

Below the simulations of the modeled variables are reported, showing the experimental and simulated trends measured during the validation assays, with the addition of $S_{H_{TOT}}$ (Fig.4.15).

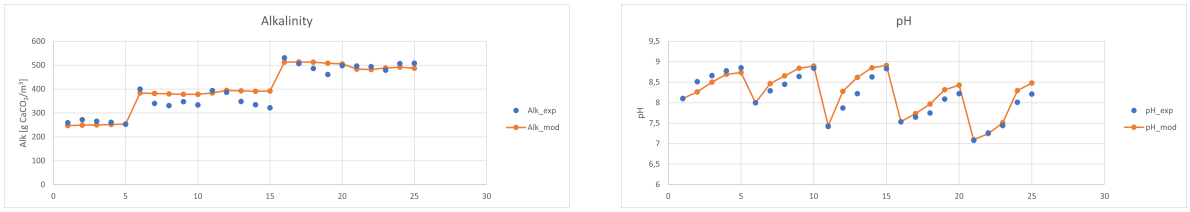

(a) Alkalinity (b) pH

(c) NHx (d) H_{TOT}

Figure 4.15: Dynamic simulations of the evolution of alkalinity, pH, NH_X and H_{TOT} in the validation tests. Experimental and modeled data are represented by markers and lines, respectively.

All the simulated curves fit quite well the experimental values and present a pattern of oscillation mostly greater than the experimental results. This behavior is particularly observed at the last points of each assay, probably induced by the higher pH values that bring less accurate results due to the chemical precipitation processes not being considered in the microalgae model adopted in the work.

Overall at first glance, the qualitative interpretation of the results derived from the tests and graphs above reported allows us to evaluate positively the goodness of the calibrated parameters μ_{ALG}, $K_{S,H}$ and $K_{I,H}$.

The validation results achieved up to now provide a positive evaluation of the goodness of the parameter calibration. However, they also present a major critical point which is the very low value of the p-value derived from the paired t-test. Indeed, a p-value of 0.03 is lower than the significance level α, thus we can not say that the two samples (experimental and modeled) are significantly similar. It is fair to state that probably the quality of the paired t-test results is affected by the degree of deviation from the assumption of normality of the differences, not completely guaranteed as previously seen from Q-Q plot and boxplot (Fig.4.13).
The difference between the p-value of the two-sample t-test and the paired one brings

us to think that the issue can be related to the magnitude of deviation of some paired observations. Thus, an analysis of the paired observations is performed visually by means of boxplots of the three single variables involved, showing both the experimental and the simulated paired boxplots (Fig.4.16).

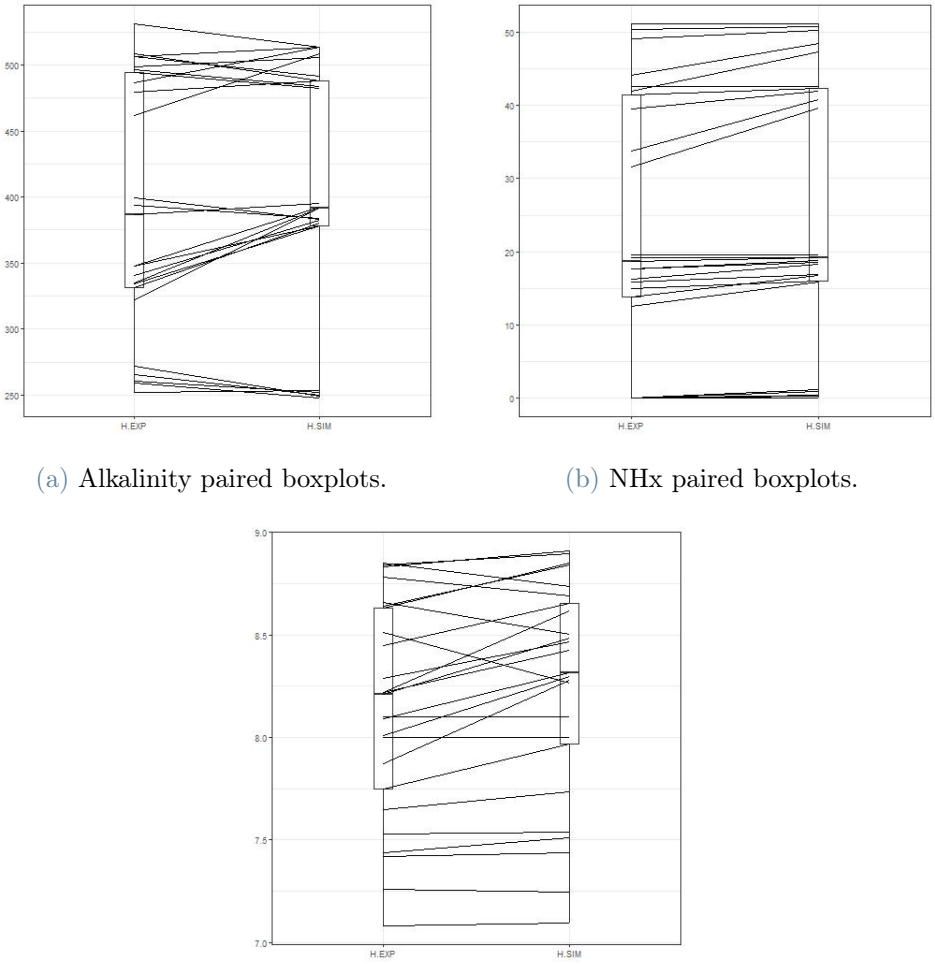

(a) Alkalinity paired boxplots.

(b) NHx paired boxplots.

(c) pH paired boxplots.

Figure 4.16: Boxplots showing the paired observations of the three variables used in validation phase. The boxplot on the left is associated to the experimental data, the one on the right to the simulated data.

While from the alkalinity (Fig.4.16a) and NHx (Fig.4.16b) relevant trends can not be detected, from the pH one (Fig.4.16c) can be noted that the differences between the paired observations increase by increasing the pH. Indeed, at higher pH is observed that the accuracy of the modeled results is lower than the values simulated at lower pH values since the connecting lines become more irregular and less straight. This result is evidence of the assumption made that the considered model does not include precipitation processes, thus

there are some normal deviations between experimental and modeled data when pH rises. This hypothesis can be valorized by reprocessing t-tests on a validation dataset including only the paired observations characterized by a pH value lower than 8.5. The cleaned dataset counts now 51 paired observations (previously 75). From the two-sample t-test is achieved a p-value of 0.94 (before 0.89), while the paired t-test provides a p-value of 0.13 (before 0.03). Comparing these values with α, we can assume that the modeled data described by lower pH are better simulated than the ones counting all the pH achieved (Tab.4.5).

Table 4.5: Summary table of the statistical analysis performed on the complete validation dataset and on the one at pH<8.5.

Dataset	**t-test**	**Paired t-test**	**R^2**
Complete	0.89	0.03	0.97
At pH<8.5	0.94	0.13	0.96

Moreover, the inaccuracy of the modeled simulation is particularly observed at the last points of each assay in Fig.4.15. As stated before, this behavior can be induced by the higher pH values that bring less accurate results due to the chemical precipitation processes not being considered in Viruela microalgae model. Another aspect to be taken into consideration about the deviations is the experimental error derived from both manual and equipment operations that can produce a systematic error in the experimental results. In addition in Fig.4.17 the scatter plot with linear regression of the cleaned data at pH lower than 8.5 is reported.

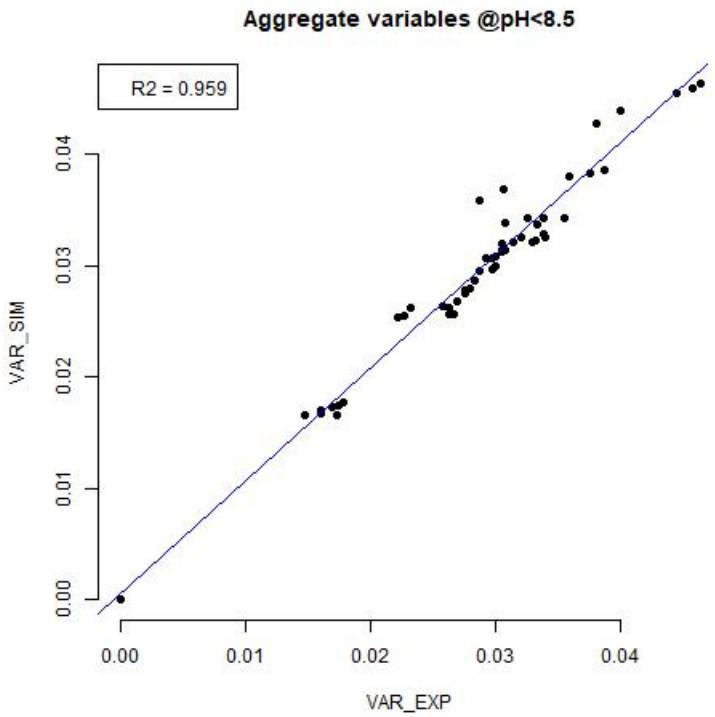

Figure 4.17: Scatter plot with validation dataset (experimental/simulated data) at pH<8.5 including all the three variables with regression line and adjusted R^2.

The adjusted R^2 is similar to the previous one computed with the complete validation dataset, equal to 0.96.

5 | Conclusions and perspectives

Once the entire experimental process has been completed and the data obtained have been analyzed, it is possible to draw conclusions from this work.

Experimental analyses to select the growth medium for microalgae led to the choice of permeate. Indeed, the handling of photobioreactors has established that the liquid fraction of the digestate from the anaerobic process after membrane treatment is a better growth medium than synthetic medium. This was verified with analyses of the TSS over time, showing a constantly increasing growth trend in contrast to the case with synthetic water.

The biological composition of the culture is a dynamic element over time. The assays performed during the calibration phase were mostly done with an algal community showing a predominance of Chlorella sp. over Scenedesmus sp. However, it was observed that in the tests performed at a higher pH, around 9, the balance between the two strains is reversed, with a greater abundance of Scenedesmus sp. over Chlorella sp. In addition, during the handling of PBRs, the culture happened to show a majority of cyanobacteria. Assays were performed including this scenario, however, the experimental results were qualitatively inconsistent with those seen from the green algae and, therefore, excluded from the calibration and validation process.

The data calibration and validation phases were carried out by means of batch tests, which allowed us to study the response of algal growth as the affecting parameters changed. In this sense, the modified boundary conditions were the initial pH, biomass concentration, and light intensity. The values of these parameters were chosen following a literature review and considering the practical working limits.

The main aim of the present work is to determine certain parameters contained in the microalgal growth model proposed by Viruela et al., 2021. The data collected in the experimental phase enabled to estimate the following values:

μ_{ALG}(@20°C) = 1.8339 d^{-1}
$K_{S,H}$ = 0.0062978 mol_{H+}/l
$K_{I,H}$ = 3.8156e-06 mol_{H+}/l

The validation of the results obtained has been performed to assess the goodness of the calibrated parameters. Through both qualitative and quantitative analysis, the goodness of the parameters is confirmed, although with noticeable limitations for scenarios characterized by higher pH levels. This was further confirmed by additional statistical analysis, which assessed that the precipitative processes occurring at alkaline pH, which are not considered in the algal model, represent a source of error in the estimation of simulated data.

Future perspectives

The perspectives of the present work are multiple and they are linked with its own limitations. As mentioned before in this section, the model simulation works more accurately when the pH presents lower values.

The experimental data embeds in their doing the precipitation phenomena, while the microalgal model adopted does not take into account these processes, so the simulated results differ from the experimental ones, in particular at alkaline pH, when precipitation processes mostly occur. It is a relevant limit especially when the research aims to study phosphorus removal since, at high pH, P-precipitation has been proven to be the most active removal route [121].

Further studies can be carried out to focus on the simulated deviation and on the accuracy of the calibrated parameters, and, in case this deviation is significant, re-calibrate them including the chemical precipitations in the model. In this perspective, running a second experimental campaign and simulating with the model that includes precipitation processes (the integrated model BNRM2A) would be interesting. Thus, it is feasible to check if the model here calibrated (no precipitation phenomena) is able to fit effectively the experimental data and verify if the observed deviations are actually associated with the precipitation processes or are due to other reasons.

Another point to be investigated is the accuracy of the calibrated model in scenarios characterized by different cultivation methods and in dark-light conditions since these settings have not been included in the present work.

Moreover, it is fundamental to assess the quality of the algal model once it is integrated with the bacterial model forming the integrated model BNRM2A (2.2.1).
Another aspect that deserves a deeper understanding is the response of the calibrated model varying the microalgae strains present in the culture. This scenario has not been monitored in the present work, but the simulation could show different responses according to the biological composition of the medium.
Regarding the assumptions made on the microalgae model in this work, we decided to operate always in excess of phosphorus in the liquid medium. Other simulations can be performed considering P-deplete conditions, taking into account the biological processes that consume the stored polyphosphate in place of the dissolved P.
Eventually, the greatest part of the data excluded from the calibration/validation datasets was due to cyanobacteria presence in the culture. The microalgal model here studied is not able to reproduce the performances of cyanobacteria because their metabolism is completely different from the one of green microalgae. However, would be interesting to study how they can be integrated into the modeling of BNRM2A since they are a valuable option for the food industry and for enriching the soil of organic carbon and nitrogen by fixation of the atmospheric one [98]. Data availability from the experimental assays performed in this work could be a starting base for further studies on this topic.

Bibliography

[1] A. Abdelfattah, S. S. Ali, H. Ramadan, E. I. El-Aswar, R. Eltawab, S.-H. Ho, T. Elsamahy, S. Li, M. M. El-Sheekh, M. Schagerl, M. Kornaros, and J. Sun. Microalgae-based wastewater treatment: Mechanisms, challenges, recent advances, and future prospects. *Environmental Science and Ecotechnology*, 13:100205, 2023. ISSN 2666-4984. doi: https://doi.org/10.1016/j.ese.2022.100205. URL `https://www.sciencedirect.com/science/article/pii/S2666498422000618`.

[2] S. Abu-Ghosh, D. Fixler, Z. Dubinsky, and D. Iluz. Flashing light in microalgae biotechnology. *Bioresource Technology*, 203:357–363, 2016. ISSN 0960-8524. doi: https://doi.org/10.1016/j.biortech.2015.12.057. URL `https://www.sciencedirect.com/science/article/pii/S0960852415016879`.

[3] G. Acien, J. M. Fernandez-Sevilla, and E. Molina-Grima. Photobioreactors for the production of microalgae. *Reviews in Environmental Science and Bio/Technology*, 12, 06 2013. doi: 10.1007/s11157-012-9307-6.

[4] V. O. Adesanya, E. Cadena, S. A. Scott, and A. G. Smith. Life cycle assessment on microalgal biodiesel production using a hybrid cultivation system. *Bioresource technology*, 163:343–355, 2014.

[5] T. V. Agbebi, E. O. Ojo, and I. A. Watson. Towards optimal inorganic carbon delivery to microalgae culture. *Algal Research*, 67:102841, 2022. ISSN 2211-9264. doi: https://doi.org/10.1016/j.algal.2022.102841. URL `https://www.sciencedirect.com/science/article/pii/S2211926422002120`.

[6] F. Almomani, S. Judd, R. Bhosale, M. Shurair, K. Aljaml, and M. Khraisheh. Intergraded wastewater treatment and carbon bio-fixation from flue gases using spirulina platensis and mixed algal culture. *Process Safety and Environmental Protection*, 124, 02 2019. doi: 10.1016/j.psep.2019.02.009.

[7] A. D. American Public Health Association, Eaton. *Standard methods for the examination of water and wastewater*. APHA-AWWA-WEF Washington, D.C., 2005.

[8] A. Anbalagan, S. Schwede, C.-F. Lindberg, and E. Nehrenheim. Influence of hy-

draulic retention time on indigenous microalgae and activated sludge process. *Water Research*, 91:277–284, 2016. ISSN 0043-1354. doi: https://doi.org/10.1016/j.watres.2016.01.027. URL https://www.sciencedirect.com/science/article/pii/S0043135416300276.

[9] S. A. Antón, A. S. Torrecillas, and L. B. Falomir. *Microalgae- bacteria consortia for urban wastewater treatment*. PhD thesis, University of Valencia, 2021.

[10] S. Aparicio, Ángel Robles, J. Ferrer, A. Seco, and L. Borrás Falomir. Assessing and modeling nitrite inhibition in microalgae-bacteria consortia for wastewater treatment by means of photo-respirometric and chlorophyll fluorescence techniques. *Science of The Total Environment*, 808:152128, 2022. ISSN 0048-9697. doi: https://doi.org/10.1016/j.scitotenv.2021.152128. URL https://www.sciencedirect.com/science/article/pii/S0048969721072041.

[11] S. Aparicio, J. González-Camejo, A. Seco, L. Borrás, Ángel Robles, and J. Ferrer. Integrated microalgae-bacteria modelling: application to an outdoor membrane photobioreactor (mpbr). *Science of The Total Environment*, 884:163669, 2023. ISSN 0048-9697. doi: https://doi.org/10.1016/j.scitotenv.2023.163669. URL https://www.sciencedirect.com/science/article/pii/S0048969723022891.

[12] R. Barat, J. Serralta, V. Ruano, E. Jiménez, J. Ribes, A. Seco, and J. Ferrer. Biological nutrient removal model no. 2 (bnrm2): a general model for wastewater treatment plants. *Water science and technology : a journal of the International Association on Water Pollution Research*, 67:1481–9, 04 2013. doi: 10.2166/wst.2013.004.

[13] E. Barbera, A. Bertucco, and S. Kumar. Nutrients recovery and recycling in algae processing for biofuels production. *Renewable and Sustainable Energy Reviews*, 90:28–42, 2018. ISSN 1364-0321. doi: https://doi.org/10.1016/j.rser.2018.03.004. URL https://www.sciencedirect.com/science/article/pii/S1364032118300923.

[14] M. Barbosa, M. Albrecht, and R. Wijffels. Hydrodynamic stress and lethal events in sparged microalgae cultures. *Biotechnology and bioengineering*, 83:112–20, 08 2003. doi: 10.1002/bit.10657.

[15] M. Barceló-Villalobos, C. G. Serrano, A. S. Zurano, L. A. García, S. E. Maldonado, J. Peña, and F. A. Fernández. Variations of culture parameters in a pilot-scale thin-layer reactor and their influence on the performance of scenedesmus almeriensis culture. *Bioresource Technology Reports*, 6:190–197, 2019. ISSN 2589-014X. doi:

https://doi.org/10.1016/j.biteb.2019.03.007. URL https://www.sciencedirect.com/science/article/pii/S2589014X19300659.

[16] M. Bartley, W. Boeing, F. Holguin, and T. Schaub. ph effects on growth and lipid accumulation of the biofuel microalgae nannochloropsis salina and invading organisms. j appl phycol. *Journal of Applied Phycology*, 26:1431–1437, 06 2014. doi: 10.1007/s10811-013-0177-2.

[17] D. Batstone, J. Keller, and J.-P. Steyer. A review of adm1 extensions, applications, and analysis: 2002-2005. *Water science and technology : a journal of the International Association on Water Pollution Research*, 54:1–10, 02 2006. doi: 10.2166/wst.2006.520.

[18] O. Bernard and B. Rémond. Validation of a simple model accounting for light and temperature effect on microalgal growth. *Bioresource Technology*, 123:520–527, 2012. ISSN 0960-8524. doi: https://doi.org/10.1016/j.biortech.2012.07.022. URL https://www.sciencedirect.com/science/article/pii/S0960852412010693.

[19] F. Casagli, G. Zuccaro, O. Bernard, J.-P. Steyer, and E. Ficara. Alba: A comprehensive growth model to optimize algae-bacteria wastewater treatment in raceway ponds. *Water Research*, 190:116734, 2021. ISSN 0043-1354. doi: https://doi.org/10.1016/j.watres.2020.116734. URL https://www.sciencedirect.com/science/article/pii/S0043135420312677.

[20] C. Chen and E. Durbin. Effects of ph on the growth and carbon uptake of marine phytoplankton. *Marine Ecology-progress Series - MAR ECOL-PROGR SER*, 109: 83–94, 06 1994. doi: 10.3354/meps109083.

[21] S. Chinnasamy, B. Ramakrishnan, A. Bhatnagar, and K. Das. Biomass production potential of a wastewater alga chlorella vulgaris arc 1 under elevated levels of co2 and temperature. *International journal of molecular sciences*, 10:518–32, 03 2009. doi: 10.3390/ijms10020518.

[22] Y. Chisti. Biodiesel from microalgae beats bioethanol. *Trends in biotechnology*, 26 (3):126–131, 2008.

[23] B. J. Collos, Y. Nitrogen metabolism in phytoplankton. URL https://www.eolss.net/sample-chapters/c09/E2-27-03-03.pdf.

[24] A. Converti, A. Casazza, E. Ortiz, P. Perego, and A. Del Borghi. Effect of temperature and nitrogen concentration on the growth and lipid content of nannochloropsis oculata and chlorella vulgaris for biodiesel production. *Chemical En-*

gineering and Processing: Process Intensification, pages 1146–1151, 06 2009. doi: 10.1016/j.cep.2009.03.006.

[25] A. F. F. M. M. e. a. Costache, T.A. Comprehensive model of microalgae photosynthesis rate as a function of culture conditions in photobioreactors. 2013. doi: 10.1007/s00253-013-5035-2.

[26] L. S. Dagnaisser, M. G. B. dos Santos, A. V. S. Rita, J. Chaves Cardoso, D. F. de Carvalho, and H. V. de Mendonça. Microalgae as Bio-fertilizer: a New Strategy for Advancing Modern Agriculture, Wastewater Bioremediation, and Atmospheric Carbon Mitigation. *Water Air and Soil Pollution*, 233(11):477, Nov. 2022. doi: 10.1007/s11270-022-05917-x.

[27] E. Derlinden, K. Bernaerts, and J. Van Impe. Accurate estimation of cardinal temperatures of escherichia coli from optimal dynamic experiments. *International journal of food microbiology*, 128:89–100, 08 2008. doi: 10.1016/j.ijfoodmicro.2008.07.007.

[28] B. Deruyck, K. H. T. Nguyen, E. Decaestecker, and K. Muylaert. Modeling the impact of rotifer contamination on microalgal production in open pond, photobioreactor and thin layer cultivation systems. *Algal Research*, 38:101398, 2019.

[29] K. Dickinson, W. Bjornsson, L. Garrison, C. Whitney, K. C. Park, A. Banskota, and P. Mcginn. Simultaneous remediation of nutrients from liquid anaerobic digestate and municipal wastewater by the microalga scenedesmus sp. amdd grown in continuous chemostats. *Journal of Applied Microbiology*, 118, 11 2014. doi: 10.1111/jam.12681.

[30] K. E. Dickinson, C. G. Whitney, and P. J. McGinn. Nutrient remediation rates in municipal wastewater and their effect on biochemical composition of the microalga scenedesmus sp. amdd. *Algal Research*, 2(2):127–134, 2013. ISSN 2211-9264. doi: https://doi.org/10.1016/j.algal.2013.01.009. URL `https://www.sciencedirect.com/science/article/pii/S221192641300026X`.

[31] D. Egger. Falling living standards during the covid-19 crisis: Quantitative evidence from nine developing countries. *Science advences*, 2021.

[32] P. Eilers and J. Peeters. A model for the relationship between light intensity and the rate of photosynthesis in phytoplankton. *Ecological Modelling*, 42(3):199–215, 1988. ISSN 0304-3800. doi: https://doi.org/10.1016/0304-3800(88)90057-9. URL `https://www.sciencedirect.com/science/article/pii/0304380088900579`.

[33] E. Eustance. Growth, nitrogen utilization and biodiesel potential for two chlorophytes grown on ammonium, nitrate or urea. *Journal of Applied Phycology*, 25, 2013. doi: https://doi.org/10.1007/s10811-013-0008-5. URL `https://link.springer.com/article/10.1007/s10811-013-0008-5#citeas`.

[34] FAO. 2.3. algal production. URL `https://www.fao.org/3/w3732e/w3732e06.htm`.

[35] I. Farag and K. Price. Resources conservation in microalgae biodiesel production. *" International Journal of Engineering and Technical Research (IJETR*, 1:49–56, 10 2013.

[36] F. A. Fernández, F. G. Camacho, and Y. Chisti. Photobioreactors: light regime, mass transfer, and scaleup. In *Progress in industrial microbiology*, volume 35, pages 231–247. Elsevier, 1999.

[37] G. Ferreira, L. Ríos Pinto, R. Maciel Filho, and L. Fregolente. A review on lipid production from microalgae: Association between cultivation using waste streams and fatty acid profiles. *Renewable and Sustainable Energy Reviews*, 109:448–466, 2019. ISSN 1364-0321. doi: https://doi.org/10.1016/j.rser.2019.04.052. URL `https://www.sciencedirect.com/science/article/pii/S1364032119302643`.

[38] L. Ferro. *Wastewater treatment and biomass generation by Nordic microalgae Growth in subarctic climate and microbial interactions.* PhD thesis, 02 2019.

[39] P. Foladori, S. Petrini, and G. Andreottola. Evolution of real municipal wastewater treatment in photobioreactors and microalgae-bacteria consortia using real-time parameters. *Chemical Engineering Journal*, 345:507–516, 2018. ISSN 1385-8947. doi: https://doi.org/10.1016/j.cej.2018.03.178. URL `https://www.sciencedirect.com/science/article/pii/S1385894718305370`.

[40] D. García, E. Posadas, S. Blanco, G. Acién, P. García-Encina, S. Bolado, and R. Muñoz. Evaluation of the dynamics of microalgae population structure and process performance during piggery wastewater treatment in algal-bacterial photobioreactors. *Bioresource Technology*, 248:120–126, 2018.

[41] S. Gatrell, K. Lum, J. Kim, and X. Lei. Nonruminant nutrition symposium: Potential of defatted microalgae from the biofuel industry as an ingredient to replace corn and soybean meal in swine and poultry diets. *Journal of animal science*, 92 (4):1306–1314, 2014.

[42] M. Ghobadi, M. Firuzi, and E. Asghari Kaljahi. Relationships between geological formations and groundwater chemistry and their effects on the concrete lining of

tunnels (case study: Tabriz metro line 2). *Environmental Earth Sciences*, 75, 06 2016. doi: 10.1007/s12665-016-5785-0.

[43] J. González-Camejo, S. Aparicio, M. Ruano, L. Borrás, R. Barat, and J. Ferrer. Effect of ambient temperature variations on an indigenous microalgae-nitrifying bacteria culture dominated by chlorella. *Bioresource Technology*, 290:121788, 2019. ISSN 0960-8524. doi: https://doi.org/10.1016/j.biortech.2019.121788. URL `https://www.sciencedirect.com/science/article/pii/S0960852419310181`.

[44] J. González-Camejo, P. Montero, S. Aparicio, M. Ruano, L. Borrás, A. Seco, and R. Barat. Nitrite inhibition of microalgae induced by the competition between microalgae and nitrifying bacteria. *Water Research*, 172:115499, 2020. ISSN 0043-1354. doi: https://doi.org/10.1016/j.watres.2020.115499. URL `https://www.sciencedirect.com/science/article/pii/S004313542030035X`.

[45] C. González-Fernández, B. Molinuevo-Salces, and M. García-González. Nitrogen transformations under different conditions in open ponds by means of microalgae-bacteria consortium treating pig slurry. *Bioresource technology*, 102:960–6, 09 2010. doi: 10.1016/j.biortech.2010.09.052.

[46] N. Hanagata, T. Takeuchi, Y. Fukuju, D. J. Barnes, and I. Karube. Tolerance of microalgae to high co2 and high temperature. *Phytochemistry*, 31(10):3345–3348, 1992. ISSN 0031-9422. doi: https://doi.org/10.1016/0031-9422(92)83682-O. URL `https://www.sciencedirect.com/science/article/pii/003194229283682O`. The International Journal of Plant Biochemistry.

[47] M. Henze, W. Gujer, T. Mino, T. Matsuo, M. C. Wentzel, G. v.R. Marais, and M. C. Van Loosdrecht. Activated sludge model no.2d, asm2d. *Water Science and Technology*, 39(1):165–182, 1999. ISSN 0273-1223. doi: https://doi.org/10.1016/S0273-1223(98)00829-4. URL `https://www.sciencedirect.com/science/article/pii/S0273122398008294`. Modelling and microbiology of activated sludge processes.

[48] M. Henze, W. Gujer, T. Mino, and M. van Loosedrecht. *Activated Sludge Models ASM1, ASM2, ASM2d and ASM3*. IWA Publishing, 10 2006. ISBN 9781780402369. doi: 10.2166/9781780402369. URL `https://doi.org/10.2166/9781780402369`.

[49] A. Herrero, A. Muro-Pastor, and E. Flores. Nitrogen control in cyanobacteria. *Journal of bacteriology*, 183:411–25, 02 2001. doi: 10.1128/JB.183.2.411-425.2001.

[50] Q. Huang, F. Jiang, L. Wang, and C. Yang. Design of photobioreactors for mass cultivation of photosynthetic organisms. *Engineering*, 3(3):318–329, 2017. ISSN

2095-8099. doi: https://doi.org/10.1016/J.ENG.2017.03.020. URL https://www.sciencedirect.com/science/article/pii/S2095809917304241.

[51] M. E. Huntley, Z. I. Johnson, S. L. Brown, D. L. Sills, L. Gerber, I. Archibald, S. C. Machesky, J. Granados, C. Beal, and C. H. Greene. Demonstrated large-scale production of marine microalgae for fuels and feed. *Algal research*, 10:249–265, 2015.

[52] I. Iacopozzi, V. Innocenti, S. Marsili-Libelli, and E. Giusti. A modified activated sludge model no. 3 (asm3) with two-step nitrification-denitrification. *Environmental Modelling and Software*, 22:847–861, 06 2007. doi: 10.1016/j.envsoft.2006.05.009.

[53] X. Ji, J. Cheng, D. Gong, X. Zhao, Y. Qi, Y. Su, and W. Ma. The effect of nacl stress on photosynthetic efficiency and lipid production in freshwater microalga—scenedesmus obliquus xj002. *Science of The Total Environment*, 633:593–599, 2018. ISSN 0048-9697. doi: https://doi.org/10.1016/j.scitotenv.2018.03.240. URL https://www.sciencedirect.com/science/article/pii/S0048969718309999.

[54] D. A. Johnson, J. Weissman, and R. Goebel. An outdoor test facility for the large-scale production of microalgae. Technical report, Solar Energy Research Inst., Golden, CO (USA); Microbial Products, Inc ..., 1988.

[55] A. Kazbar, G. Cogne, B. Urbain, H. Marec, B. Le-Gouic, J. Tallec, H. Takache, A. Ismail, and J. Pruvost. Effect of dissolved oxygen concentration on microalgal culture in photobioreactors. *Algal Research*, 39:101432, 2019. ISSN 2211-9264. doi: https://doi.org/10.1016/j.algal.2019.101432. URL https://www.sciencedirect.com/science/article/pii/S2211926418305216.

[56] A. Kliphuis, D. Martens, M. Janssen, and R. Wijffels. Effect of o-2:co2 ratio on the primary metabolism of chlamydomonas reinhardtii. *Biotechnology and bioengineering*, 108, 10 2011. doi: 10.1002/bit.23194.

[57] A. Koyande, C. Kit Wayne, R. K, Y. Tao, and P.-L. Show. Microalgae: A potential alternative to health supplementation for humans. *Food Science and Human Wellness*, 8, 03 2019. doi: 10.1016/j.fshw.2019.03.001.

[58] N. Langenfeld, P. Kusuma, T. Wallentine, C. Criddle, L. Seefeldt, and B. Bugbee. Optimizing nitrogen fixation and recycling for food production in regenerative life support systems. *Frontiers in Astronomy and Space Sciences*, 8, 06 2021. doi: 10.3389/fspas.2021.699688.

[59] J. Lv, F. Zhao, J. Feng, Q. Liu, F. Nan, X. Liu, and S. Xie. Transcriptomic

analysis reveals the mechanism on the response of chlorococcum sp. gd to glucose concentration in mixotrophic cultivation. *Bioresource Technology*, 288:121568, 2019. ISSN 0960-8524. doi: https://doi.org/10.1016/j.biortech.2019.121568. URL https://www.sciencedirect.com/science/article/pii/S0960852419307989.

[60] J. Masojídek and G. Torzillo. Mass cultivation of freshwater microalgae. In *Reference Module in Earth Systems and Environmental Sciences*. Elsevier, 2014. ISBN 978-0-12-409548-9. doi: https://doi.org/10.1016/B978-0-12-409548-9.09373-8. URL https://www.sciencedirect.com/science/article/pii/B9780124095489093738.

[61] J. Masojídek, M. Koblížek, and G. Torzillo. *Photosynthesis in Microalgae*, chapter 2, pages 20–39. John Wiley Sons, Ltd, 2003. ISBN 9780470995280. doi: https://doi.org/10.1002/9780470995280.ch2. URL https://onlinelibrary.wiley.com/doi/abs/10.1002/9780470995280.ch2.

[62] T. M. Mata, A. A. Martins, and N. S. Caetano. Microalgae for biodiesel production and other applications: A review. *Renewable and Sustainable Energy Reviews*, 14(1):217–232, 2010. ISSN 1364-0321. doi: https://doi.org/10.1016/j.rser.2009.07.020. URL https://www.sciencedirect.com/science/article/pii/S1364032109001646.

[63] Y. MATSUDA, T. G. WILLIAMS, and B. COLMAN. Quantification of the rate of co2 formation in the periplasmic space of microalgae during photosynthesis. a comparison of whole-cell rate constants for co2 and hco3– uptake among three species of the green alga chlorella. *Plant, Cell & Environment*, 22(4):397–405, 1999. doi: https://doi.org/10.1046/j.1365-3040.1999.00399.x. URL https://onlinelibrary.wiley.com/doi/abs/10.1046/j.1365-3040.1999.00399.x.

[64] K. Maxwell and G. N. Johnson. Chlorophyll fluorescence—a practical guide. *Journal of Experimental Botany*, 51(345):659–668, 04 2000. ISSN 0022-0957. doi: 10.1093/jexbot/51.345.659. URL https://doi.org/10.1093/jexbot/51.345.659.

[65] L. Meier, D. Stará, J. Bartacek, and D. Jeison. Removal of h2s by a continuous microalgae-based photosynthetic biogas upgrading process. *Process Safety and Environmental Protection*, 119:65–68, 2018. ISSN 0957-5820. doi: https://doi.org/10.1016/j.psep.2018.07.014. URL https://www.sciencedirect.com/science/article/pii/S0957582018305536.

[66] R. Mitra, A. Das Gupta, R. R. Kumar, and R. Sen. A cleaner and smarter way to achieve high microalgal biomass density coupled with facilitated self-flocculation

by utilizing bicarbonate as a source of dissolved carbon dioxide. *Journal of Cleaner Production*, 391:136217, 2023. ISSN 0959-6526. doi: https://doi.org/10.1016/j.jclepro.2023.136217. URL https://www.sciencedirect.com/science/article/pii/S095965262300375X.

[67] M. Moazami-Goudarzi and B. Colman. Changes in carbon uptake mechanisms in two green marine algae by reduced seawater ph. *Journal of Experimental Marine Biology and Ecology*, 413:94–99, 2012. ISSN 0022-0981. doi: https://doi.org/10.1016/j.jembe.2011.11.017. URL https://www.sciencedirect.com/science/article/pii/S0022098111005168.

[68] R. E. Moosbrugger, M. C. Wentzel, G. A. Ekama, and G. v. R. Marais. A 5 pH Point Titration Method for Determining the Carbonate and SCFA Weak Acid/Bases in Anaerobic Systems. *Water Science and Technology*, 28(2):237–245, 07 1993. ISSN 0273-1223. doi: 10.2166/wst.1993.0112. URL https://doi.org/10.2166/wst.1993.0112.

[69] J. Moroney, N. Jungnick, R. Dimario, and D. Longstreth. Photorespiration and carbon concentrating mechanisms: Two adaptations to high o2, low co2 conditions. *Photosynthesis research*, 117, 06 2013. doi: 10.1007/s11120-013-9865-7.

[70] N. Murata, S. Takahashi, Y. Nishiyama, and S. I. Allakhverdiev. Photoinhibition of photosystem ii under environmental stress. *Biochimica et Biophysica Acta (BBA) - Bioenergetics*, 1767(6):414–421, 2007. ISSN 0005-2728. doi: https://doi.org/10.1016/j.bbabio.2006.11.019. URL https://www.sciencedirect.com/science/article/pii/S0005272806003665. Structure and Function of Photosystems.

[71] R. Narala, S. Garg, K. Sharma, S. Thomas-Hall, M. Deme, Y. Li, and P. Schenk. Comparison of microalgae cultivation in photobioreactor, open raceway pond, and a two-stage hybrid system. *Frontiers in Energy Research*, 4, 08 2016. doi: 10.3389/fenrg.2016.00029.

[72] U. Nations. *ADOPTION OF THE PARIS AGREEMENT*. 2015.

[73] Y. Nishiyama, S. I. Allakhverdiev, and N. Murata. A new paradigm for the action of reactive oxygen species in the photoinhibition of photosystem ii. *Biochimica et Biophysica Acta (BBA) - Bioenergetics*, 1757(7):742–749, 2006. ISSN 0005-2728. doi: https://doi.org/10.1016/j.bbabio.2006.05.013. URL https://www.sciencedirect.com/science/article/pii/S0005272806001344.

[74] A. Olabi, N. Shehata, E. T. Sayed, C. Rodriguez, R. Chinyere Anyanwu, C. Russell,

and M. Ali Abdelkareem. Role of microalgae in achieving sustainable development goals and circular economy. *Science of the Total Environment*, 2022.

[75] W. J. Oswald. Micro-algal and waste-water treatment. *Micro-algal biotechnology*, pages 305–328, 1988.

[76] N. Pang, X. Gu, S. Chen, H. Kirchhoff, H. Lei, and S. Roje. Exploiting mixotrophy for improving productivities of biomass and co-products of microalgae. *Renewable and Sustainable Energy Reviews*, 112:450–460, 2019. ISSN 1364-0321. doi: https://doi.org/10.1016/j.rser.2019.06.001. URL `https://www.sciencedirect.com/science/article/pii/S1364032119303867`.

[77] J. C. Pires, M. C. Alvim-Ferraz, and F. G. Martins. Photobioreactor design for microalgae production through computational fluid dynamics: A review. *Renewable and Sustainable Energy Reviews*, 79(C):248–254, 2017. doi: 10.1016/j.rser.2017.05.06. URL `https://ideas.repec.org/a/eee/rensus/v79y2017icp248-254.html`.

[78] E. Posadas, M. del Mar Morales, C. Gomez, F. G. Acién, and R. Muñoz. Influence of ph and co2 source on the performance of microalgae-based secondary domestic wastewater treatment in outdoors pilot raceways. *Chemical Engineering Journal*, 265:239–248, 2015. ISSN 1385-8947. doi: https://doi.org/10.1016/j.cej.2014.12.059. URL `https://www.sciencedirect.com/science/article/pii/S1385894714016738`.

[79] G. Procházková, I. Brányiková, V. Zachleder, and T. Brányik. Effect of nutrient supply status on biomass composition of eukaryotic green microalgae. *Journal of Applied Phycology*, 26(3):1359–1377, 2014. doi: 10.1007/s10811-013-0154-9.

[80] R. Qiu, S. Gao, P. A. Lopez, and K. L. Ogden. Effects of ph on cell growth, lipid production and co2 addition of microalgae chlorella sorokiniana. *Algal Research*, 28:192–199, 2017. ISSN 2211-9264. doi: https://doi.org/10.1016/j.algal.2017.11.004. URL `https://www.sciencedirect.com/science/article/pii/S2211926417305684`.

[81] M. Ras, J.-P. Steyer, and O. Bernard. Temperature effect on microalgae: A crucial factor for outdoor production. *Reviews in Environmental Science and Bio/Technology*, 12, 06 2013. doi: 10.1007/s11157-013-9310-6.

[82] S. Raso, B. Genugten, M. Vermuë, and R. Wijffels. Effect of oxygen concentration on the growth of nannochloropsis sp. at low light intensity. *Journal of applied phycology*, 24:863–871, 08 2012. doi: 10.1007/s10811-011-9706-z.

[83] B. Rath. Commercial and industrial applications of micro algae – a review. *J. Algal Biomass Utln. 2012,*, 3:89–100, 01 2012.

[84] D. A. Ratkowsky, J. Olley, and T. Ross. Unifying temperature effects on the growth rate of bacteria and the stability of globular proteins. *Journal of Theoretical Biology*, 233(3):351–362, 2005. ISSN 0022-5193. doi: https://doi.org/10.1016/j.jtbi.2004.10.016. URL https://www.sciencedirect.com/science/article/pii/S0022519304004941.

[85] J. Reilly. The covid-19 effect on the paris agreement. *HUMANITIES AND SOCIAL SCIENCES COMMUNICATIONS*, 2021.

[86] C. S. Reynolds. *The Ecology of Phytoplankton*. Ecology, Biodiversity and Conservation. Cambridge University Press, 2006. doi: 10.1017/CBO9780511542145.

[87] S. Rossi, F. Casagli, M. Mantovani, V. Mezzanotte, and E. Ficara. Selection of photosynthesis and respiration models to assess the effect of environmental conditions on mixed microalgae consortia grown on wastewater. *Bioresource Technology*, 305:122995, 2020. ISSN 0960-8524. doi: https://doi.org/10.1016/j.biortech.2020.122995. URL https://www.sciencedirect.com/science/article/pii/S0960852420302649.

[88] S. Rossi, R. Díez-Montero, E. Rueda, F. Castillo Cascino, K. Parati, J. García, and E. Ficara. Free ammonia inhibition in microalgae and cyanobacteria grown in wastewaters: Photo-respirometric evaluation and modelling. *Bioresource Technology*, 305:123046, 2020. ISSN 0960-8524. doi: https://doi.org/10.1016/j.biortech.2020.123046. URL https://www.sciencedirect.com/science/article/pii/S0960852420303151.

[89] A. Ruiz-Martínez, J. Serralta, I. Romero, A. Seco, and J. Ferrer. Effect of intracellular p content on phosphate removal in scenedesmus sp. experimental study and kinetic expression. *Bioresource Technology*, 175:325–332, 2015. ISSN 0960-8524. doi: https://doi.org/10.1016/j.biortech.2014.10.081. URL https://www.sciencedirect.com/science/article/pii/S096085241401503X.

[90] F. Sangiovanni. Analisi foto-respirometriche e modellazione matematica applicate alla descrizione e all'ottimizzazione di sistemi di coltivazione di microalghe. Master's thesis, ING I - Scuola di Ingegneria Civile, Ambientale e Territoriale, 2022.

[91] K. Satyanarayana, A. Mariano, and J. Vargas. A review on microalgae: A versatile source for sustainable energy and materials. *International Journal of Energy Research*, 35:291 – 311, 03 2011. doi: 10.1002/er.1695.

[92] P. M. Schenk, S. R. Thomas-Hall, E. Stephens, U. C. Marx, J. H. Mussgnug, C. Posten, O. Kruse, and B. Hankamer. Second generation biofuels: high-efficiency microalgae for biodiesel production. *Bioenergy research*, 1:20–43, 2008.

[93] A. Seco, S. Aparicio, J. Gonzalez-Camejo, A. Jiménez-Benítez, O. Mateo, J. Mora, G. Noriega-Hevia, P. Sanchis-Perucho, R. Serna-García, N. Zamorano-López, et al. Resource recovery from sulphate-rich sewage through an innovative anaerobic-based water resource recovery facility (wrrf). *Water Science and Technology*, 78(9):1925–1936, 2018.

[94] R. Serna-García, J. Mora-Sánchez, P. Sanchis-Perucho, A. Bouzas, and A. Seco. Anaerobic membrane bioreactor (anmbr) scale-up from laboratory to pilot-scale for microalgae and primary sludge co-digestion: Biological and filtration assessment. *Bioresource Technology*, 316:123930, 2020. ISSN 0960-8524. doi: https://doi.org/10.1016/j.biortech.2020.123930. URL `https://www.sciencedirect.com/science/article/pii/S0960852420312025`.

[95] J. Serralta, J. Ferrer, L. Borrás, and A. Seco. An extension of asm2d including ph calculation. *Water Research*, 38(19):4029–4038, 2004. ISSN 0043-1354. doi: https://doi.org/10.1016/j.watres.2004.07.009. URL `https://www.sciencedirect.com/science/article/pii/S0043135404003410`.

[96] P. Shanahan, D. Borchardt, M. Henze, W. Rauch, P. Reichert, L. Somlyody, and P. Vanrolleghem. River water quality model no. 1 (rwqm1): I. modelling approach. *Water science and technology : a journal of the International Association on Water Pollution Research*, 43:1–9, 02 2001. doi: 10.2166/wst.2001.0238.

[97] B. D. Shoener, S. M. Schramm, F. Béline, O. Bernard, C. Martínez, B. G. Plósz, S. Snowling, J.-P. Steyer, B. Valverde-Pérez, D. Wágner, and J. S. Guest. Microalgae and cyanobacteria modeling in water resource recovery facilities: A critical review. *Water Research X*, 2:100024, 2019. ISSN 2589-9147. doi: https://doi.org/10.1016/j.wroa.2018.100024. URL `https://www.sciencedirect.com/science/article/pii/S2589914718300240`.

[98] J. S. Singh, A. Kumar, A. N. Rai, and D. P. Singh. Cyanobacteria: A precious bio-resource in agriculture, ecosystem, and environmental sustainability. *Frontiers in Microbiology*, 7, 2016. ISSN 1664-302X. doi: 10.3389/fmicb.2016.00529. URL `https://www.frontiersin.org/articles/10.3389/fmicb.2016.00529`.

[99] J. S. Singh, A. Kumar, A. N. Rai, and D. P. Singh. Cyanobacteria: A precious bio-resource in agriculture, ecosystem, and environmental sustainability. *Frontiers*

in Microbiology, 7, 2016. ISSN 1664-302X. doi: 10.3389/fmicb.2016.00529. URL https://www.frontiersin.org/articles/10.3389/fmicb.2016.00529.

[100] A. Solimeno, R. Samsó, E. Uggetti, B. Sialve, J.-P. Steyer, A. Gabarró, and J. García. New mechanistic model to simulate microalgae growth. *Algal Research*, 12:350–358, 2015. ISSN 2211-9264. doi: https://doi.org/10.1016/j.algal.2015.09.008. URL https://www.sciencedirect.com/science/article/pii/S221192641530062X.

[101] A. Solimeno, C. Gómez-Serrano, and F. Acién. Bioalgae 2: improved model of microalgae and bacteria consortia for wastewater treatment. *Environmental Science and Pollution Research*, 26, 09 2019. doi: 10.1007/s11356-019-05824-5.

[102] J. H. Steele. Environmental control of photosynthesis in the sea. *Limnology and Oceanography*, 7(2):137–150, 1962. doi: https://doi.org/10.4319/lo.1962.7.2.0137. URL https://aslopubs.onlinelibrary.wiley.com/doi/abs/10.4319/lo.1962.7.2.0137.

[103] R. J. Strasser, M. Tsimilli-Michael, and A. Srivastava. *Analysis of the Chlorophyll a Fluorescence Transient*, pages 321–362. Springer Netherlands, Dordrecht, 2004. ISBN 978-1-4020-3218-9. doi: 10.1007/978-1-4020-3218-9_12. URL https://doi.org/10.1007/978-1-4020-3218-9_12.

[104] C.-H. Su, L.-J. Chien, J. Gomes, Y.-S. Lin, Y.-K. Yu, J.-S. Liou, and R.-J. Syu. Factors affecting lipid accumulation by nannochloropsis oculata in a two-stage cultivation process. *Journal of Applied Phycology*, 23:903–908, 2011.

[105] G. Su, H. C. Ong, Y. Y. Gan, W.-H. Chen, C. T. Chong, and Y. S. Ok. Co-pyrolysis of microalgae and other biomass wastes for the production of high-quality bio-oil: progress and prospective. *Bioresource technology*, 344:126096, 2022.

[106] J. Sánchez, J. M. Fernandez-Sevilla, G. Acien, M. Cerón, J. Pérez-Parra, and E. Molina-Grima. Biomass and lutein productivity of scenedesmus almeriensis: Influence of irradiance, dilution rate and temperature. *Applied microbiology and biotechnology*, 79:719–29, 08 2008. doi: 10.1007/s00253-008-1494-2.

[107] M. J. E. L. S. P. Tibbetts, Sean M. Chemical composition and nutritional properties of freshwater and marine microalgal biomass cultured in photobioreactors. *Journal of Applied Phycology*, 03 2015. doi: 10.1007/s10811-014-0428-x. URL https://doi.org/10.1007/s10811-014-0428-x.

[108] G. Torzillo and A. Vonshak. *Handbook of Microalgal Culture: Applied Phycology*

and Biotechnology, Second Edition, pages 90–113. 04 2013. ISBN 9780470673898. doi: 10.1002/9781118567166.ch6.

[109] C. A. Tracker, 2022. URL `https://climateactiontracker.org/countries/`.

[110] A. Trebst. Energy conservation in photosynthetic electron transport of chloroplasts. *Annual Review of Plant Physiology*, 25(1):423–458, 1974. doi: 10.1146/annurev.pp.25.060174.002231. URL `https://doi.org/10.1146/annurev.pp.25.060174.002231`.

[111] *World Population Prospects 2022*. UN Department of Economic and Social Affairs Population Division, 2022.

[112] *HUMAN DEVELOPMENT REPORT 2007/2008*. United Nations Development Programme, 2008.

[113] *HUMAN DEVELOPMENT REPORT 2021/2022 OVERVIEW - Uncertain times, unsettled lives Shaping our future in a transforming world*. United Nations Development Programme, 2022.

[114] G. Van Vooren, F. Le Grand, J. Legrand, S. Cuiné, G. Peltier, and J. Pruvost. Investigation of fatty acids accumulation in nannochloropsis oculata for biodiesel application. *Bioresource Technology*, 124:421–432, 2012. ISSN 0960-8524. doi: https://doi.org/10.1016/j.biortech.2012.08.009. URL `https://www.sciencedirect.com/science/article/pii/S0960852412011777`.

[115] J. Velazquez, R. Rodriguez-Jasso, L. Colla, A. Galindo, D. Cervantes, C. Aguilar, B. Fernandes, and H. Ruiz. Microalgal biomass pretreatment for bioethanol production: A review. *Biofuel Research Journal*, 5, 03 2018. doi: 10.18331/BRJ2018.5.1.5.

[116] A. Viruela, Robles, F. Durán Pinzón, M. Ruano, R. Barat, J. Ferrer, and A. Seco. Performance of an outdoor membrane photobioreactor for resource recovery from anaerobically treated sewage. *Journal of Cleaner Production*, 178, 12 2017. doi: 10.1016/j.jclepro.2017.12.223.

[117] A. Viruela, S. Aparicio, Ángel Robles, L. Borrás Falomir, J. Serralta, A. Seco, and J. Ferrer. Kinetic modeling of autotrophic microalgae mainline processes for sewage treatment in phosphorus-replete and -deplete culture conditions. *Science of The Total Environment*, 797:149165, 2021. ISSN 0048-9697. doi: https://doi.org/10.1016/j.scitotenv.2021.149165. URL `https://www.sciencedirect.com/science/article/pii/S0048969721042388`.

[118] A. Viruela, S. Aparicio, Ángel Robles, L. Borrás Falomir, J. Serralta, A. Seco, and

J. Ferrer. Kinetic modeling of autotrophic microalgae mainline processes for sewage treatment in phosphorus-replete and -deplete culture conditions. *Science of The Total Environment*, 797:149165, 2021. ISSN 0048-9697. doi: https://doi.org/10.1016/j.scitotenv.2021.149165. URL https://www.sciencedirect.com/science/article/pii/S0048969721042388.

[119] S. Walke. Protein extraction from spirulina platensis. 8:1524–1530, 10 2019. doi: 10.35940/ijitee.L3110.1081219.

[120] H. Wang, W. Zhang, L. Chen, J. Wang, and T. Liu. The contamination and control of biological pollutants in mass cultivation of microalgae. *Bioresource technology*, 128:745–750, 2013.

[121] J.-H. Wang, T.-y. Zhang, G.-H. Dao, X.-Q. Xu, X.-X. Wang, and H.-Y. Hu. Microalgae-based advanced municipal wastewater treatment for reuse in water bodies. *Applied Microbiology and Biotechnology*, 101, 04 2017. doi: 10.1007/s00253-017-8184-x.

[122] R. Wayne. Chapter 13 - chloroplasts. In R. Wayne, editor, *Plant Cell Biology (Second Edition)*, pages 235–267. Academic Press, second edition edition, 2019. ISBN 978-0-12-814371-1. doi: https://doi.org/10.1016/B978-0-12-814371-1.00013-8. URL https://www.sciencedirect.com/science/article/pii/B9780128143711000138.

[123] Wikipedia contributors. Planetary boundaries — Wikipedia, the free encyclopedia, 2022. URL https://en.wikipedia.org/w/index.php?title=Planetary_boundaries&oldid=1118644719.

[124] P. J. l. B. Williams and L. M. L. Laurens. Microalgae as biodiesel biomass feedstocks: Review analysis of the biochemistry, energetics economics. *Energy Environ. Sci.*, 3:554–590, 2010. doi: 10.1039/B924978H. URL http://dx.doi.org/10.1039/B924978H.

[125] M.-K. H. Winkler, P. Boets, B. Hahne, P. Goethals, and E. I. P. Volcke. Effect of the dilution rate on microbial competition: r-strategist can win over k-strategist at low substrate concentration. *PLOS ONE*, 12:1–12, 03 2017. doi: 10.1371/journal.pone.0172785. URL https://doi.org/10.1371/journal.pone.0172785.

[126] D. Wágner, B. Valverde Pérez, and B. Plosz. Light attenuation in photobioreactors and algal pigmentation under different growth conditions – model identification and complexity assessment. *Algal Research*, 35:488–499, 11 2018. doi: 10.1016/j.algal.2018.08.019.

[127] D. S. Wágner, B. Valverde-Pérez, M. Sæbø, M. Bregua de la Sotilla, J. Van Wagenen, B. F. Smets, and B. G. Plósz. Towards a consensus-based biokinetic model for green microalgae – the asm-a. *Water Research*, 103:485–499, 2016. ISSN 0043-1354. doi: https://doi.org/10.1016/j.watres.2016.07.026. URL https://www.sciencedirect.com/science/article/pii/S0043135416305309.

[128] A. Xia and J. D. Murphy. Microalgal cultivation in treating liquid digestate from biogas systems. *Trends in Biotechnology*, 34(4):264–275, 2016. ISSN 0167-7799. doi: https://doi.org/10.1016/j.tibtech.2015.12.010. URL https://www.sciencedirect.com/science/article/pii/S016777991500270X.

[129] M. Xu, M. Bernards, and Z. Hu. Algae-facilitated chemical phosphorus removal during high-density chlorella emersonii cultivation in a membrane bioreactor. *Bioresource Technology*, 153:383–387, 2014. ISSN 0960-8524. doi: https://doi.org/10.1016/j.biortech.2013.12.026. URL https://www.sciencedirect.com/science/article/pii/S0960852413018440.

[130] A. Y. Effect of ph on inorganic carbon uptake in algal cultures. *Appl Environ Microbiol.*, 1982. doi: 10.1128/aem.43.6.1300-1306.1982. URL https://pubmed.ncbi.nlm.nih.gov/16346029/.

[131] S. R. M. R. M. A.-G. A. G. R. A. . A. R. R. Yaakob, M. A. Influence of nitrogen and phosphorus on microalgal growth, biomass, lipid, and fatty acid production: An overview. *National library of medicine*, 2021. doi: https://doi.org/10.3390/cells10020393. URL https://www.ncbi.nlm.nih.gov/pmc/articles/PMC7918059/.

[132] S. Zaher and A. Helal. How culture medium ph range influence phytoplankton growth performance and biochemical content. *Egyptian Journal of Aquatic Biology and Fisheries*, 24:103–116, 09 2020. doi: 10.21608/ejabf.2020.111001.

[133] S. Zhang, L. Zhang, G. Xu, F. Li, and X. Li. A review on biodiesel production from microalgae: Influencing parameters and recent advanced technologies. *Frontiers in Microbiology*, 13, 2022. ISSN 1664-302X. doi: 10.3389/fmicb.2022.970028. URL https://www.frontiersin.org/articles/10.3389/fmicb.2022.970028.

[134] Çağla Yarkent, C. Gürlek, and S. S. Oncel. Potential of microalgal compounds in trending natural cosmetics: A review. *Sustainable Chemistry and Pharmacy*, 17:100304, 2020. ISSN 2352-5541. doi: https://doi.org/10.1016/j.scp.2020.100304. URL https://www.sciencedirect.com/science/article/pii/S2352554120301169.

A | Appendix A

A.1. Flask average depth

Table A.1: Average depth flask.

Flask horizontal section	Radius d[cm]	Radius d[m]
Top	2	0.02
1000ml	3.5	0.035
700ml	5	0.05
Base	6.5	0.065
d average	4.25	0.0425

A.2. Viruela et al. microalgae model

Parameters	Description	Value	Unit	Source
μ_{ALG}	Maximum growth rate of X_{ALG}	1.8	d^{-1}	Calibrated
$b_{ALG,1}$	Maximum inactivation rate of X_{ALG}	0.1	d^{-1}	(Reichert et al., 2001)
$b_{ALG,2}$	Maximum decay rate of X_{ALG}	0.15	d^{-1}	Calibrated
q_{XPP}	Rate constant for storage of $X_{PP\text{-}ALG}$	0.01	d^{-1}	Calibrated
K_{O2}	Half saturation parameter for S_{O2}	0.2	g O_2 m^{-3}	(Reichert et al., 2001)
$K_{Ig,C}$	Half saturation parameter for $S_{Ig,C}$	$4.32 \cdot 10^{-3}$	g C m^{-3}	(Solimeno et al., 2015)
K_{NHX}	Half saturation parameter for S_{NHX} in a phosphorus-replete medium	0.1	g N m^{-3}	Calibrated
$K_{NHX\text{-}qXPP}$	Half saturation parameter for S_{NHX} in a phosphorus-deplete medium	3	g N m^{-3}	Calibrated
K_{NO3}	Half saturation parameter for S_{NO3}	12.61	g N m^{-3}	(Wágner et al., 2016)
η_{NO3}	Reduction factor for X_{ALG} growth of S_{NO3}	0.59	–	(Eze et al., 2018)
K_{PO4}	Half saturation parameter for S_{PO4}	0.05	g P m^{-3}	Calibrated
$K_{I,PO4}$	Inhibition parameter for $X_{PP\text{-}ALG}$ use in a phosphorus-replete medium	0.15	g P m^{-3}	Calibrated
K_{XPP}	Half saturation parameter of X_{ALG} growth for $X_{PP\text{-}ALG}$	0.0027	g P m^{-3}	(Ruiz-Martinez et al., 2014)
K_{XPP_qXPP}	Half saturation parameter of X_{PP} storage for $X_{PP\text{-}ALG}$	0.003	g P m^{-3}	(Ruiz-Martínez et al., 2015a)
n	Regulation coefficient or Hill number	0.006	–	(Ruiz-Martínez et al., 2015a)
K_{Mg}	Half saturation parameter for S_{Mg}	0.13	g Mg m^{-3}	(Sydney et al., 2010)
K_K	Half saturation parameter for S_K	8.78	g K m^{-3}	(Sydney et al., 2010)
T_{MIN}	Minimum temperature for microalgae growth	2	°C	Calibrated
T_{MAX}	Maximum temperature for microalgae growth	40	°C	Calibrated
b	Intrinsic model parameter	87.13	–	Calibrated
c	Intrinsic model parameter	1.46	–	Calibrated
I_{OPT}	Optimal light intensity for X_{ALG} growth	230	µmol m^{-2} s^{-1}	Calibrated
k_w	Attenuation coefficient due to water	1.97	m^{-3}	(Sun et al., 2016)
K_I	Attenuation coefficient due to particulate components	0.025	m^2 g TSS^{-1}	Calibrated
$K_{I,H}$	Lower half saturation parameter for S_H	0.00001	mol H^+ L^{-1}	(Siegrist et al., 1993)
$K_{S,H}$	Upper half saturation parameter for S_H	0.00063	mol H^+ L^{-1}	(Siegrist et al., 1993)
$S_{H,opt}$	Optimal pH for X_{ALG} growth	7.50	pH	Calculated
$K_{La,O2}$	Mass transfer coefficient for oxygen	16.2	h^{-1}	Calibrated
$K_{La,CO2}$	Mass transfer coefficient for dioxide carbon	16.2	h^{-1}	Calibrated
$K_{La,NH3}$	Mass transfer coefficient for free ammonia	16.2	h^{-1}	Calibrated
k	Constants of mass transfer coefficient equation	0.05	–	Calibrated
r	Constants of mass transfer coefficient equation	1	–	Calibrated

Figure A.1: Parameters values used in the microalgae model [118].

Stoichiometric coefficients	Unit
X_{ALG} growth on S_{NHX} and S_{PO4}	
$v_{1,1} = 1$	g O_2 g COD^{-1}
$v_{2,1} = -i_{N,ALG}$	g N g COD^{-1}
$v_{4,1} = -i_{P,ALG}$	g P g COD^{-1}
$v_{5,1} = \frac{-i_{C,ALG}}{10^3}$	mol C g COD^{-1}
$v_{6,1} = \frac{i_{N,ALG}}{14} \cdot \frac{1}{10^3} - \frac{2i_{C,ALG}}{10^3} - \frac{3i_{P,ALG}}{31} \cdot \frac{1}{10^3}$	mol H g COD^{-1}
$v_{11,1} = 1$	g COD g COD^{-1}
X_{ALG} growth on S_{NO3} and S_{PO4}	
$v_{1,2} = 1 + \frac{64}{14} \cdot i_{N,ALG}$	g O_2 g COD^{-1}
$v_{3,2} = -i_{N,ALG}$	g N g COD^{-1}
$v_{4,2} = -i_{P,ALG}$	g P g COD^{-1}
$v_{5,2} = \frac{-i_{C,ALG}}{10^3}$	mol C gCOD^{-1}
$v_{6,2} = -\frac{i_{N,ALG}}{14} \cdot \frac{1}{10^3} - \frac{2i_{C,ALG}}{10^3} - \frac{3i_{P,ALG}}{31} \cdot \frac{1}{10^3}$	mol H g COD^{-1}
$v_{11,2} = 1$	g COD g COD^{-1}
X_{ALG} growth on S_{NHX} and X_{PP-ALG}	
$v_{1,3} = 1$	g O_2 g COD^{-1}
$v_{2,3} = -i_{N,ALG}$	g N g COD^{-1}
$v_{5,3} = \frac{-i_{C,ALG}}{10^3}$	mol C g COD^{-1}
$v_{6,3} = \frac{i_{N,ALG}}{14} \cdot \frac{1}{10^3} - \frac{2i_{C,ALG}}{10^3} - \frac{2i_{P,ALG} \cdot i_{Mg,XPP-ALG}}{24.3} \cdot \frac{1}{10^3} - \frac{i_{P,ALG} \cdot i_{K,XPP-ALG}}{39.1} \cdot \frac{1}{10^3}$	mol H g COD^{-1}
$v_{7,3} = i_{P,ALG} \cdot i_{Mg,XPP-ALG}$	g Mg g COD^{-1}
$v_{8,3} = i_{P,ALG} \cdot i_{K,XPP-ALG}$	g K g COD^{-1}
$v_{11,3} = 1$	g COD g COD^{-1}
$v_{13,3} = -i_{P,ALG}$	g P g COD^{-1}
X_{ALG} growth on S_{NO3} on X_{PP-ALG}	
$v_{1,4} = 1 + \frac{64}{14} \cdot i_{N,ALG}$	g O_2 g COD^{-1}
$v_{3,4} = -i_{N,ALG}$	g N g COD^{-1}
$v_{5,4} = \frac{-i_{C,ALG}}{10^3}$	mol C g COD^{-1}
$v_{6,4} = -\frac{i_{N,ALG}}{14} \cdot \frac{1}{10^3} - \frac{2i_{C,ALG}}{10^3} - \frac{2i_{P,ALG} \cdot i_{Mg,XPP-ALG}}{24.3} \cdot \frac{1}{10^3} - \frac{i_{P,ALG} \cdot i_{K,XPP-ALG}}{39.1} \cdot \frac{1}{10^3}$	mol H g COD^{-1}
$v_{7,4} = i_{P,ALG} \cdot i_{Mg,XPPALG}$	g Mg g COD^{-1}
$v_{8,4} = i_{P,ALG} \cdot i_{K,XPP-ALG}$	g K g COD^{-1}
$v_{11,4} = 1$	g COD g COD^{-1}
$v_{13,4} = -i_{P,ALG}$	g P g COD^{-1}
X_{PP-ALG} storage	
$v_{4,5} = -1$	g P g COD^{-1}
$v_{6,5} = -\frac{3}{31 \cdot 10^3} + \frac{2i_{Mg,XPPALG}}{24.3} \frac{1}{10^3} + \frac{i_{K,XPPALG}}{39.1} \cdot \frac{1}{10^3}$	mol H g COD^{-1}
$v_{7,5} = -i_{Mg,XPPALG}$	g Mg g COD^{-1}
$v_{8,5} = -i_{K,XPPALG}$	g K g COD^{-1}
$v_{13,5} = 1$	g P g COD^{-1}

Figure A.2: Stoichiometric coefficients in microalgae model, continued [118].

X_{ALG} endogenous respiration	
$v_{1,6} = -1$	g COD g COD^{-1}
$v_{2,6} = i_{N,ALG}$	g N g COD^{-1}
$v_{4,6} = i_{P,ALG}$	g P g COD^{-1}
$v_{5,6} = \frac{i_{C,ALG}}{10^3}$	mol C g COD^{-1}
$v_{6,6} = 3 \cdot \frac{i_{P,ALG}}{31} + 2 \cdot \frac{i_{C,ALG}}{10^3} - \frac{i_{N,ALG}}{14}$	mol H g COD^{-1}
$v_{11,6} = -1$	g COD g COD^{-1}
X_{ALG} lysis	
$v_{2,7} = i_{N,ALG} - (1 - f_{SI} - f_{XI}) \cdot i_{N,SS} - f_{SI} \cdot i_{N,SIALG} - f_{XI} \cdot i_{N,XIALG}$	g N g COD^{-1}
$v_{4,7} = i_{P,ALG} - (1 - f_{SI} - f_{XI}) \cdot i_{P,SS} - f_{SI} \cdot i_{P,SIALG} - f_{XI} \cdot i_{P,XIALG}$	g P g COD^{-1}
$v_{5,7} = \frac{i_{C,ALG} - (1 - f_{SI} - f_{XI}) \cdot i_{C,SS} - f_{SI} \cdot i_{C,SIALG} - f_{XI} \cdot i_{C,XIALG}}{10^3}$	mol C g COD^{-1}
$v_{6,7} = \frac{3 \cdot (i_{P,ALG} - (1 - f_{SI} - f_{XI}) \cdot i_{P,SS} - f_{SI} \cdot i_{P,SIALG} - f_{XI} \cdot i_{P,XIALG})}{31} + \frac{2 \cdot (i_{C,ALG} - (1 - f_{SI} - f_{XI}) \cdot i_{C,SS} - f_{SI} \cdot i_{C,SIALG} - f_{XI} \cdot i_{C,XIALG})}{10^3} - \frac{i_{N,ALG} - (1 - f_{SI} - f_{XI}) \cdot i_{N,SS} - f_{SI} \cdot i_{N,SIALG} - f_{XI} \cdot i_{N,XIALG}}{14}$	mol H g COD^{-1}
$v_{9,7} = (1 - f_{SI} - f_{XI})$	g COD g COD^{-1}
$v_{10,7} = f_{SI}$	g COD g COD^{-1}
$v_{11,7} = -1$	g COD g COD^{-1}
$v_{12,7} = f_{XI}$	g COD g COD^{-1}
$X_{PP\text{-}ALG}$ lysis	
$v_{4,8} = 1$	g P g COD^{-1}
$v_{6,8} = -\frac{3}{31 \cdot 10^3} - \frac{2i_{Mg,XPPALG}}{24.3} \frac{1}{10^3} - \frac{i_{K,XPPALG}}{39.1} \cdot \frac{1}{10^3}$	mol H g COD^{-1}
$v_{7,8} = i_{Mg,XPPALG}$	g Mg g COD^{-1}
$v_{8,8} = i_{K,XPPALG}$	g K g COD^{-1}
$v_{13,8} = -1$	g P g COD^{-1}
$S_{[CO2]}$ stripping	
$v_{5,9} = \frac{-1}{10^3}$	-
$v_{6,9} = \frac{-2}{10^6}$	-
S_{O2} stripping	
$v_{1,10} = -1$	-
$S_{[NH3]}$ stripping	
$v_{2,11} = -1$	-

Figure A.3: Stoichiometric coefficients in microalgae model, continued [118].

Parameters	Equations
Chemical equilibrium $NH_4^+ \leftrightarrow NH_3$	$K_{eq,1} = 10^{2.891-\frac{2727}{T+273.15}}$
Chemical equilibrium $CO_2 \leftrightarrow HCO_3^-$.	$K_{eq,2} = 10^{17.843-\frac{3404.71}{T+273.15}-0.032786(T+273.15)}$
Chemical equilibrium $HCO_3^- \leftrightarrow CO_3^{2-}$	$K_{eq,3} = 10^{9.494-\frac{2902.39}{T+273.15}-0.02379(T+273.15)}$
Chemical equilibrium $CO_2 \leftrightarrow HCO_3^-$.	$K_{eq,1} = 10^{17.843-\frac{3404.71}{T+273.15}-0.032786(T+273.15)}$

Kinetic parameters

Parameters	Description	Value	Unit	Source
$k_{eq,1}$	Dissociation constant of $NH_4^+ \leftrightarrow NH_3$	1000	d^{-1}	(Reichert et al., 2001)
$k_{eq,2}$	Dissociation constant of $CO_2 \leftrightarrow HCO_3^-$.	10000	d^{-1}	(Reichert et al., 2001)
$k_{eq,3}$	Dissociation constant of $HCO_3^- \leftrightarrow CO_3^{2-}$	1000	d^{-1}	(Reichert et al., 2001)
$k_{eq,w}$	Dissociation constant of $H^+ \leftrightarrow OH^-$	1000	g m^{-1} d^{-1}	(Reichert et al., 2001)
Stoichiometric parameters				
$i_{N,ALG}$	Fraction of nitrogen in microalgae	0.060	g N g COD^{-1}	Calculated from Oswald (1988)
$i_{P,ALG}$	Fraction of phosphorus in microalgae	0.0016	g P g COD^{-1}	(Ruiz-Martínez et al., 2015)
$i_{C,ALG}$	Fraction of carbon in microalgae	0.3372	g C g COD^{-1}	Calculated from Oswald (1988)
$i_{TSS,ALG}$	Fraction of total suspended solids in microalgae	0.646	g TSS g COD^{-1}	Calculated from Oswald (1988)
$i_{N,XI}$	Fraction of nitrogen in X_I	0.01	g N g COD^{-1}	Current study
$i_{P,XI}$	Fraction of phosphorus in X_I	0.005	g P g COD^{-1}	Current study
$i_{C,XI}$	Fraction of carbon in X_I	0.025	g C g COD^{-1}	Current study
$i_{TSS,XI}$	Fraction of total suspended solids in X_I	0.60	g TSS g COD^{-1}	Current study
$i_{Mg,XPP-ALG}$	Fraction of magnesium in X_{PP-ALG}	0.26	g Mg g P^{-1}	Calculated from $(K_{0.34}Mg_{0.33}PO_3)n$
$i_{K,XPP-ALG}$	Fraction of potassium in X_{PP-ALG}	0.42	g K g P^{-1}	Calculated from $(K_{0.34}Mg_{0.33}PO_3)n$
$i_{TSS,XPP-ALG}$	Fraction of total suspended solids in X_{PP-ALG}	3.23	g TSS g P^{-1}	Calculated from $(K_{0.34}Mg_{0.33}PO_3)n$
$i_{N,SS}$	Fraction of nitrogen in S_S	0.01	g N g COD^{-1}	Current study
$i_{P,SS}$	Fraction of phosphorus in S_S	0.001	g P g COD^{-1}	Current study
$i_{C,SS}$	Fraction of carbon in S_S	0.025	g C g COD^{-1}	Current study
$i_{N,SI}$	Fraction of nitrogen in S_I	0.001	g N g COD^{-1}	Current study
$i_{P,SI}$	Fraction of phosphorus in S_I	0.001	g P g COD^{-1}	Current study
$i_{C,SI}$	Fraction of carbon in S_I	0.03	g C g COD^{-1}	Current study
F_{XI}	Fraction of X_I generated microalgae decay	0.25	g COD g COD^{-1}	Current study
F_{SI}	Fraction of S_I generated microalgae decay	0.6	g C g COD^{-1}	Current study

Figure A.4: Stoichiometric coefficients in microalgae model [118].

B | Appendix B

B.1. Optimization function with MATLAB genetic algorithm

```
function [F]=SIMULACIONES_OPTIMIZACION_ALG(X)

%% parámetros del modelo
% Coeficientes de conversión de la matriz de composición
  Eso.CO_Itssalg = 0.646;  % Contenido de TSS en las algas
  Eso.CO_Itssxialg = 0.6;  % Contenido de TSS en la Xialg
  Eso.CO_Itssxppalg = 3.23;  % Contenido de TSS en el Xppalg
  Eso.CO_Inalg = 0.06;  % Contenido de nitrógeno en las algas (C106H181O45N16P)
  Eso.CO_Inxialg = 0.01;  % Contenido de nitrógeno en la Xialg.
  Eso.CO_Ipalg = 0.001/Eso.CO_Itssalg; % Contenido de fósforo en las algas
  Eso.CO_Ipxialg = 0.005;  % Contenido de fósforo en la Xialg.
  Eso.CO_Icalg = 0.0281;  % en moles - Contenido de carbono en las algas
  Eso.CO_Icxialg = 0.025;  % Contenido de carbono en la Xialg
  Eso.CO_Imgxialg = 0.0015;  %Contenido de magnesio en la Xialg
  Eso.CO_Imgxppalg = 0.26;  %Contenido de magnesio en la Xialg.
  Eso.CO_Imgalg = 0.0018;  %Contenido de magnesio en la Xalg;
  Bibliografía https://doi.org/10.1016/j.biortech.2010.02.088;
  También podría ser 0.0032
  Chemical composition and nutritional properties of freshwater and marine
  microalgal biomass cultured in photobioreactors
  Eso.CO_Ikalg = 0.0207;  %Contenido de potasio en la Xalg;
  Bibliografía https://doi.org/10.1016/j.biortech.2010.02.088;
  También podría ser 0.01
  Chemical composition and nutritional properties of freshwater and marine
  microalgal biomass cultured in photobioreactors
  Eso.CO_Ikxialg = 0.0008;  %Contenido de potasio en la Xialg
  Eso.CO_Ikxppalg = 0.42;  %Contenido de potasio en la Xppalg
```

```
Eso.CO_Ipss = 0.001;% Contenido de fósforo en la Ss
Eso.CO_Ipsi = 0.001;% Contenido de fósforo en la Si
Eso.CO_Inss = 0.01;%0.01;% Contenido de nitrógeno en la Ss
Eso.CO_Insi = 0.001;% Contenido de nitrógeno en la Si
Eso.CO_Icss = 0.025;% Contenido de nitrógeno en la Ss
Eso.CO_Icsi = 0.03;% Contenido de nitrógeno en la Si

% Parámetros estequiométricos Algas modelo simplificado
Eso.CO_Fxialg = 0.25;  %
Eso.CO_Fsi = 0.6; %

% Parámetros cinéticos y coeficientes cinéticos para la biomasa
Eso.CO_Ualg_20 = 1.8; %Velocidad máxima de crecimiento de algas a 20ºC
Eso.CO_Qpp_20 =0.010; %Velocidad máxima de acumulación de polifosfato a 20ºC
Eso.CO_balg1_20 = 0.15; %Velocidad de muerte de algas a 20ºC %%y poliP
Eso.CO_balg2_20 = 0.1; %Velocidad de mantenimiento de algas a 20ºC
Eso.CO_Nno2 = 0.8; %Rendimiento para el nitrito
Eso.CO_Nno3 = 0.59; %Rendimiento para el nitrato
Eso.CO_Ktotc = 0.00432; %Constante de semisaturación para el CO2
Eso.CO_Ko2 = 0.2; %Constante de semisaturación para el O2
Eso.CO_Kxppalg_alg = 0.027; %Constante de semisaturación para el Xpp en el crecimiento
Eso.CO_Knh4 = 0.1; %Constante de semisaturación para el amonio
Eso.CO_Knh4_qpp = 3; %Constante de semisaturación para el amonio
Eso.CO_Kno2 = 10; %Constante de semisaturación para el nitrito
Eso.CO_Kno3 = 12.61; %Constante de semisaturación para el nitrato
Eso.CO_Kpo4 = 0.05; %Constante de semisaturación para el fosfato
Eso.CO_Kmg = 0.13;  %Constante de semisaturación para el magnesio
Eso.CO_Kk = 8.78; %Constante de semisaturación para el potasio
Eso.CO_n_xppalg = 0.006;  %Máxima concentración de Xppalg almacenada
Eso.CO_Kxppalg_xppalg = 0.003; %Constante de semisaturación para el
polifosfato en la acumulación de polifosfatos
Eso.CO_Kla_O2 = 1.36;% se calcula a partir del base; 1.36-1.80 h-1
Eso.CO_Kla_CO2 = Eso.CO_Kla_O2;%
Eso.CO_KipH = 0.00063;
Eso.CO_KpH = 0.000001;  %Me da un pH óptimo de 7,5
Eso.CO_Kipo4 = 0.15; %Inhibición del uso del Xpp cuando hay Spo4
Eso.CO_Kla_NH3 = Eso.CO_Kla_CO2;% se calcula a partir del base
Eso.CO_Kla_k = 0.05; %constante ajuste Kla en función de Q
```

```
  Eso.CO_Kla_r = 1; %constante ajuste Kla en función de Q

  % Coeficientes de la función lumínica
  Eso.CO_kw = 0.1986; %Coeficiente de atenuación del agua (valor para Xtss medido
  como DQO)
  Eso.CO_kb = 0.025; %Coeficiente de atenuación de la biomasa
  Eso.CO_Ioptimo = 230; %Coeficiente de saturación de la luz

  % Coeficientes de la función de datos.Temperatura (Ratkowski)
  Eso.CO_Tmin_Ualg = 2; %Coeficiente para calcular Ualg a cualquier temperatura
  Eso.CO_Tmax_Ualg = 40; %Coeficiente para calcular Ualg a cualquier T
  Eso.CO_b_Ualg = 87.1329461911729; %Coeficiente para calcular Ualg a cualquier T
  Eso.CO_c_Ualg = 1.46349934667002E-08; %Coeficiente para calcular Ualg a cualquier T
  Eso.CO_Tmin_balg1 = Eso.CO_Tmin_Ualg; %Coeficiente para calcular balg a cualquier T
  Eso.CO_Tmax_balg1 = Eso.CO_Tmax_Ualg; %Coeficiente para calcular balg a cualquier T
  Eso.CO_b_balg1 = Eso.CO_b_Ualg;%Coeficiente para calcular balg a cualquier T
  Eso.CO_c_balg1 = Eso.CO_c_Ualg; %Coeficiente para calcular balg a cualquier T
  Eso.CO_Tmin_balg2 = Eso.CO_Tmin_Ualg; %Coeficiente para calcular balg a cualquier T
  Eso.CO_Tmax_balg2 = Eso.CO_Tmax_Ualg; %Coeficiente para calcular balg a cualquier T
  Eso.CO_b_balg2 = Eso.CO_b_Ualg; %Coeficiente para calcular balg a cualquier T
  Eso.CO_c_balg2 = Eso.CO_c_Ualg; %Coeficiente para calcular balg a cualquier T

  % Coeficientes de la función de pH
  Eso.CO_pHoptimo = 7.5;

  Eso.CO_Ualg_20  = X(1) ;
  Eso.CO_KipH   = X(2)/1000 ;
  Eso.CO_KpH  = X(3)/1000000;
  Eso.CO_Kla_O2 = 5.84;
  Eso.CO_Kla_CO2 = Eso.CO_Kla_O2;
  Eso.CO_Kla_NH3 = Eso.CO_Kla_CO2;


PARAMETROS = Eso;

load Datos_calibracion_modelo_TODOS.txt
DATOS2 = Datos_calibracion_modelo_TODOS;
DATOS2(DATOS2(:,:)<0)=0;
```

```
j=1;
experimento=1;
for i=1:DATOS2(length (DATOS2(:,1)),1) %experimentos tomados

DATOS=DATOS2(j:j+4,:); %primer exp
pHmod=[];
Alkmod=[];

So2 = 10;
Snh4 = DATOS(1,4);
Sno2 = 0;
Sno3 = 0;
Spo4 = DATOS(1,5);
Sco2 = 0;
Stotc = DATOS(1,18);
Salk = DATOS(1,8);
Stoth = DATOS(1,19);
Smg = DATOS(1,10);
Sk = DATOS(1,11);
Xs = 0;
Ss = 0;
Si = 0;
Xalg =(DATOS(1,22)-Xs)/Eso.CO_Itssalg;
Xialg = 0;
Xppalg = 5;

x0=[So2,Snh4,Sno2,Sno3,Spo4,Sco2,Stotc,Salk,Stoth,Smg,Sk,Xs,Xalg,Xialg,Xppalg,Ss,Si];

if i==1
    texp=DATOS(:,2)./24;
    pHexp=DATOS(:,17);
    Alkexp=DATOS(:,8);
else
    texp = [texp; DATOS(:,2)./24+5/24.*(i-1)];
    pHexp = [pHexp; DATOS(:,17)];
    Alkexp = [Alkexp; DATOS(:,8)];
end

tiempo=DATOS(:,2)./24;
```

```
options = odeset('MaxStep',0.1,'InitialStep',0.000005);
[t,Y] = ode45('Generacion_ALG',tiempo,x0,options,PARAMETROS,DATOS(1,:),experimento);

calculopH=1;
if calculopH==1
    %siFI1 = 0; % PARA INTRODUCIR LA FUERZA IÓNICA
    siFI1 = 1; % PARA QUE MINTEQA2 CALCULE LA FUERZA IÓNICA
    if siFI1==0
        FuerzaIonica=0.1;
    elseif siFI1==1
        FuerzaIonica=0;
    end
    for jjj=1:length (Y(:,1))
        datos.Temp = 25;
        datos.ORP = 100;
        datos.totAl = 0;
        datos.Sa = DATOS (1,3);
        datos.Spro = DATOS (1,6);
        datos.totFe = DATOS (1,12);
        datos.totCa = DATOS (1,9);
        datos.Sh2s = DATOS (1,16);
        datos.Sso4 = DATOS (1,15);
        totH = Y(jjj,9);
        totC = Y(jjj,7);
        sialk = 0;
        datos.pH = 0;
        datos.Snh4 = Y(jjj,2);
        datos.Sno2 = Y(jjj,3);
        datos.Sno3 = Y(jjj,4);
        datos.Spo4 = Y(jjj,5);
        datos.Smg = Y(jjj,10);
        datos.Sk = Y(jjj,11);

        %Calculo de pH
        MatrizDatos=[datos.Temp datos.pH datos.ORP totH totC datos.Smg datos.Sk
        datos.totAl datos.Sa datos.Spro datos.Snh4 datos.Spo4 datos.totFe
        datos.totCa datos.Sno2 datos.Sh2s datos.Sso4 FuerzaIonica sialk];
        MatrizResultados=LeerDLL(MatrizDatos,1);
```

```
        pH = MatrizResultados(1);
        datos.pH = pH;
        if isempty(pHmod)
            pHmod=pH;
        else
            pHmod = [pHmod; pH];
        end

         %Calculo equilibrio
        MatrizDatos=[datos.Temp datos.pH datos.ORP totH totC datos.Smg datos.Sk
        datos.totAl datos.Sa datos.Spro datos.Snh4 datos.Spo4 datos.totFe
        datos.totCa datos.Sno2 datos.Sh2s datos.Sso4 FuerzaIonica sialk];
        MatrizResultados=LeerDLL(MatrizDatos,0);

        datos.Sco3= MatrizResultados(10);
        datos.Shco3= MatrizResultados(12);
        datos.Sco2= MatrizResultados(14);

        datos.Seq_alk = ((datos.Shco3 + 2 * datos.Sco3) / 2 * 100) * 1000;
        if isempty(Alkmod)
            Alkmod=datos.Seq_alk;
        else
            Alkmod = [Alkmod; datos.Seq_alk];
        end

    end
end

 %Componentes
 if i==1
     sim.t = t;
     sim.So2 = Y(:,1);
     sim.Snh4 = Y(:,2);
     sim.Sno2 = Y(:,3);
     sim.Sno3 = Y(:,4);
     sim.Spo4 = Y(:,5);
     sim.Sco2 = Y(:,6);
     sim.Stotc = Y(:,7);
     sim.Salk = Y(:,8);
```

```
    sim.Stoth = Y(:,9);
    sim.Smg = Y(:,10);
    sim.Sk = Y(:,11);
    sim.Xs = Y(:,12);
    sim.Xalg = Y(:,13);
    sim.Xialg = Y(:,14);
    sim.Xppalg = Y(:,15);
    sim.Ss = Y(:,16);
    sim.Si = Y(:,17);
    sim.pH = pHmod;
    sim.Alk = Alkmod;

 else
    sim.t = [sim.t; t+5/24*(i-1)];
    sim.So2 = [sim.So2; Y(:,1)];
    sim.Snh4 = [sim.Snh4; Y(:,2)];
    sim.Sno2 = [sim.Sno2; Y(:,3)];
    sim.Sno3 = [sim.Sno3; Y(:,4)];
    sim.Spo4 = [sim.Spo4; Y(:,5)];
    sim.Sco2 = [sim.Sco2; Y(:,6)];
    sim.Stotc = [sim.Stotc; Y(:,7)];
    sim.Salk = [sim.Salk; Y(:,8)];
    sim.Stoth = [sim.Stoth; Y(:,9)];
    sim.Smg = [sim.Smg; Y(:,10)];
    sim.Sk = [sim.Sk; Y(:,11)];
    sim.Xs = [sim.Xs; Y(:,12)];
    sim.Xalg = [sim.Xalg; Y(:,13)];
    sim.Xialg = [sim.Xialg; Y(:,14)];
    sim.Xppalg = [sim.Xppalg; Y(:,15)];
    sim.Ss = [sim.Ss; Y(:,16)];
    sim.Si = [sim.Si; Y(:,17)];
    sim.pH = [sim.pH; pHmod];
    sim.Alk = [sim.Alk; Alkmod];
 end

j=j+5;
experimento=experimento+1;
end
```

```
sim.Xtss = (sim.Xalg .* Eso.CO_Itssalg)+(sim.Xialg .* Eso.CO_Itssxialg)+
(sim.Xppalg .* Eso.CO_Itssxppalg);
sim.Xvss = (sim.Xalg .* Eso.CO_Itssalg)+(sim.Xialg .* Eso.CO_Itssxialg);
sim.Porgsusp = (sim.Xalg .* Eso.CO_Ipalg)+(sim.Xialg .* Eso.CO_Ipxialg)+(sim.Xppalg);
sim.Nsol = sim.Snh4 + sim.Sno2 + sim.Sno3 + sim.Ss .*Eso.CO_Inss + sim.Si .*Eso.CO_Insi;
sim.Norgsol = sim.Ss .*Eso.CO_Inss + sim.Si .*Eso.CO_Insi;
sim.DQOs = sim.Ss + sim.Si;
sim.DBOs = sim.Ss;


exp.Snh4 = DATOS2(:,4);
exp.Spo4 = DATOS2(:,5);
exp.pH = pHexp;
exp.Alk = Alkexp;

Dif.Snh4= abs(sim.Snh4-exp.Snh4);
Dif.Spo4= abs(sim.Spo4-exp.Spo4);
Dif.pH= abs(sim.pH-exp.pH);
Dif.Alk= abs(sim.Alk-exp.Alk);

Res.Snh4= Dif.Snh4 .*sqrt(abs(1./std(exp.Snh4)));
Res.Snh4 (isnan(Res.Snh4))=0;
Res.Spo4 = Dif.Spo4.*sqrt(abs(1./std(exp.Spo4)));
Res.Spo4 (isnan(Res.Spo4))=0;
Res.pH = Dif.pH .*sqrt(abs(1./std(exp.pH)));
Res.pH (isnan(Res.pH))=0;
Res.Alk = Dif.Alk .*sqrt(abs(1./std(exp.Alk)));
Res.Alk (isnan(Res.Alk))=0;

%ga optimización
F = sum(sum([Res.Alk,Res.pH,Res.Snh4]));

end
```

```
%%PARÁMETROS A OPTIMIZAR
Eso.CO_Ualg_20 = 1.8 ;
```

```
Eso.CO_KipH = 0.00063*1000;
Eso.CO_KpH = 0.000001*1000000;

X0=[Eso.CO_Ualg_20 Eso.CO_KipH Eso.CO_KpH];

s3=10;
LB = X0./s3;
UB=X0.*s3;

options = gaoptimset('TolFun',1e-3);
ObjectiveFunction = @(x) SIMULACIONES_OPTIMIZACION_ALG(x);
[X, fval, EXITFLAG, OUTPUT, final_pop, scores] =
ga(ObjectiveFunction,length(LB),[],[],[],[],LB,UB,[],[],options);

if EXITFLAG >0
    Eso.CO_Ualg_20  = X(1) ;
    Eso.CO_KipH   = X(2)/1000 ;
    Eso.CO_KpH  = X(3)/1000000 ;
    Missatge= ['GA converged to a solution:\n\r', ...
        ' Eso.CO_Ualg_20 = ',num2str(Eso.CO_Ualg_20),';\n', ...
        ' Eso.CO_KipH  = ',num2str(Eso.CO_KipH),';\n', ...
        ' Eso.CO_KpH= ',num2str(Eso.CO_KpH),';\n'];

elseif EXITFLAG ==0
    Missatge= 'The maximum number of function evaluations was reached.\n';
elseif EXITFLAG <0
    Missatge= 'LSQNONLIN did not converge to a solution.\n';
end

fprintf(1,'\r');
fprintf(1,Missatge);

fprintf(1,['EXITFLAG = ',num2str(EXITFLAG),'\n']);
fprintf(1,['Number of generations taken = ',num2str(OUTPUT.generations),'\n']);
fprintf(1,['Number of function evaluations = ',num2str(OUTPUT.funccount),'\n']);
fprintf(1,['Algorithm used = ',num2str(OUTPUT.problemtype),'\n']);
```

```
%% Results
%  Eso.CO_Ualg_20 = 1.8339;
%  Eso.CO_KipH  = 0.0062978;
%  Eso.CO_KpH= 3.8156e-06;
```

B.2. Microalgal modelling code

```
%% parámetros del modelo
% Coeficientes de conversión de la matriz de composición
  Eso.CO_Itssalg = 0.646;  % Contenido de TSS en las algas
  Eso.CO_Itssxialg = 0.6;  % Contenido de TSS en la Xialg
  Eso.CO_Itssxppalg = 3.23;  % Contenido de TSS en el Xppalg
  Eso.CO_Inalg = 0.06;  % Contenido de nitrógeno en las algas (C106H181O45N16P)
  Eso.CO_Inxialg = 0.01;  % Contenido de nitrógeno en la Xialg.
  Eso.CO_Ipalg = 0.001/Eso.CO_Itssalg; % Contenido de fósforo en las algas
  Eso.CO_Ipxialg = 0.005;  % Contenido de fósforo en la Xialg.
  Eso.CO_Icalg = 0.0281;  % en moles - Contenido de carbono en las algas
  Eso.CO_Icxialg = 0.025;  % Contenido de carbono en la Xialg
  Eso.CO_Imgxialg = 0.0015;  %Contenido de magnesio en la Xialg
  Eso.CO_Imgxppalg = 0.26;  %Contenido de magnesio en la Xialg.
  Eso.CO_Imgalg = 0.0018;  %Contenido de magnesio en la Xalg;
  Bibliografía https://doi.org/10.1016/j.biortech.2010.02.088;
  También podría ser 0.0032
  Chemical composition and nutritional properties of freshwater and marine
  microalgal biomass cultured in photobioreactors
  Eso.CO_Ikalg = 0.0207;  %Contenido de potasio en la Xalg;
  Bibliografía https://doi.org/10.1016/j.biortech.2010.02.088;
  También podría ser 0.01
  Chemical composition and nutritional properties of freshwater and marine
  microalgal biomass cultured in photobioreactors
  Eso.CO_Ikxialg = 0.0008;  %Contenido de potasio en la Xialg
  Eso.CO_Ikxppalg = 0.42;  %Contenido de potasio en la Xppalg

  Eso.CO_Ipss = 0.001;% Contenido de fósforo en la Ss
  Eso.CO_Ipsi = 0.001;% Contenido de fósforo en la Si
  Eso.CO_Inss = 0.01;%0.01;% Contenido de nitrógeno en la Ss
```

```
Eso.CO_Insi = 0.001;% Contenido de nitrógeno en la Si
Eso.CO_Icss = 0.025;% Contenido de nitrógeno en la Ss
Eso.CO_Icsi = 0.03;% Contenido de nitrógeno en la Si

% Parámetros estequiométricos Algas modelo simplificado
Eso.CO_Fxialg = 0.25;  %
Eso.CO_Fsi = 0.6; %

% Parámetros cinéticos y coeficientes cinéticos para la biomasa
Eso.CO_Ualg_20 = 1.8; %Velocidad máxima de crecimiento de algas a 20ºC
Eso.CO_Qpp_20 =0.010; %Velocidad máxima de acumulación de polifosfato a 20ºC
Eso.CO_balg1_20 = 0.15; %Velocidad de muerte de algas a 20ºC %%y poliP
Eso.CO_balg2_20 = 0.1; %Velocidad de mantenimiento de algas a 20ºC
Eso.CO_Nno2 = 0.8; %Rendimiento para el nitrito
Eso.CO_Nno3 = 0.59; %Rendimiento para el nitrato
Eso.CO_Ktotc = 0.00432; %Constante de semisaturación para el CO2
Eso.CO_Ko2 = 0.2; %Constante de semisaturación para el O2
Eso.CO_Kxppalg_alg = 0.027; %Constante de semisaturación para el Xpp
en el crecimiento
Eso.CO_Knh4 = 0.1; %Constante de semisaturación para el amonio
Eso.CO_Knh4_qpp = 3; %Constante de semisaturación para el amonio
Eso.CO_Kno2 = 10; %Constante de semisaturación para el nitrito
Eso.CO_Kno3 = 12.61; %Constante de semisaturación para el nitrato
Eso.CO_Kpo4 = 0.05; %Constante de semisaturación para el fosfato
Eso.CO_Kmg = 0.13;  %Constante de semisaturación para el magnesio
Eso.CO_Kk = 8.78; %Constante de semisaturación para el potasio
Eso.CO_n_xppalg = 0.006;  %Máxima concentración de Xppalg almacenada
Eso.CO_Kxppalg_xppalg = 0.003; %Constante de semisaturación para el polifosfato
en la acumulación de polifosfatos
Eso.CO_Kla_O2 = 1.36;% se calcula a partir del base; 1.36-1.80 h-1
Eso.CO_Kla_CO2 = Eso.CO_Kla_O2;%
Eso.CO_KipH = 0.00063;
Eso.CO_KpH = 0.000001;  %Me da un pH óptimo de 7,5
Eso.CO_Kipo4 = 0.15; %Inhibición del uso del Xpp cuando hay Spo4
Eso.CO_Kla_NH3 = Eso.CO_Kla_CO2;% se calcula a partir del base
Eso.CO_Kla_k = 0.05; %constante ajuste Kla en función de Q
Eso.CO_Kla_r = 1; %constante ajuste Kla en función de Q
```

```
  % Coeficientes de la función lumínica
  Eso.CO_kw = 0.1986; %Coeficiente de atenuación del agua (valor para Xtss
  medido como DQO)
  Eso.CO_kb = 0.025; %Coeficiente de atenuación de la biomasa
  Eso.CO_Ioptimo = 230; %Coeficiente de saturación de la luz

  % Coeficientes de la función de datos.Temperatura (Ratkowski)
  Eso.CO_Tmin_Ualg = 2; %Coeficiente para calcular Ualg a cualquier temperatura
  Eso.CO_Tmax_Ualg = 40; %Coeficiente para calcular Ualg a cualquier T
  Eso.CO_b_Ualg = 87.1329461911729; %Coeficiente para calcular Ualg a cualquier T
  Eso.CO_c_Ualg = 1.46349934667002E-08; %Coeficiente para calcular Ualg a cualquier T
  Eso.CO_Tmin_balg1 = Eso.CO_Tmin_Ualg; %Coeficiente para calcular balg a cualquier T
  Eso.CO_Tmax_balg1 = Eso.CO_Tmax_Ualg; %Coeficiente para calcular balg a cualquier T
  Eso.CO_b_balg1 = Eso.CO_b_Ualg;%Coeficiente para calcular balg a cualquier T
  Eso.CO_c_balg1 = Eso.CO_c_Ualg; %Coeficiente para calcular balg a cualquier T
  Eso.CO_Tmin_balg2 = Eso.CO_Tmin_Ualg; %Coeficiente para calcular balg a cualquier T
  Eso.CO_Tmax_balg2 = Eso.CO_Tmax_Ualg; %Coeficiente para calcular balg a cualquier T
  Eso.CO_b_balg2 = Eso.CO_b_Ualg; %Coeficiente para calcular balg a cualquier T
  Eso.CO_c_balg2 = Eso.CO_c_Ualg; %Coeficiente para calcular balg a cualquier T

  % Coeficientes de la función de pH
  Eso.CO_pHoptimo = 7.5;


 Eso.CO_Ualg_20 = 1.8339;
 Eso.CO_KipH  = 0.0062978;
 Eso.CO_KpH= 3.8156e-06;


 Eso.CO_Kla_O2= 5.84;


PARAMETROS = Eso;

load Datos_calibracion_modelo_TODOS.txt
DATOS2 = Datos_calibracion_modelo_TODOS;
```

```
DATOS2(DATOS2(:,:)<0)=0;

j=1;
experimento=1;
for i=1:DATOS2(length (DATOS2(:,1)),1) %experimentos tomados

DATOS=DATOS2(j:j+4,:); %primer exp
pHmod=[];
Alkmod=[];
CO2mod=[];
NH3mod=[];

So2 = 10;
Snh4 = DATOS(1,4);
Sno2 = 0;
Sno3 = 0;
Spo4 = DATOS(1,5);
Sco2 = 0;
Stotc = DATOS(1,18);
Salk = DATOS(1,8);
Stoth = DATOS(1,19);
Smg = DATOS(1,10);
Sk = DATOS(1,11);
Xs = 0;
Ss = 0;
Si = 0;
Xalg =(DATOS(1,22)-Xs)/Eso.CO_Itssalg;
Xialg = 0;
Xppalg = 5;

x0=[So2,Snh4,Sno2,Sno3,Spo4,Sco2,Stotc,Salk,Stoth,Smg,Sk,Xs,Xalg,
Xialg,Xppalg,Ss,Si];

if i==1
    texp=DATOS(:,2)./24;
    pHexp=DATOS(:,17);
    Alkexp=DATOS(:,8);
```

```
else
    texp = [texp; DATOS(:,2)./24+5/24.*(i-1)];
    pHexp = [pHexp; DATOS(:,17)];
    Alkexp = [Alkexp; DATOS(:,8)];
end



tfinal=length (DATOS(:,2))/24;

espacio=0.001;
tiempo=0:espacio:tfinal;
tiempo=tiempo';

options = odeset('MaxStep',0.1,'InitialStep',0.000005);
[t,Y] = ode45('Generacion_ALG',tiempo,x0,options,PARAMETROS,DATOS(1,:),
experimento);

calculopH_equil=1;
if calculopH_equil==1
    %siFI1 = 0; % PARA INTRODUCIR LA FUERZA IÓNICA
    siFI1 = 1; % PARA QUE MINTEQA2 CALCULE LA FUERZA IÓNICA
    if siFI1==0
        FuerzaIonica=0.1;
    elseif siFI1==1
        FuerzaIonica=0;
    end
    for jjj=1:length (Y(:,1))
        datos.Temp = 25;
        datos.ORP = 100;
        datos.totAl = 0;
        datos.Sa = DATOS (1,3);
        datos.Spro = DATOS (1,6);
        datos.totFe = DATOS (1,12);
        datos.totCa = DATOS (1,9);
        datos.Sh2s = DATOS (1,16);
```

```
datos.Sso4 = DATOS (1,15);
totH = Y(jjj,9);
totC = Y(jjj,7);
sialk = 0;
datos.pH = 0;
datos.Snh4 = Y(jjj,2);
datos.Sno2 = Y(jjj,3);
datos.Sno3 = Y(jjj,4);
datos.Spo4 = Y(jjj,5);
datos.Smg = Y(jjj,10);
datos.Sk = Y(jjj,11);

%Calculo de pH
MatrizDatos=[datos.Temp datos.pH datos.ORP totH totC datos.Smg datos.Sk
datos.totAl datos.Sa datos.Spro datos.Snh4 datos.Spo4 datos.totFe
datos.totCa datos.Sno2 datos.Sh2s datos.Sso4 FuerzaIonica sialk];
MatrizResultados=LeerDLL(MatrizDatos,1);
pH = MatrizResultados(1);
datos.pH = pH;
if isempty(pHmod)
    pHmod=pH;
else
    pHmod = [pHmod; pH];
end


%Calculo equilibrio
MatrizDatos=[datos.Temp datos.pH datos.ORP totH totC datos.Smg datos.Sk
datos.totAl datos.Sa datos.Spro datos.Snh4 datos.Spo4 datos.totFe
datos.totCa datos.Sno2 datos.Sh2s datos.Sso4 FuerzaIonica sialk];
MatrizResultados=LeerDLL(MatrizDatos,0);

datos.Sco3= MatrizResultados(10);
datos.Shco3= MatrizResultados(12);
datos.Sco2= MatrizResultados(14);
datos.Snh3= MatrizResultados(21);
```

```
        datos.Seq_alk = ((datos.Shco3 + 2 * datos.Sco3) / 2 * 100) * 1000;
        if isempty(Alkmod)
            Alkmod=datos.Seq_alk;
            NH3mod=datos.Snh3;
            CO2mod=datos.Sco2;
        else
            Alkmod = [Alkmod; datos.Seq_alk];
            NH3mod = [NH3mod; datos.Snh3];
            CO2mod = [CO2mod; datos.Sco2];
        end

    end
end


 %Componentes
 if i==1
     sim.t = t;
     sim.So2 = Y(:,1);
     sim.Snh4 = Y(:,2);
     sim.Sno2 = Y(:,3);
     sim.Sno3 = Y(:,4);
     sim.Spo4 = Y(:,5);
     sim.Sco2 = Y(:,6);
     sim.Stotc = Y(:,7);
     sim.Salk = Y(:,8);
     sim.Stoth = Y(:,9);
     sim.Smg = Y(:,10);
     sim.Sk = Y(:,11);
     sim.Xs = Y(:,12);
     sim.Xalg = Y(:,13);
     sim.Xialg = Y(:,14);
     sim.Xppalg = Y(:,15);
     sim.Ss = Y(:,16);
     sim.Si = Y(:,17);
     sim.pH = pHmod;
     sim.Alk = Alkmod;
```

```
    sim.NH3 = NH3mod;
    sim.CO2 = CO2mod;

 else
    sim.t = [sim.t; t+5/24*(i-1)];
    sim.So2 = [sim.So2; Y(:,1)];
    sim.Snh4 = [sim.Snh4; Y(:,2)];
    sim.Sno2 = [sim.Sno2; Y(:,3)];
    sim.Sno3 = [sim.Sno3; Y(:,4)];
    sim.Spo4 = [sim.Spo4; Y(:,5)];
    sim.Sco2 = [sim.Sco2; Y(:,6)];
    sim.Stotc = [sim.Stotc; Y(:,7)];
    sim.Salk = [sim.Salk; Y(:,8)];
    sim.Stoth = [sim.Stoth; Y(:,9)];
    sim.Smg = [sim.Smg; Y(:,10)];
    sim.Sk = [sim.Sk; Y(:,11)];
    sim.Xs = [sim.Xs; Y(:,12)];
    sim.Xalg = [sim.Xalg; Y(:,13)];
    sim.Xialg = [sim.Xialg; Y(:,14)];
    sim.Xppalg = [sim.Xppalg; Y(:,15)];
    sim.Ss = [sim.Ss; Y(:,16)];
    sim.Si = [sim.Si; Y(:,17)];
    sim.pH = [sim.pH; pHmod];
    sim.Alk = [sim.Alk; Alkmod];
    sim.NH3 = [sim.NH3; NH3mod];
    sim.CO2 = [sim.CO2; CO2mod];

 end


j=j+5;
experimento=experimento+1;
end

sim.Xtss = (sim.Xalg .* Eso.CO_Itssalg)+(sim.Xialg .* Eso.CO_Itssxialg)+
(sim.Xppalg .* Eso.CO_Itssxppalg);
sim.Xvss = (sim.Xalg .* Eso.CO_Itssalg)+(sim.Xialg .* Eso.CO_Itssxialg);
```

```
sim.Porgsusp = (sim.Xalg .* Eso.CO_Ipalg)+(sim.Xialg .* Eso.CO_Ipxialg)+
(sim.Xppalg);
sim.Nsol = sim.Snh4 + sim.Sno2 + sim.Sno3 +
sim.Ss .*Eso.CO_Inss + sim.Si .*Eso.CO_Insi;
sim.Norgsol = sim.Ss .*Eso.CO_Inss + sim.Si .*Eso.CO_Insi;
sim.DQOs = sim.Ss + sim.Si;
sim.DBOs = sim.Ss;

figure(1)

    subplot(2,1,1)
    grid
    plot(sim.t,sim.Xalg,'g');
    ylabel('Xalg');
    xlabel('Time (days)');

    subplot(2,1,2)
    grid
    plot(sim.t,sim.Xppalg,'b');
    ylabel('Xppalg');
    xlabel('Time (days)');

figure(2)
    subplot(2,1,1)
    title('Nutrients');
    plot(sim.t,sim.Snh4,'r')
    hold on;
    plot(texp,DATOS2(:,4),'o')
    hold off;
    grid;
    ylabel('NH4 (g N/m3)');
    xlabel('Time (days)');

    subplot(2,1,2)
    plot(sim.t,sim.Spo4,'r')
    hold on;
    plot(texp,DATOS2(:,5),'o')
```

```
    hold off;
    grid;
    ylabel('PO4 (g COD/m3)');
    xlabel('Time (days)');


figure(3)
    subplot(1,1,1)
    plot(sim.t,sim.Xvss,'r')
    hold on;
    plot(texp,DATOS2(:,22),'o')
    hold off;
    title('Particulates');
    ylabel('Xvss (gSS/m3)');
    xlabel('Time (days)');

figure(4)
    subplot(2,1,1)
    plot(sim.t,sim.Stotc,'r')
    hold on;
    plot(texp,DATOS2(:,18),'o')
    hold off;
    grid;
    ylabel('totC (mol C/m3)');
    xlabel('Time (days)');

    subplot(2,1,2)
    plot(sim.t,sim.Stoth,'r')
    hold on;
    plot(texp,DATOS2(:,19),'o')
    hold off;
    grid;
    ylabel('totH (mol H+/m3)');
    xlabel('Time (days)');


figure(5)
```

```
    subplot(2,1,1)
    plot(sim.t,sim.pH,'r')
    hold on;
    plot(texp,DATOS2(:,17),'o')
    hold off;
    grid;
    ylabel('pH');
    xlabel('Time (days)');

    subplot(2,1,2)
    plot(sim.t,sim.Alk,'r')
    hold on;
    plot(texp,DATOS2(:,8),'o')
    hold off;
    grid;
    ylabel('Alk');
    xlabel('Time (days)');
```

```
function [sys]=Generacion_ALG(t,x,~,Parametros,OPERACION,experimento)

x(x(:,1)<0)=0;

if t == 0
    datos.pH = OPERACION(1,17);
end

%t
%% Componentes
datos.SO2 = x(1);
datos.Snh4 = x(2);
datos.Sno2 = x(3);
datos.Sno3 = x(4);
datos.Spo4 = x(5);
```

```
datos.SCO2 = x(6);
datos.totc = x(7);
datos.Salk = x(8);
datos.Stoth =x(9);
datos.Smg = x(10);
datos.Sk = x(11);
datos.Xs = x(12);
datos.Xalg = x(13);
datos.Xialg = x(14);
datos.Xppalg = x(15);
datos.Ss = x(16);
datos.Si = x(17);


persistent ConstantesCargadas
persistent Eso
if t<0.1
    ConstantesCargadas = 0;
end
if ConstantesCargadas==0
  Eso= CargarConstantes(Parametros);
   ConstantesCargadas=1;
end

datos.Xtss = datos.Xs + datos.Xalg + datos.Xialg; %ESTÁ SIMANDO COMO
DQOparticulada. kb (m2 gDQOp/1)


%% datos de operación LUZ y T
datos.Io = OPERACION (1,24);
datos.Temp = 25;

datos.V = 1/1000; %m3
datos.d = 0.0425; %m

%% cálculo pH y equil
calculopH = 1;
```

```
calculoEquil = 1;

%siFI1 = 0; % PARA INTRODUCIR LA FUERZA IÓNICA
siFI1 = 1; % PARA QUE MINTEQA2 CALCULE LA FUERZA IÓNICA
if siFI1==0
    FuerzaIonica=0.1;
elseif siFI1==1
    FuerzaIonica=0;
end

if calculopH==1
    datos.ORP = 100;
    datos.totAl = 0;
    datos.Sa = OPERACION (1,3);
    datos.Spro = OPERACION (1,6);
    datos.totFe = OPERACION (1,12);
    datos.totCa = OPERACION (1,9);
    datos.Sh2s = OPERACION (1,16);
    datos.Sso4 = OPERACION (1,15);
    totH = datos.Stoth;
    totC = datos.totc;
    sialk = 0;
    datos.pH = 0;

    %Calculo de pH
    MatrizDatos=[datos.Temp datos.pH datos.ORP totH totC datos.Smg datos.Sk
    datos.totAl datos.Sa datos.Spro datos.Snh4 datos.Spo4 datos.totFe
    datos.totCa datos.Sno2 datos.Sh2s datos.Sso4 FuerzaIonica sialk];
    MatrizResultados=LeerDLL(MatrizDatos,1);
    datos.pH = MatrizResultados(1);

end

if calculoEquil == 1

    datos.ORP = 100;
    datos.totAl = 0;
```

```
    datos.Sa = OPERACION (1,3);
    datos.Spro = OPERACION (1,6);
    datos.totFe = OPERACION (1,12);
    datos.totCa = OPERACION (1,9);
    datos.Sh2s = OPERACION (1,16);
    datos.Sso4 = OPERACION (1,15);
    sialk = 0;
    %Calculo de equilibrio
    MatrizDatos=[datos.Temp datos.pH datos.ORP datos.Stoth datos.totc datos.Smg
    datos.Sk datos.totAl datos.Sa datos.Spro datos.Snh4 datos.Spo4 datos.totFe
    datos.totCa datos.Sno2 datos.Sh2s datos.Sso4 FuerzaIonica sialk];
    MatrizResultados=LeerDLL(MatrizDatos,0);
    datos.Seq_H = MatrizResultados(1);
    protonH_mod = datos.Seq_H;
    datos.pH_eq=-1*(log10(protonH_mod));
    datos.Sco3= MatrizResultados(10);
    datos.Shco3= MatrizResultados(12);
    datos.Seq_h2co3= MatrizResultados(13);
    datos.Sco2= MatrizResultados(14);
    datos.Snh3= MatrizResultados(21);
    datos.FuerzaIonica= MatrizResultados(31);

    datos.Seq_alk = (datos.totc * 1000 - datos.Sco2) / 2 * 100;

end


%% Cálculo matriz estequiométrica
persistent MatrizCargada
persistent MATRIZESTEQUIOMETRICA
if t<0.1
    MatrizCargada=0;
end
if MatrizCargada==0
   MATRIZESTEQUIOMETRICA = CalculoMatriz(Eso);
   MatrizCargada=1;
end
```

```
%% Cálculo vector cinético
    %ratio Xpp/PAO
    Eso.CO_fpp_alg = datos.Xppalg/datos.Xalg ;

    %función luz
    Eso.CO_Fluz = datos.Io * (1 - exp(-(Eso.CO_kw + Eso.CO_kb * datos.Xtss) *
    datos.d)) / ((Eso.CO_kw + Eso.CO_kb * datos.Xtss) *
    datos.d) / Eso.CO_Ioptimo * exp(1 - (datos.Io *
    (1 - exp(-(Eso.CO_kw + Eso.CO_kb * datos.Xtss) * datos.d)) /
    ((Eso.CO_kw + Eso.CO_kb * datos.Xtss) * datos.d) / Eso.CO_Ioptimo));

    %función de pH
    Eso.CO_pHoptimo = sqrt(Eso.CO_KpH * Eso.CO_KipH) / (sqrt(Eso.CO_KpH *
    Eso.CO_KipH) + Eso.CO_KpH) * Eso.CO_KipH / (sqrt(Eso.CO_KpH * Eso.CO_KipH)
    + Eso.CO_KipH);
    Eso.CO_FpH = (Eso.CO_KipH / (Eso.CO_KipH + 10 ^ (-(datos.pH) + 3))) *
    (10 ^ (-(datos.pH) + 3) / (Eso.CO_KpH + 10 ^ (-(datos.pH) + 3))) *
    1 / Eso.CO_pHoptimo;

    %función datos.Temperatura (Ratkowski)
    T=0:0.01:50;
    Ftemp=(Eso.CO_b_Ualg .* (T - Eso.CO_Tmin_Ualg)) .^ 2 .*
    (1 - exp(Eso.CO_c_Ualg .* (T - Eso.CO_Tmax_Ualg)));
    f_Topt=max(Ftemp);
    Ftemp_norm = (Eso.CO_b_Ualg * (datos.Temp - Eso.CO_Tmin_Ualg)) ^ 2 *
    (1 - exp(Eso.CO_c_Ualg * (datos.Temp - Eso.CO_Tmax_Ualg)))/f_Topt;

    Eso.CO_Ualg = Eso.CO_Ualg_20 * Ftemp_norm;
    Eso.CO_Qpp = Eso.CO_Qpp_20 * Ftemp_norm;
    Eso.CO_Balg1 = Eso.CO_Balg1_20 * Ftemp_norm;
    Eso.CO_Balg2 = Eso.CO_Balg2_20 * Ftemp_norm;


    Iav = datos.Io * (1 - exp(-(Eso.CO_kw + Eso.CO_kb * datos.Xtss) * datos.d)) /
    ((Eso.CO_kw + Eso.CO_kb * datos.Xtss) * datos.d);
    Eso.CO_Fluz = Iav / (Iav +  Eso.CO_Ioptimo);
```

```
% Crecimiento de Xalg con Snh4 y Xpp (PROCESO 3 MODELO PUBLICADO)
VECTORCINETICO(1) = Eso.CO_Ualg * (datos.totc / (Eso.CO_Ktotc + datos.totc)) *
(datos.Snh4 / (Eso.CO_Knh4_qpp + datos.Snh4)) * (Eso.CO_Kipo4 /
(Eso.CO_Kipo4 + datos.Spo4)) * (Eso.CO_fpp_alg /
(Eso.CO_Kxppalg_alg + Eso.CO_fpp_alg)) * datos.Xalg * Eso.CO_Fluz * Eso.CO_FpH;

% Crecimiento de Xalg con Sno2 y Xpp
VECTORCINETICO(2) = 0;

% Crecimiento de Xalg con Sno3 y Xpp (PROCESO 4 MODELO PUBLICADO)
VECTORCINETICO(3) = 0;

% Almacenamiento de Xppalg (PROCESO 5 MODELO PUBLICADO)
VECTORCINETICO(4) = Eso.CO_Qpp * (datos.Spo4 / (Eso.CO_Kpo4 + datos.Spo4)) * ((
(Eso.CO_Kxppalg_xppalg^Eso.CO_n_xppalg + Eso.CO_fpp_alg^Eso.CO_n_xppalg)) *
datos.Xalg * Eso.CO_Fluz * Eso.CO_FpH;

% Lisis de Xalg (PROCESO 7 MODELO PUBLICADO)
VECTORCINETICO(5) = Eso.CO_Balg1 * datos.Xalg;

% Lisis de Xppalg (PROCESO 8 MODELO PUBLICADO)
VECTORCINETICO(6) = Eso.CO_Balg1 * datos.Xppalg;

% Mantenimiento de Xalg (PROCESO 6 MODELO PUBLICADO)
VECTORCINETICO(7) = Eso.CO_Balg2 * datos.Xalg;

KlaBase=Eso.CO_Kla_CO2;

VolumenMolar.CO2 = 0.037278;
viscosidad = exp(-52.843 + 3703.6 / (datos.Temp + 273.15) + 5.866 *
log((datos.Temp + 273.15)) - 5.879E-29 * (datos.Temp + 273.15) ^ 10.0);
PesoMolecularH2O = 18;
Difusividad.CO2 = 0.00000000000000011728 * (datos.Temp + 273.15) *
(2.6 * PesoMolecularH2O) ^ 0.5 / viscosidad / (VolumenMolar.CO2 ^ 0.6);
DifusBase = Difusividad.CO2;
KLa.CO2 = KlaBase * (Difusividad.CO2 / DifusBase) ^ (0.5);
```

```
PresionParcial.CO2 =  0.030*10000;
datos.SCO2_sat = CalculoSaturacionCO2(datos.Temp,PresionParcial.CO2);%co2

%Stripping CO2 (PROCESO 9 MODELO PUBLICADO)
VECTORCINETICO(8) = KLa.CO2 * (datos.Sco2 - datos.SCO2_sat/44);

VolumenMolar.O2 = 0.02802;
Difusividad.O2 = 0.00000000000000011728 * (datos.Temp + 273.15) *
(2.6 * PesoMolecularH2O) ^ 0.5 / viscosidad / (VolumenMolar.O2 ^ 0.6);
KLa.O2 = KlaBase * (Difusividad.O2 / DifusBase) ^ (0.5);
PresionParcial.O2 = 20.95*10000;
datos.SO2_sat = CalculoSaturacionO2(datos.Temp,PresionParcial.O2);%o2

%Stripping O2 (PROCESO 10 MODELO PUBLICADO)
VECTORCINETICO(9) = KLa.O2 * (datos.SO2 - datos.SO2_sat);

 %% AMPLIACIÓN MODELO ALGAS CON DOBLE VÍA CRECIMIENTO
VolumenMolar.NH3 = 0.03693;
Difusividad.NH3 = 0.00000000000000011728 * (datos.Temp + 273.15) *
(2.6 * PesoMolecularH2O) ^ 0.5 / viscosidad / (VolumenMolar.NH3 ^ 0.6);
KLa.NH3 = KlaBase * (Difusividad.NH3 / DifusBase) ^ (0.5);
PresionParcial.NH3 = 0.001*10000;
datos.NH3_sat = CalculoSaturacionNH3(datos.Temp,PresionParcial.NH3);%nh3
datos.NH3_sat = 0;

%Stripping NH3 (PROCESO 11 MODELO PUBLICADO)
VECTORCINETICO(10) = KLa.NH3 * (datos.Snh3 - datos.NH3_sat * 14 / 17);

 % Crecimiento de Xalg con Snh4  y Spo4 (PROCESO 1 MODELO PUBLICADO)
VECTORCINETICO(11) = Eso.CO_Ualg * (datos.totc /
(Eso.CO_Ktotc + datos.totc)) * (datos.Snh4 / (Eso.CO_Knh4 + datos.Snh4)) *
(datos.Spo4 / (Eso.CO_Kpo4 + datos.Spo4)) * datos.Xalg *
Eso.CO_Fluz * Eso.CO_FpH;

% Crecimiento de Xalg con Sno2  y Spo4
VECTORCINETICO(12) = 0;
```

```
    % Crecimiento de Xalg con Sno3  y Spo4 (PROCESO 2 MODELO PUBLICADO)
    VECTORCINETICO(13) = 0;

    GEN = MATRIZESTEQUIOMETRICA'*VECTORCINETICO';

sys=GEN;
```

B.3. R statistical code

```
library("readxl")
library("gmodels")
library("car")
library("DescTools")
library("ggplot2")
library("qqplotr")
library("dplyr")
data = read_excel("C:\\Users\\EG\\OneDrive - Politecnico di Milano\\Desktop\\
Excel resumen.xlsx",sheet = "Foglio2")
#cambia foglioX e numerosità sotto in T-TEST
dfdata = data.frame(data)

my_data = dfdata

x <- my_data$H_EXP
y <- my_data$H_SIM

#SCATTER PLOT ALL VAR

Model<-lm(y ~ x, data = my_data)
summary(Model)
jpeg(file="scatterplot_norm_2.jpeg")
plot(x, y, main = "Aggregate variables",
     xlab = "VAR_EXP", ylab = "VAR_SIM",
     pch = 19, frame = FALSE)
abline(lm(y ~ x, data = my_data), col = "blue")
legend("topleft",legend=paste("R2 =", format(summary(Model)$r.squared,digits=3)))
```

```
dev.off()

#T-TEST
my_data <- data.frame(
                group = rep(c("x", "y"), each = 75),
                weight = c(x,  y)
                )
# Print all data
print(my_data)

library("dplyr")
group_by(my_data, group) %>%
  summarise(
    count = n(),
    mean = mean(weight, na.rm = TRUE),
    sd = sd(weight, na.rm = TRUE)
  )

# Plot weight by group and color by group
library("ggpubr")
ggboxplot(my_data, x = "group", y = "weight",
          color = "group", palette = c("#00AFBB", "#E7B800"),
          order = c("H.EXP", "H.SIM"),
          ylab = "Weight", xlab = "Groups")

# Subset weight data before treatment
H.EXP <- subset(my_data,  group == "x", weight,
                drop = TRUE)
# subset weight data after treatment
H.SIM <- subset(my_data,  group == "y", weight,
                drop = TRUE)
# Plot paired data
library(PairedData)
pd <- paired(H.EXP, H.SIM)
plot(pd, type = "profile") + theme_bw()

#Preleminary test to check paired t-test assumptions
```

```
#Assumption 1: Are the two samples paired?
#Yes, since the data have been collected from measuring twice the H variable of
#the sample in the same boundary conditions.
#Assumption 2: Is this a large sample?
#Yes, because n > 30 (35). Since the sample size is large enough (more than 30),
#we do not need to check whether the differences of the pairs follow a normal
#distribution, we assume they do. Anyway, we check it in the code.
#How to check the normality of the data differences?
#Use Shapiro-Wilk normality test as described at: Normality Test in R.
#Null hypothesis: the data differences are normally distributed
#Alternative hypothesis: the data differences are not normally distributed

# compute the difference
d <- with(my_data,
        weight[group == "x"] - weight[group == "y"])
# Shapiro-Wilk normality test for the differences
shapiro.test(d)

jpeg(file="boxplot_norm_2.jpeg")
ggboxplot(d) +
  stat_boxplot(geom ="errorbar", width = 0.5) +
  geom_boxplot(fill = "light blue") +
  stat_summary(fun.y=mean, geom="point", shape=10, size=3.5, color="black") +
  theme_bw() + theme(legend.position="none")
dev.off()

jpeg(file="qqplot_norm_2.jpeg")
qqPlot(d)
dev.off()

library("ggpubr")
ggdensity(d,
          main = "Density plot of differences")

# => p-value = XXX
#  p-value > 0.05 implying that the distribution of the data are not
#significantly different from normal distribution.
```

```
#In other words, we can assume the normality.
#Is there any significant changes in the weights of mice after treatment?
#1) Compute paired t-test - Method 1: The data are saved in two different
#numeric vectors.
# Compute t-test no paired
res <- t.test(H.EXP, H.SIM, paired = FALSE)
res
# Compute paired t-test
res <- t.test(H.EXP, H.SIM, paired = TRUE)
res

#t is the t-test statistic value (t = 20.88),
#df is the degrees of freedom (df= 9),
#p-value is the significance level of the t-test (p-value = 6.210^{-9}).
#conf.int is the confidence interval (conf.int) of the mean differences at 95%
#is also shown (conf.int= [173.42, 215.56])
#sample estimates is the mean differences between pairs (mean = 194.49).

#Interpretation of the result
#The p-value of the test is 6.210^{-9}, which is less than the significance level
#alpha = 0.05. We can then reject null hypothesis and conclude that the
#average H variable experimental is significantly different
```

List of Figures

List of Tables

Acknowledgements

Per prima cosa desidero esprimere i miei più sinceri ringraziamenti alla professoressa Elena Ficara per avermi dato l'opportunità di poter svolgere questo lavoro di tesi su un argomento cosi attuale. Ringrazio con gratitudine inoltre sia la professoressa Ficara sia il professore José Ferrer Polo per il sempre rapido aiuto nelle pratiche burocratiche legate a questa esperienza cosi arricchente chiamata Erasmus.
Un profondo grazie va poi al professor Ángel Robles, primo ad accogliermi in una nuova realtà, senza il quale non sarei stato in grado di portare avanti il mio lavoro. Ringrazio anche il professor Luis Borrás e la dottoressa Stéphanie Aparicio per i preziosi aiuti che mi hanno sempre dato durante il lavoro fatto.
Ringrazio la mia famiglia per il supporto che mi hanno dato per tutti questi anni di università e, in special modo, in questo ultimo anno vissuto a distanza.
Quiero dar las gracias a todos los compañeros con los que he compartido mi trabajo, desde Javier, el primero que me ayudó a instalarme, hasta Ángela con la que he compartido momentos especiales, pasando por Patricia, Ivana, Berta, María, Valeria y Melissa que siempre me han ayudado desde el primer día. También saludo con afecto a Carlos, Abril, Jesús, Alejandro, Laura, Jordi por todos los bellos momentos que hemos vivido juntos, guardaré un precioso recuerdo de todos vosotros, con la esperanza de volver a veros pronto.
Chiaramente non posso che ringraziare i miei coinquilini, e amici, che mi hanno accompagnato durante questo starordinario anno, mamma Norma, zio Walter, Ralph, Bea e il nostro baby Lucas.
Un grazie lo dedico anche ai soci e compari con cui ci siamo tenuti compagnia lungo questo viaggio universitario, zio Andrew, il vecio Luca, il Tino.
Infine, voglio ringraziare i BMBR® per questi anni fatti di reciproca sopportazione e supporto, amici sempre fedeli e presenti.